SYNTHESIS, CHARACTERIZATION AND CATALYTIC PROPERTIES OF THE ZEOLITE MCM-22

A THESIS

SUBMITTED TO THE

UNIVERSITY OF POONA

FOR THE DEGREE OF

DOCTOR OF PHILOSOPHY

(IN CHEMISTRY)

BY

R. RAVISHANKAR

CATALYSIS DIVISION

NATIONAL CHEMICAL LABORATORY

PUNE - 411 008, INDIA.

APRIL 1996

DEDICATED TO MY PARENTS

AND

MY LATE GRANDFATHER

CERTIFICATE

Certified that the work incorporated in the thesis "**Synthesis, Characterization and Catalytic Properties of the Zeolite MCM-22**" submitted by Mr. R. Ravishankar, for the degree of Doctor of Philosophy, was carried out by the candidate under my supervision in the Catalysis Division, National Chemical Laboratory, Pune, India. **Materials** obtained from other sources have been duly acknowledged in the thesis.

[S. SIVASANKER]

(Research Guide)

ACKNOWLEDGEMENTS

[R. RAVISHANKAR]

C O N T E N T S . . . .

ABSTRACT

MCM-22 is a high silica zeolite patented by the Mobil group (Rubin and Chu, US Patent No. 4,954,325) in 1990. However, no publications on this zeolite appeared till 1994, eventhough a large number of patents dealt with the applications of this zeolite. This thesis describes a study of the synthesis of MCM-22 with different Si/Al ratios, their characterization by different physico-chemical methods and investigation of their catalytic properties. Hexamethyleneimine was used as the template for the synthesis. The influences of some of the synthesis parameters like Si/Al ratio, crystallization temperature, mode of crystallization, silica source, amount of template concentration and base concentration on the kinetics of crystallization were investigated. The samples were characterized by XRD, SEM, TGA/DTA, NMR and I.R. spectroscopic methods besides adsorption of gases and hydrocarbons. The catalytic reactions studied were the isomerization of m-xylene, hydroisomerization and cracking of n-hexane and transformation of methanol to hydrocarbons.

The objective of the present thesis is to study the synthesis, characterization and catalytic properties of the zeolite MCM-22.

Chapter I deals with a general introduction to zeolites, their synthesis using organic template molecules, their characterization using experimental techniques such as, XRD, SEM, I.R., MAS NMR, thermal analysis and sorption of probe molecules and properties exhibited by zeolites such as acid-base properties and shape selectivity. Test reactions carried out to determine the pore topology of unknown zeolite structures are discussed in detail in the latter part of this chapter and finally the applications of zeolites as catalysts is briefly mentioned.

Chapter II describes the experimental procedures used to synthesize MCM-22 and the parameters affecting the synthesis, such as temperature of crystallization, mode of crystallization, Si/Al ratios, OH^-/SiO_2 and R/Na_2O ratios of the synthesis gel and the nature of silica source. Optimum synthesis conditions for obtaining the most crystalline sample were

found out and samples synthesized under these conditions were used for charactrization and catalytic applications.

Chapter III deals with the characterization of the zeolite samples using various instrumental techniques. XRD has been used to calculate the unit cell parameters of the samples with different Si/Al ratios. High resolution solid state nuclear magnetic resonance spectroscopic experiments over highly siliceous samples have been utilized to study the nature of the silicon environments and to find out the number of crystallographically distinct 'T' sites. Multi-nuclear MAS NMR studies of various nucleii such as ^{13}C, ^{29}Si, ^{1}H and ^{27}Al have been carried out over both as-synthesized and calcined samples to gather information about the framework species. Thermal analyses coupled with temperature programmed decomposition of the template molecules have been carried out to learn about the template-lattice interactions.

Chapter IV describes the sorption properties of MCM-22. Sorption of various probe molecules namely, water, n-hexane, cyclohexane, m-xylene and mesitylene were carried out over MCM-22 samples with different SiO_2/Al_2O_3 ratios. The results were compared with the sorption uptake over other large pore zeolites such as, zeolite ß, mordenite, ZSM-12 and USY and medium pore zeolite, ZSM-5. Sorption of ammonia was carried out over MCM-22 samples with different Si/Al ratios at different temperatures. The results obtained were fitted into the various equations and isosteric heats of ammonia adsorption and chemical potentials were determined.

Chapter V describes the use of zeolite MCM-22 as a catalyst in a wide variety of reactions. Four reactions, viz., isomerization of m-xylene, hydroisomerization and cracking of n-hexane and transformation of methanol to hydrocarbons were carried out. The effect of various parameters have been studied and the results are presented in this chapter.

Chapter VI summarizes the conclusions drawn from the above studies and the salient features of the thesis.

CHAPTER I

INTRODUCTION

1.1 INTRODUCTION

Zeolites are crystalline microporous materials containing cavities and channels of molecular dimensions (3 Å to 13 Å) and possess large internal surface areas. The access of molecules into the pores of these materials is determined by the relative sizes of the molecules and the size of the pores. Thus, all the zeolites can be classified under the broad class of molecular sieves.[1a]

By virtue of possessing uniform pores and high surface area, zeolites have found applications in adsorption and separation processes and in catalysis. They are widely used in the industry, especially in petroleum refineries and petrochemical units as adsorbents and in processes such as hydrocracking, cracking, isomerization and alkylation.

1.1.1 ZEOLITES

In 1756, a Swedish mineralogist, Cronsted[1b], observed that the mineral stilbite when heated liberated steam. This led him to coin the term "Zeolite" from the two Greek words, "Zeo" to boil and "lithos" stone.

Zeolites are crystalline aluminosilicates with rigid three dimensional framework of $[SiO_4]$ and $[AlO_4]$ tetrahedra linked to each other by corner sharing of oxygen ions. Each $[AlO_4]$ tetrahedron creates a negative charge on the framework of the zeolite. The framework negative charge is balanced by cations, which occupy non-framework/exchangeable positions. The crystal structure of a zeolite is determined by the specific order in which the tetrahedral units are linked together. A representative empirical formula[2] for a zeolite is given below:

$$M_{2/n}O \cdot Al_2O_3 \cdot x\,SiO_2 \cdot y\,H_2O.$$
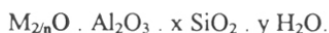
where "M" represents the exchangeable charge balancing cations belonging to group I or II with a valency of 'n'. Sometimes, other metal or organic cations and ions such as NH_4^+, and H^+ also

balance the framework charge. The value of 'x' is always equal to or greater than 2, since two aluminum atoms cannot occupy two adjacent tetrahedral positions in accordance with the Lowenstein's Rule.[3] When H^+ ions are the charge balancing cations, then the zeolite possess Brönsted acid characteristics.

1.1.2 BUILDING UNITS OF ZEOLITE STRUCTURES

The primary building unit of any zeolite structure is the tetrahederal $[TO_4]$ unit, where, T is either Si or Al. A secondary building unit (SBU) consists of selected geometric groups of these tetrahedra consisting of 4, 6 and 8 membered rings, 4-4, 6-6 and 8-8 membered double rings (DR) and 4-1, 5-1 and 4-4-1 branched rings.[4] All the zeolitic structures known so far have been found to be made up of combinations of the above SBUs. A schematic representation of these SBUs is presented in Figure 1.1. New combinations of the various polyhedra would lead to new structures.[5]

The crystalline framework structures contain voids and channels of discrete sizes. The pore or channel openings generally range from 3 - 20 Å. Thus, zeolites are classified as microporous materials. Water molecules and other cations are present in the channels or voids to neutralize the framework charge created by the $[AlO_4]$ tetrahedra. The cations occupy non-framework or exchangeable positions. The ions encountered often are listed below :

Alkali/alkaline earth metals : Na^+, K^+, Rb^+, Cs^+, Ca^{2+}, Mg^{2+}, Ba^{2+} and Sr^{2+}.

Organic cations : TMA^+, TEA^+, TPA^+, TBA^+, H_3O^+, NH_4^+ and ions of other nitrogen and oxygen containing molecules.

Rare earth and noble metal ions like La^{3+}, Ce^{3+} and Pt^{2+}, Pd^{2+}.

1.2 CLASSIFICATION OF ZEOLITES

Zeolites can be classified based on their morphology,[6-9] crystal structures,[6,7] chemical composition (SiO_2/Al_2O_3 ratios),[6,7,10] pore topology[6,11] and their natural occurrence.[6] They can

4   5   6   8

4-1   4-1   5-1   6-2

4-4-1   6-6
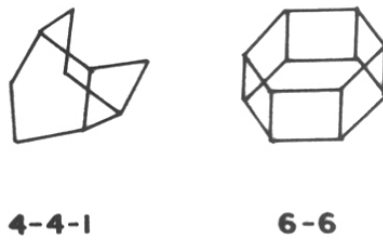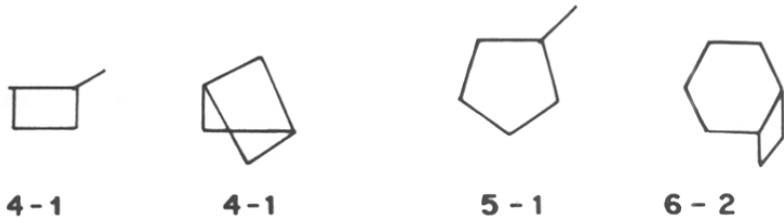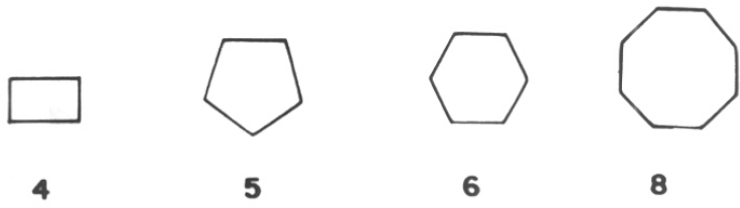
Figure 1.1   Secondary building units of zeolite structures.[4]

be classified on the basis of their silica to alumina ratio into three groups,[10] namely, (a) low silica zeolites, Si/Al = 1 - 1.5, (b) medium silica zeolites, Si/Al = 1.5 - 5.0 and (c) high silica zeolites, Si/Al = 5 - several thousands and silica polymorphs, Si/Al $\simeq$ infinity. Silicalite-1 is the silica polymorph of ZSM-5 [MFI] type structure. They can also be conveniently classified based on their effective pore diameters.

Barrer[12] had classified zeolites into five groups, which was later modified by Sand[11] into three groups, namely, small pore zeolites (pore diameter 3 Å - 4 Å; 8-membered ring pore openings; erionite, chabazite, A, rho, etc.), medium pore zeolites (pore diameter 5 - 6 Å; 10-membered ring pore openings; ZSM-5, ZSM-11, ZSM-48, EU-1, ferrierite, etc.) and large pore zeolites (pore diameter > 7 Å; 12-membered ring pore openings; beta, X, Y, mordenite and ZSM-12). The shape of the pores varies from one zeolite to another, for example, it is circular in ZSM-11, circular and sinusoidal in ZSM-5, elliptical in AlPO$_4$-11 and tear-drop shaped in ZSM-23. Zeolites can also be classified based on the dimensionality of the pores; one-dimensional (1D) in the case of ZSM-12 and ZSM-48, two-dimensional (2D) in the case of ZSM-5 and ZSM-11 and three-dimensional (3D) in the case of X, Y and beta. Surface properties like hydrophobicity and hydrophilicity depend on the SiO$_2$/Al$_2$O$_3$ ratios of the zeolites. Silica rich zeolites are hydrophobic in nature, whereas, aluminum rich zeolites are hydrophilic in nature, reflected by the uptake of water molecules. Davis et al.[13,14] have synthesized a new aluminophosphate molecular sieve designated as VPI-5 with a pore opening of 13 Å and Estermann et al.[15] have reported the synthesis of a new gallophosphate molecular sieve called cloverite with 20 MR pore openings (super cage diameter, 29 Å - 30 Å). A new ultra large pore molecular sieve designated as JDF-20 has been reported recently.[16] Very recently, a new mesoporous silica polymorph[17,18] called MCM-41 possessing one-dimensional regular array of uniformly sized mesopores in the range of 16 Å to 100 Å has been reported. A listing of the zeolites based on their pore dimensions are presented in Table 1.1.

Table 1.1   Classification of some typical zeolites based on their pore geometry.[4]

8 - Membered Ring (Small Pore)	10 - Membered Ring (Medium Pore)	12 - Membered Ring (Large Pore)
Linde A	Dachiardite	Cancrinite
Bikitaite	Epistilbite	Linde X, Y, L, EMT
Brewsterite	Ferrierite	Gmelinite
Chabazite	Heulandite	Mazzite
Edingtonite	ZSM-5	Mordenite (Large pore)
Erionite	ZSM-11	Offretite
Mordenite (Small pore)	Stilbite	ZSM-12
Levynite	ZSM-22, -23, -48	Omega
Paulingite	ZSM-39	Beta
Phillipsite	ZSM-47	NCL-1
ZK-4 and ZK-5	EU-1 (ZSM-40)	$AlPO_4$ -5

Low silica zeolites are thermally stable upto about 923 K - 1023 K, whereas, high silica and aluminum free silica polymorphs are stable upto about 1273 K - 1473 K. As framework Si/Al ratio increases, the cation exchange capacity and total acidity decrease, but the strength of the acid sites increase.

1.2.1 NATURAL ZEOLITES

To date, about 40 natural zeolites are known, of which some have synthetic analogs. Very recently, a natural material called Tacherikite[19] was discovered and found to be a natural counterpart of zeolite beta; the latter was synthesized 20 years ago by Wadlinger et al.[20-23] Very recently, a natural zeolite termed as Boggosite[24a] was reported to have both 10 MR and 12 MR channels (synthetic zeolites NU-87 and SSZ-26 also have 10 and 12 MR intersecting channels[24b,c]).

1.2.2 SYNTHETIC ZEOLITES

Zeolites can also be synthesized under hydrothermal conditions in the laboratory. Hydrothermal methods typically involve crystallization at high temperatures (270 K - 500 K) under autogeneous pressure (0.5 - 3 MPa) from aqueous systems containing the necessary chemical components for their formation. Schafhautle, in 1845, reported the preparation of quartz by heating silica gel with water in an autoclave.[6] Later, many groups have synthesized zeolites under hydrothermal conditions. At present, at least 160 synthetic zeolites have been prepared. Variation of the Si/Al ratio in the reaction mixture leads to a variety of zeolites. Most of the synthetic zeolites are considered to be metastable phases in a thermodynamic sense and are produced under non-equilibrium conditions. From a mixture of components of identical chemical composition, widely different zeolite species may be formed as metastable phases in closed systems at temperatures lower than 473 K. The important parameters that govern the formation of a synthetic zeolite are the nature of the starting materials, the rate of nucleation and crystallization, the crystallization temperature and duration of crystallization.[6]

Earlier, in general, the synthesis was carried out at temperatures below 473 K with gels of very high pH (>12), the gels generally containing alkali metal ions as mineralizing agents. These usually resulted in zeolites with high aluminum content (Si/Al < 5) such as, A,[25] X,[26] and Y.[27] The general conditions for the synthesis of zeolites are :

1. Reactive starting materials.

2. High pH.

3. Low temperature hydrothermal conditions.

4. High degree of supersaturation of the silicate and aluminate species.

Later, the presence of tetraalkyl ammonium cations and other anions in the reaction mixture was found to produce zeolites with new structures; these zeolites had high Si/Al ratios (> 20). Typical examples of such zeolites are ZSM-5, ZSM-11, ZSM-48 and ZSM-12. Barrer,[28-31] Kerr[32-37] and Kokotailo[38] have done pioneering research using new templates.

High silica zeolites such as ZSM-5, by virtue of having high acid strength, are very useful in adsorption processes and are used as catalysts. Synthetic zeolites such as zeolite A and X have found extensive application in adsorption and separation processes and in detergent industries. Zeolite Y and mordenite exchanged with rare earth and noble metals are used in important petrochemical processes such as catalytic hydroisomerization, hydrocracking and alkylation/dealkylation.[39-41] Medium pore zeolites, mainly ZSM-5, due to their shape selective property are used in petroleum and petrochemical processes such as hydrodewaxing, alkylation and isomerization reactions.[42,43]

1.3 ROLE OF TEMPLATES

Templates play an important role in the synthesis of known and new zeolite structures. The use of templates was discovered in late 1960s by Barrer.[28-31] This has now become important in the synthesis of high silica zeolites.[31-38,44] The same organic cation can sometimes lead to different structures,[29,32,45,46] for example, the tetramethyl ammonium (TMA) cation leads

to the formation of 17 different structures. Table 1.2 lists the structures formed by using the TMA cation. Similarly, a variety of templates could lead to the formation of the same structure, a few examples of which are listed in Table 1.3. It has been generally found that the zeolites synthesized using templates have voids large enough to accommodate these molecules. TMA is used to synthesize both erionite and offretite,[47,48] two zeolites with related structures. It fits into the pore system of erionite tightly but loosely in the offretite pores. Thus, the use of TMA as the templating agent prevents the intergrowth of erionite during offretite synthesis.[48] The templating effect of the TMA cation is attributed to the stability offered by the electric-dipole interactions and the stereospecificity due to its size and shape.[48,49]

The tetraethyl ammonium (TEA) cation makes a good template in synthesizing zeolites with channels such as ZSM-8 (a 10 membered ring (10 MR) zeolite), $AlPO_4$-5 (an open 12 ring molecular sieve) and mordenite (a zeolite with puckered pore (12 MR) openings). The template fits in tightly in the pores of ZSM-8 but fits in loosely in the channels of $AlPO_4$-5. The hydrated TEA cation also acts as a templating agent of the cage structure in ZSM-20.[49]

The zeolite ZSM-5 was originally prepared by Argauer and Landolt[50] in 1972 with Si/Al ratios in the range of 30 - 400 in the presence of tetrapropyl ammonium (TPA) cations. This range was then extended to several thousands and a silica polymorph of ZSM-5 structure has also been prepared. Eventhough, template free synthesis of ZSM-5 has been carried out,[51-53] it has been found suitable for synthesis in only a limited range of Si/Al ratios. It has generally been observed that TEA, TPA and tetrabutyl ammonium (TBA) cations tend to template the channel type structures. They are typical templates for the synthesis of beta, ZSM-5 and ZSM-11, respectively. The cations have been shown to sit in the channel intersection extending the hydrophobic arms of alkyl groups into the channels.[48,49,54]

Non-zeolite molecular sieves such as $AlPO_4$-5 can also be synthesized[55] with the aid of organic templates. The size of the template molecules vary from ~ 6 Å to ~ 8 Å. As zeolites

Table 1.2   Typical examples of templates used in zeolites synthesis and the structures obtained.[28-38]

Templates	Zeolite structures obtained
Tetramethyl ammonium ion (TMA)	Zeolite A, E, FU-1, NU-1, O, ZSM-4, ZSM-6, ZSM-39, ZSM-47 and sodalite.
Tetraethyl ammonium ion (TEA)	ZSM-5, ZSM-8, ZSM-12, ZSM-20, ZSM-25, ZSM-48 and beta.
Tetrapropyl ammonium ion (TPA) and Tetrapropyl phosphonium ion (TPP)	ZSM-5 and $AlPO_4$-5.
Tetrabutyl ammonium ion (TBA) and Tetrabutyl phosphonium ion (TBP)	ZSM-11.
TMA + TEA	ZSM-39.
Pyrrolidine	ZSM-21, ZSM-23 and ZSM -25.
Hexamethyleneimine	MCM-22, PSH-3, $AlPO_4$-5 and nonasil.
Ethanolamine	ZSM-5.
Glycerol	ZSM-5.
Hexamethylene bis(ethylammonium bromide)	NCL-1.
Hexamethylene bis(ethyldimethylammonium bromide)	ZSM-12.
Hexamethylene bis(tripropyl ammonium bromide)	ZSM-5.

Table 1.3   Some examples of different organic templates directing a single structure.[49]

Zeolite Structure	Templates
ZSM-5	TEA, TPA, TPP, Tripropyl amine, Ethanolamine, Alcohols, Methyl qinuclidine, Glycerol, Propyl amine, Morpholine, Hexanediol, Di-n-butyl amine, Pyrrolidine and 1,6-diamino hexane.
Omega	Tetramethyl ammonium salt, Choline chloride, DABCO, Pyrrolidine.
$AlPO_4$-5	Tetraethyl ammonium hydroxide, Choline hydroxide, Tetrapropyl ammonium hydroxide, Triethyl amine, 2-Picoline, Cyclohexylamine and Dicyclohexylamine.
Ferrierite	Choline, Pyrrolidine, Ethylenediamine, Piperidine, 1,3-Diaminopropane and 2,4-pentane diol.

and AlPO's have been synthesized both with templates fitting into the pores tightly and loosely, it appears that template fit is not the only criterion for obtaining a particular zeolite structure.[49]

Lok et al.[49] have reviewed the role of organic guest molecules and have reached some conclusions about the role of organic templates in the synthesis of zeolites. A template theory[49] has been proposed to explain the structure directing effect of the organic guest molecules. The charge distribution and the size and the geometric shape of the templates are believed to be responsible for their structure directing effect. Some observations on the role of the template molecules are listed below.[48,49]

A)   They are structure directing agents.

B)   They modify the gel and aid the formation of new structures.

C)   They increase the Si/Al ratio of the zeolites; Na-A, ZK-4 and alpha can be synthesized with higher Si/Al ratios in the presence of templates.

D)   Templates alter the pH of the synthesis gel.

E)   They act as mineralizing agents, keeping the reactive species in solution.

F)   They decrease the time of crystallization; the synthesis of ETS-10, a large pore titanosilicate molecular sieve, is carried out in 10 days in the absence of template,[56] and in 3.5 days in the presence TMA and Cetyltrimethyl ammonium ions.[57]

G)   Templates act as a void fillers, around which the zeolite structure is formed.

Non-nitrogen containing organic molecules like alcohols,[58-61] ketones,[62] glycerol[63] and cationic polymers[47,64] have also been used as templates in the synthesis of zeolites. Table 1.3 lists some examples of zeolite structures directed by different templates. Use of bis-quartenary ammonium salts[65,66] instead of the conventional mono-quarternary ones has led to the synthesis of some more new zeolites. The mere substitution of alkyl groups can often lead to new structures. Recently, a new zeolite designated as NCL-1[67] was synthesized with a bis

quarternary ammonium salt. Nitrogen containing cyclic compounds (such as, morpholine, pyridine, piperidine and homopiperidine) have also been used as templates.

PSH-3 was first synthesized by Puppe and Weisser using hexamethyleneimine (homopiperidine) as the templating agent in 1984.[68] Later, MCM-22 and SSZ-25, two new molecular sieves,[69,70] believed to be iso-structural with PSH-3, were synthesized by Mobil and Chevron research groups, in 1990 and 1987, respectively, using hexamethyleneimine and N,N,N-trimethyl admantammonium hydroxide as organic templates. Numerous patents have been filed during the last few years claiming the use of MCM-22 in reactions normally carried out over both medium and large pore zeolites.[71-73] It was believed that MCM-22 was a medium pore zeolite,[74] but, Leonowicz et al.[75] have recently unraveled the structure of the zeolite and have claimed that the zeolite possesses both 10 MR channels and 12 MR cages. Later, many research groups[76] have used a variety of reactions to explore the pore topology of MCM-22. We have carried out different acid-catalyzed reactions and have found that MCM-22 behaves more as a wide pore zeolite than as a medium pore one. Rubin[77a] has reported the synthesis of a crystalline material iso-structural with ZSM-12 using hexamethyleneimine as the template. The synthesis of FU-1, a medium pore zeolite was reported by Dewing et al.[77b] It has been found that FU-1 and MCM-22 have a few common XRD lines.[74]

1.4 MODIFICATION OF ZEOLITES

Modification of zeolites could be carried out during hydrothermal synthesis or after the synthesis has been carried out (post-synthesis modifications).

1.4.1 HYDROTHERMAL MODIFICATION OF ZEOLITES

Substitution of Si^{4+} by ions of other bi, tri, tetra and penta- valent elements like Be, B, Ga, In, Ge, Ti, V, Sn, Cr, Fe, Co, W, Zr, Mo and P has been reported. The substitution by transition metal ions has extended the use of zeolites in redox reactions with potential applications in the synthesis of fine chemicals and drugs intermediates.

Barrer[78] has summarized four types of isomorphous substitution possible in a zeolite lattice.

A)   One guest molecule by another.

B)   One cation by another.

C)   An element by its isotope.

D)   One element in a tetrahedral co-ordination (framework element) by another element.

All the four methods of substitutions have been found to be useful in the practical application of zeolites. The fourth method leads to the substitution of one element by another in the zeolite lattice, essentially altering many of the properties of the zeolite. Goldsmith[79] was the first to initiate the substitution of Si^{4+} by Ge^{4+}. This was later followed by the substitution of Al by B, Ga and In. Taramasso et al.[80] in 1980, first reported the hydrothermal synthesis of TS-1, an isomorph of silicalite-1 having titanium ions in lattice. This invention has resulted in a major breakthrough in oxidation catalysis and has spurred the synthesis of other transition metal containing molecular sieves by hydrothermal procedures. Physico-chemical characterization techniques such as XRD, UV-Vis, I.R. and NMR spectroscopies have been used to confirm the isomorphous substitution by metal ions.[81-83] Recently, Castro-Martins et al.[84] have used an electrochemical method (cyclic voltammetry) to confirm the isomorphous substitution of Si by Ti in silicalite-1 lattice.

To date, many metallosilicate molecular sieves possessing catalytic activities have been synthesized. Ione et al.[85] have reported the incorporation of a large number of metal ions in the zeolite lattice. They have claimed that many metals ions can be introduced into the framework of ZSM-5 at very low concentrations.

In 1982, Wilson et al.[86,87] reported the synthesis of a new class of non-zeolite molecular sieves called aluminophosphates ($AlPO_4$).[87] Later, incorporation of metals like Co, Ti, Mn and

13

V into these materials was reported. When Si^{4+} ions were incorporated in the $AlPO_4$ framework, the resulting silicoaluminophosphate (SAPO) acquired ion-exchange capacites and acidic properties. Different metals have also been incorporated in SAPOs to produce metallo-silicoaluminophosphates or **MeAPSO** molecular sieves. These non-zeolitic molecular sieves have been found to exhibit excellent thermal and hydrothermal stability and weak to moderate acidic properties.

A new ultra large pore aluminophosphate containing 18-MR channels, termed VPI-5, was reported by Davis *et al.*[13,14] Estermann *et al.*[15] have reported the synthesis of another ultra large pore gallophosphate molecular sieve with 20 MR pores called cloverite.

1.4.2 POST-SYNTHETIC MODIFICATION OF ZEOLITES

Recently, Be^{2+} has been incorporated in the lattice of ZSM-5, ie., isomorphous substitution of Al^{3+} by Be^{2+}, by post-synthetic treatments, the incorporation being confirmed by Be-NMR spectroscopy.[88] Similarly, Ti was incorporated in the lattice of zeolite beta by post-synthetic treatments, very effectively.[89] Four methods of post-synthetic modifications are possible. These are :

1) Ion-exchange through solution

2) Impregnation

3) Solid-state exchange

4) Chemical vapour deposition

1.4.2.1 Cation exchange

The cations present in the non-framework or exchange positions can be substituted by other cations through ion-exchange. The exchange capacity is large in the case of materials with low Si/Al ratios. Ion Sieve Effect,[6] ie., the penetration of only some types of cations through the channels or cages of the zeolite, is observed in some cases. For example, Rb^+ (radius = 1.48 Å) can be exchanged in analcime but not Cs^+ (radius = 1.65 Å).

The cation-exchange capacity of a zeolite is determined by its chemical composition, the density and nature of the cationic sites present and their distribution. The size of the cation and the exchange temperature also affect the degree of exchange. Ag^+ (radius = 1.26 Å) can exchange all the Na^+ ions including those trapped in the ß cages of zeolite A, whereas, Tl^+ (radius = 1.40 Å) cannot enter the ß cages.[90] The exchange of Na^+ by Li^+ is temperature dependent.[91]

1.4.2.2 Metal loading

Bifunctional catalysts used in hydroconversion reactions are prepared by cation exchange or impregnation techniques. Metallic salts or complexes are generally used. Typically, the metals that catalyze hydrogenation-dehydrogenation reactions such as, Pt, Pd, Ru, Zn, Cu, Ni, Co, Fe, Mo, Cr and W are the components of bifunctional catalysts. Other methods of loading metals over a zeolite support include solid state ion-exchange[92] and chemical vapour deposition.[93]

1.5 ACIDIC AND BASIC PROPERTIES OF ZEOLITES

Zeolites exhibit acid-base properties depending on the presence of extraframework, charge balancing cations.

1.5.1 ACIDITY

The acidity in zeolites is due to the presence of the trivalent metal ion in the framework creating a net negative charge on the framework.[6,7,48] When this charge is balanced by a proton, it imparts Brönsted acidity to the zeolite. The contribution of Brönsted acidity to total acidity is much more than that by Lewis acid centers (originating from the framework aluminum) or other metal ions. Thermal treatment of the protonic zeolites converts many of the Brönsted sites into Lewis acid sites. The H^+ content of the zeolite is related to the framework Al content. Acidity increases with aluminum content, but the strength of the acid sites tends to decrease.

Recently, Farneth et al.[94] have reviewed various methods of determining and measuring the zeolite acidity. They are listed below :[95]

1) I.R. spectroscopy of structural hydroxyl groups and sorbed bases like ammonia, pyridine and pyrrole.

2) Alkane cracking.

3) UV-Vis spectroscopy.

4) Microcalorimetry : adsorption of bases.

5) Temperature Programmed Desorption : desorption of bases.

6) Solid State NMR of OH groups and sorbed bases.

7) ESR spectroscopy.

1.5.2 BASICITY

Acidity and Basicity are corollary properties exhibited by zeolites. Basicity in zeolites may be either due to Lewis or Brönsted centers.[96] Lewis base is the oxygen ion in the framework and the Brönsted base is the basic hydroxyl group. Brönsted basicity is dominated by Lewis basicity and is determined by the extent of charge located on oxygen atoms. Barthomeuf et al.[97] have carried out extensive work on characterizing the basic sites and have shown that the actual basic strength of a zeolite depends not only on the chemical composition, but also on the structural environment of the framework oxygen atoms.

1.6 CHARACTERIZATION OF ZEOLITES

New synthetic materials can be characterized by using various physico-chemical techniques like XRD, electron microscopy, IR, UV-Vis, High resolution solid state NMR, ESCA, ESR, EXAFS, Laser Raman spectroscopic techniques, adsorption of sorbates and through catalytic test reactions. The estimation of pore structure and dimensions through catalytic reactions provides an excellent basis for classification of zeolites under realistic

catalytic conditions. This provides additional support to the inferences obtained from instrumental techniques.

1.6.1 *PHYSICO-CHEMICAL CHARACTERIZATION OF ZEOLITES*

A variety of techniques are used to characterize zeolites, a few of which are discussed in detail in the succeeding sections.

1.6.1.1 X-Ray Diffraction

X-Ray Diffraction (XRD) is a powerful technique used to identify a zeolite,[4,5,98] as each system has its own finger-print diffraction pattern. XRD is used qualitatively to identify the structures and phase purity. In the quantitative sense, it is used to calculate unit cell parameters,[99a] symmetry groups, crystallite size and even chemical composition.[99b] The unit cell parameters are refined using mathematical methods like Rietveld refinements[100] and Distant Least Square (DLS) fitting methods, which are often used for the determination of unknown structures.

When the zeolites are large single crystals, the determination of their structures becomes simple. So far, only a few zeolites have been synthesized as large single crystals.[101-104] Structure determination of zeolites with powder diffraction patterns is more difficult. High resolution electron microscopy (HREM) is sometimes used alongwith XRD techniques for structure determination. Some zeolites whose structures were established recently are VPI-5,[13,14] cloverite,[15] MCM-22,[75] and ETS-10.[105]

1.6.1.2 I.R. Spectroscopy

Infrared spectroscopy was earlier used exhaustively in the identification of organic compounds.[106] Like most organic functional groups, the secondary building units in zeolites have their own finger-print vibrations.[107,108] Flanigen has assigned the I.R. bands of zeolites to the different structure sensitive vibrational modes associated with zeolite lattices.[107] Zeolites exhibit I.R. spectra in the range of 200 - 1350 cm^{-1} and 3500 - 3700 cm^{-1}, bands in the former

17

range being from structure sensitive lattice vibrations and the latter due to zeolitic water and structural hydroxyl groups.[107,108] The typical IR stretching frequencies exhibited by zeolites and their corresponding vibrational modes are given below.

Structure sensitive vibrations or vibrations due to external linkages of the TO₄ units

Asymmetric stretching	1050 - 1150 cm^{-1}
Symmetric stretching	750 - 820 cm^{-1}
Double ring	650 - 500 cm^{-1}
Pore opening	300 - 420 cm^{-1}

Structure insensitive vibrations or internal vibrations of the TO₄ units

Asymmetric stretching	1250 - 950 cm^{-1}
Symmetric stretching	720 - 650 cm^{-1}
T - O bend	500 - 420 cm^{-1}

I.R. spectroscopy has also been used to study the acidity in zeolites using sorption of probe molecules like ammonia, pyrrole and pyridine.[109,110] Information about the extra-framework cations, viz., octahedral aluminum ions,[111] can also obtained from I.R. spectral data.

Confirmation of isomorphous substitution of elements can also be obtained from I.R. studies.[112,113] The incorporation of heavier metal ions such as Ti, P, Ga, Fe, V and Sn into the framework of zeolite lattice shifts the vibrations to lower wavenumbers, whereas, the incorporation of a lighter element such as boron causes a shift towards higher wavenumbers.[114]

I.R. spectroscopy can be used to identify the SBUs in zeolites (see Figure 1.1).[115-117] ZSM-5 and ZSM-11 exhibit a band around 550 cm^{-1}, characteristic of pentasil zeolites, and is attributed to structure sensitive modes caused by D5R blocks of type 5-3 and 5-5 rings. Similarly, an absorption band around 560 cm^{-1} exhibited by mordenite is attributed to pentasil rings of type 5-3.[116, 117]

Flanigen and Ward have discussed the framework and hydroxyl I.R. bands of zeolites.[107,108] Acidity of zeolites (Lewis and Brönsted sites) can be studied both qualitatively and quantitatively by I.R. spectroscopic methods using the characteristic bands in the region 3500 - 3700 cm^{-1}.[118] Zeolitic water and structural hydroxyl groups also exhibit bands in the same region.

1.6.1.3 Nuclear Magnetic Resonance Spectroscopy
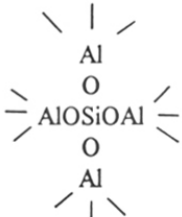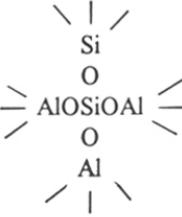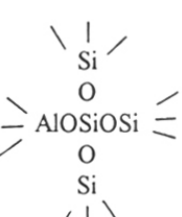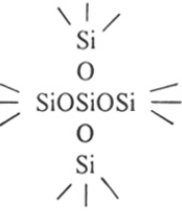
Solid State NMR has emerged as a powerful technique to characterize zeolites. Its applications have increased after the discovery of the "**Magic Angle Spinning (MAS)**" technique. High resolution NMR of zeolite samples yields useful and valuable information about the nature of the atoms and the environment of the corresponding nuclei. 2D NMR studies of zeolites yield greater information on the nature of sites and their exact environment. A lattice walk could be performed which gives the relative densities of the species and their environments.

Lippmaa et al.[119] were the first to initiate the study of silicate species in zeolites by NMR. Later on, Nagy et al.[120] have used NMR to study zeolites containing different nuclei (isomorphous substitutions). NMR studies are also useful to crystallographers to arrive at unknown structures. It has become a complimentary technique to XRD and HREM.

In low silica zeolites, the presence of large amounts of aluminum affects the Si-signals considerably. Engelhardt et al.[121] have identified 5 major types of silicate species in the first co-ordination sphere of silicon atoms. The range of signals originating from silicate species extend from $\delta = -90$ ppm to -125 ppm (with respect to tetramethyl silane).[121] The presence of an aluminum ion in the first co-ordination sphere shifts the ^{29}Si signals to the low field by about 5 ppm. The different silicate species and their corresponding chemical shift regions are presented in Table 1.4.

The intensities of the different ^{29}Si MAS NMR spectral lines of zeolites are directly related to the amounts of the non-repeating, crystallographically non-equivalent distinct T

Table 1.4   Types of silicate species, "Q" notation and their corresponding chemical shift ranges.[121]

"Q" notation	Silicate species	Chemical shift range (ppm)
Q^4 (4 Al)	Al–O–AlOSiOAl–O–Al	– 80 to – 93
Q^4 (3 Al)	Si–O–AlOSiOAl–O–Al	– 85 to – 95
Q^4 (2 Al)	Si–O–AlOSiOSi–O–Al	– 93 to – 100
Q^4 (1 Al)	Si–O–AlOSiOSi–O–Si	– 97 to – 107
Q^4 (0 Al)	Si–O–SiOSiOSi–O–Si	– 101 to – 117

sites.[122] Thus, based on the number of such distinct T sites and their relative occupancies in the framework, framework Si/Al ratios can be estimated from NMR spectra.[123]

^{27}Al MAS NMR of zeolites is mainly used to study the co-ordination of aluminum atoms.[122] Tetrahedral and octahedral aluminum species are characterized by the presence of signals at 45 - 55 ppm and 0 - 5 ppm, respectively, with reference to $[Al(H_2O)_6]^{3+}$.[121]

Fyfe et al.[124-127] have conducted 2D NMR experiments and have determined T-O-T connectivities in highly siliceous zeolites. T-O and T-O-T bond lengths and bond angles and T-O-T-O dihedral angles of ZSM-5[124] and ZSM-11[125] have been calculated using 2D NMR experiments. Spectral correlation with Si-O-T bond angles and Si-O bond lengths have also been obtained.[128,129]

Klinowski[130] has used NMR techniques to follow the course of the reaction and to identify the intermediates in the transformation of methanol to hydrocarbons over ZSM-5. Kumar et al.[131] have carried out ^{13}C MAS NMR and ^1H - ^{13}C cross-polarization experiments to locate the organic templates inside the zeolite channels and their interaction with the lattice. NMR studies of other nuclei such as Be, Ti, Sn, Ga, Fe, V and B are also known. Study of extra-framework cations has also been carried out using NMR techniques.[132]

High Resolution NMR studies of liquid samples have been used to follow the course of crystallization of zeolites. These studies have led to the identification of intermediate species of aluminum and silicon species resulting in newer insights in understanding zeolite structure formation.[133]

1.6.2 ADSORPTION PHENOMENON IN ZEOLITES

Zeolites are crystalline aluminosilicates having a regularity in the internal pore system. They have well defined and uniform channels. Adsorption takes place mainly in the intra-crystalline voids, which contribute to nearly 99 % of the total surface area. The walls of the channels are the origins of the internal surface area. Zeolites possess high surface area of

several hundred square metres per gram, thus providing a large surface for adsorption and reaction to occur. Zeolites are also used as selective adsorbents due to their high sorption capacity[4] and their ability to separate molecules based upon size and orientation with respect to the size of the pores in them.

1.6.2.1 Diffusion in Zeolites

Heterogeneous catalysis is a surface phenomenon.[134] The reactants diffuse into pores where the active sites are located, undergo reaction and the products diffuse out through the pores. The diffusion of both reactants and products takes place through the minute channels. During the process of diffusion through a pore, the chemical potential decreases along the direction of diffusion.

There are three types of diffusion phenomena that could possibly take place in zeolite catalysts. They are briefly summarized below :

1.   Ordinary or bulk diffusion : Ordinary or bulk diffusion is encountered, for example in a system containing large pores or at high pressures when the mean free path of the reactants is negligibly small when compared to the diameter of the pores or inter-particle voids. This diffusion phenomena often determines the rate at which the reactant reaches the external surface of the microporous catalyst (zeolite) particles or the rate at which the products diffuse from the surface of the catalyst into the bulk (gas).

2.   Knudsen diffusion : This type of diffusion process is encountered typically inside the pores of diameter comparable to the mean free path of the reactant or product under consideration. When a gas diffuses through the pores, it often collides with the walls (of channels) leading to momentary adsorption and desorption. When the concentration of the gas is low, the frequency of colliding with walls is more than the frequency of two molecules colliding with each other. The momentary adsorption and desorption leading to slow diffusion through the pores is termed as Knudsen diffusion. Typically one would encounter this type of

22

diffusion inside the pores of binder materials used in the formulation of catalysts from zeolite srystallites.

3.   Configurational diffusion[135] : This type of diffusion occurs when the diameter of the pores approaches the dimensions of the molecules. Diffusion is extremely slow and the diffusion rate is highly susceptible to even minor changes (of a fraction an Å) in the pore or molecular dimensions. Configurational diffusion is most commonly encountered in zeolites whose pore dimensions are very similar to the dimensions of the reactant molecules.

1.6.2.2 Sorption in zeolites

Many theories such as those by Langmuir, Brunauer, Emmett and Teller (BET), Dubinin and Freundlich have been put forth to explain the different types of adsorption isotherms. The more common isotherm equations and their assumptions are listed in Table 1.5. Each theory has its own assumptions and restrictions to be applied realistically. From these equations, surface area, pore volume, isosteric heats and chemical potential of sorption process could be calculated. Some of these theories have been applied in the present study for characterizing the zeolite through sorption of ammonia.

1.7 CATALYTIC PROPERTIES

Nowadays, zeolites are replacing conventional acid catalysts such as concentrated sulfuric acid and hydrofluoric acid, which are environmentally unsafe and hazardous. The main advantages of the use of zeolites as catalysts are as follows :

⇒   They are environment friendly.

⇒   Highly stable (both thermal and hydrothermal).

⇒   Porous and exhibit shape selective properties.

⇒   Easy to regenerate and reuse.

⇒   Non toxic and non-hazardous.

⇒   Cheap and easily available.

Table 1.5   Isotherm equations and their assumptions.

TYPE	Equation	Assumption
Langmuir	$\dfrac{P}{V} = \dfrac{P}{V_m} + \dfrac{1}{bV_m}$	Monolayer Adsorption
BET	$\dfrac{(P/P_o)}{V(1 - P/P_o)} = \dfrac{1}{CV_m} + \left(\dfrac{P}{P_o} \times \dfrac{(C-1)}{CV_m}\right)$	Multilayer Adsorption
Freundlich	$q_{ads} = [\ln(k)].q_o - q_o \ln(\theta)$	Similar to Langmuir's Model.
Dubinin	$\log(W) = \log(W_o) - \left(\dfrac{B}{2.303\,\beta^2} \times [T.\log(P/P_o)]^2\right)$	Pore Filling Theory

⇒   Exhibit ion-exchange properties facilitating the preparation of bifunctional catalysts.

⇒   Properties could be tailored by isomorphous substitution of framework elements.

However, they suffer from the disadvantages of faster deactivation due to irreversible adsorption of heavier molecules. The above disadvantage, however, is easily overcome by regenerative procedures. Some examples of the application of zeolites as industrial catalysts are listed in Table 1.6.

1.7.1 SHAPE SELECTIVITY IN ZEOLITES

Shape selectivity is the combination of sieving property of a zeolite operating when a catalytic reaction is carried out over it.

Weisz and Frillete[136] identified shape selectivity exhibited by zeolites. Later, Csicsery,[137,138] Chen et al.[139] and Miale et al.[140] have published in detail on shape selective catalysis by zeolites. Atleast three types of shape selectivity are reported to exist. Derouane et al.[141] have proposed an additional type, termed as "Molecular Traffic Control". Figure 1.2 depicts the three important types of shape selectivities exhibited by zeolites.

1.7.1.1 Reactant Shape Selectivity

Out of a mixture of reactants of all shapes and sizes, the ability of zeolite pores to discriminate the bulkier reactants, preventing their entry is termed as Reactant Shape Selectivity (RSS), Figure 1.2 (A). Thus, bulkier reactants do not reach the active sites and do not react. At best, they undergo reaction on the surface. Competitive cracking of n- and iso- paraffins over ZSM-5 is a good example. Entry of the linear alkane is favorable and leads to products whereas those from the iso-paraffins are absent.[136-138]

1.7.1.2 Product Shape Selectivity

The reactants are sufficiently small enough to diffuse into the pores and lead to products. Among the products formed, only one or a few them are sufficiently small to diffuse out of the pores. Eventhough, the other products may be formed inside the pores in major amounts, they

Table 1.6   Industrially important zeolite based catalytic reactions.

Process	Use	Process	Use
MTG	Methanol to Gasoline	Xylene isomerization	Production of p-xylene.
MDDW	Dewaxing of Middle Distillates	Toluene Disproportionation	Production of xylenes
LDW	Dewaxing of Lube oils	Alkylation of toluene	Production of xylenes.
MOGD	Methanol to light olefins and middle distillates.	Hydroxylation of Phenol	Production of catechol and hydroquinone.
Alkylation of benzene	Production of ethyl benzene and cumene	F.C.C.	Cracking of heavy oils.
Isomerization	Isomerization of light naphtha.	Hydrocracking	Hydrocracking of heavy oils.
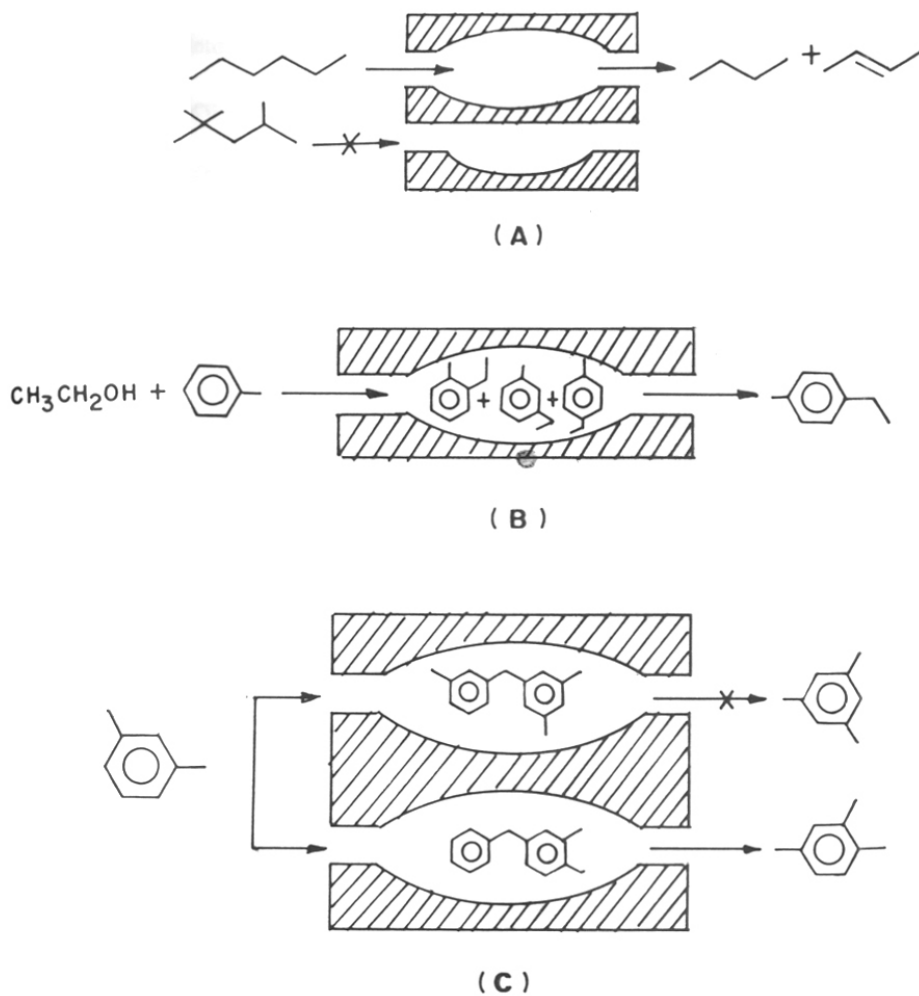
Figure 1.2   Different types of Shape selectivities encountered inside zeolite pores.[136-138]
        (A) :   Reactant shape selectivity [RTSS] RSS
        (B) :   Product shape selectivity   [PSS]
        (C) :   Restricted transition state shape selectivity [RTSS]

are not detected in the reaction products. They are formed in the intersections or cages and are too bulky to diffuse out through the pores which have smaller dimensions than the cages. Thus, they are trapped inside the cages and finally crack into smaller molecules and come out or get converted into coke deposits which lead to the deactivation of the catalysts, (Figure 1.2(B)). In the ethylation of toluene, among all the three isomers formed, p-ethyl toluene is the smallest isomer and o-ethyl toluene is the bulkiest one. Over medium pore zeolites, the product stream is found to contain mostly the p-isomer.[142] Thus, the formation of high diffusivity products is favored in systems exhibiting product shape selectivity (PSS).

1.7.1.3 Restricted Transition State Shape Selectivity (RTSS)

In this case, both the reactants and products diffuse easily out of the pores. This type of shape-selectivity is observed when restriction or hindrance is posed by the zeolite channels in the formation of the transition states, (Figure 1.2 (C)). A bulkier transition state is more hindered and its formation is suppressed, whereby the products formed from that transition state is absent. Thus, other products formed from the less bulky transition states are observed. In a system with enough room to accommodate all types of transition states, no selectivity would be observed and the products will be in equilibrium concentrations. RTSS is due to the intrinsic chemical effects emerging from the limited space around the intracrystalline active sites. It has been found that there is no dependence on intra-crystalline diffusion path. The best example is the isomerization-disproportionation of m-xylene. It has been found that in medium pore zeolites, a combination of both PSS and RTSS exists, whereas, in large pore zeolites, only PSS was found to operate.[137]

1.7.1.4 Molecular Traffic Control

A new type of shape selectivity called Molecular Traffic Control was coined by Derouane et al.[141] They have proposed that this operates in systems with inter-connecting channels of different diameters. According to this concept, reactants diffuse through one set of

pore system, while the products diffuse out through the other, the reaction occurring in the intersection of channels or cages minimizing the counter diffusion. But it has not received much attention due to lack of experimental support.

1.7.2 CATALYTIC TEST REACTIONS

Test reactions are carried out for characterizing the pore width of molecular sieves with unknown structures.[143] They are first carried out over catalysts with known pore topology and dimensions and the results obtained are compared with that obtained over unknown materials. Always, a single test reaction is insufficient to gauge the pore topology. Thus, a series of reactions have to be carried out to draw the final conclusions. Martens *et al.*[143] have estimated the void structure of zeolites by test reactions. Some of the criteria, a good test reaction should satisfy are listed below :[143, 144]

⇒ Reaction should be carried out under non-deactivating conditions (use of bifunctional catalysts is preferred).

⇒ The disappearance of the reactants should preferably not be diffusion controlled.

⇒ Systems with wide range of pore sizes and structures should be chosen (as standards).

⇒ The reaction mechanism of the test-reaction should be well established.

⇒ Results obtained should be from independent sets choosing different feeds; reactions should be carried out at different conversion levels to account for the formation of minor products.

⇒ Simple experimental setup encompassing a continuous flow reactor with GC.

⇒ Maximum information should be gained through the reaction.

Some of the test reactions are discussed in detail in the following sections.

1.7.2.1 Constraint Index (CI)

Branched alkanes crack at a faster rate than their unbranched counterparts. A reverse trend was observed in the rate of cracking over ZSM-5 catalysts. This led to the pursuit or research in this area by the Mobil research group. They have coined the term "Constraint Index (CI)" to quantify the pore-size characteristics of zeolites. CI[145] is the ratio of the first order rate constants of the competitive cracking of n-hexane and 3-methyl pentane obtained using a feed containing equal amounts of the two compounds.

$$CI = \frac{Log(1 - X_{n-Hex})}{Log(1 - X_{3-MP})}$$

where, X_{n-Hex} and X_{3-MP} denote the conversion of n-hexane and 3-methyl pentane, respectively. It has been found that as the numerical value of CI increases, pore width decreases. Typical values of CI are :[142]

CI < 1	$\Rightarrow$	Large pore molecular sieves.
1 < CI < 12	$\Rightarrow$	Medium pore molecular sieves.
CI > 12	$\Rightarrow$	Small pore molecular sieves.

Haag et al.[146] have studied the mechanism of cracking over zeolites and the parameters that influence the product selectivities. They have found that the rate controlling step in the complex chain reactions via carbocations is the chain propagating hydride transfer step between a cracked carbenium ion and a feed molecule and this hydride transfer proceeds via a bimolecular transition state. Thus, in effect, RTSS operates rather than RSS or PSS. These observations have been confirmed by others.[147,148]

This test reaction has some disadvantages. **Frilette** et al.[145] have found that the reaction is temperature dependent. For large pore zeolites, the range is very small (0.4 in the case of X and Y to 1.0 in the case of mordenite). It is very difficult to gauge large pores within the small range of CI. Also, the large pore zeolites deactivate faster.[149,150] Thus, it is difficult to carry

out this test reaction under non-deactivating conditions, thereby limiting its usefulness in testing large pore materials.

1.7.2.2 m-Xylene Isomerization

Isomerization of m-xylene is useful as a test reaction[151] as the selectivity of the ortho- and para- isomers are dependent on the pore width of the zeolites. RTSS enables this reaction to be used as a test reaction for the estimation of pore width of zeolites. Corma et al.[152] have proposed a bimolecular pathway for the isomerization of m-Xylene. It was Gnep et al.[153] who first proposed the use of this reaction as a test reaction. The following three factors could yield vital information about the pore architecture of the zeolite.

1. The relative rates of formation of o- and p- isomers.

2. Ratio of isomerization to disproportionation.

3. Distribution of trimethyl benzene isomers.

From para/ortho ratio, one could know to which class of pore system a zeolite belongs to:

p-/o- Xylene = 1 - 1.1   ⇒ Large pore molecular sieves. Here RTSS is absent, so
equilibrium distribution of isomers.

p-/o- Xylene = 1.5 - 2 ⇒ Medium pore molecular sieves. In this case RTSS operates in
addition to PSS. So more formation of p- isomer.

Martens et al.[154] have correlated the pore topology with respect to the distribution of trimethyl benzenes (from the disproportionation of xylenes) by analyzing the space requirements for the formation of the different bulky (diphenyl methane type) transition states.

Dewing applied Thiele's equations[155] and arrived at a ratio of rate constants of o- and p- xylenes under conditions of diffusional limitations and has called the ratio as the 'R' value. It is dependent on the ratio of the diffusion co-efficients of o- and p- xylenes inside the pores. Joensen et al.[156] have subsequently formulated the "Shape Selective Index (SSI)" to quantify

31

the shape-selective characteristics of zeolites. It is defined as the molar ratio of o- and p-xylenes in the product observed under shape selective conditions minus the above ratio obtained under identical experimental conditions over a large pore molecular sieve, ie., under non-shape selective conditions.

1.7.2.3 Ethyl Benzene Disproportionation

Disproportionation of ethyl benzene was first proposed by Karge et al.[157] as a test reaction to characterize the pore widths of zeolites. The mechanism involved the formation of diphenyl methane type of transition states. Various criteria have been proposed based on the ratio of yields of diethylbenzene and benzene and the distribution of diethyl benzene isomers. Medium and large pore zeolites were discriminated based on the yields of the diethyl benzene isomers and benzene. The ratio of diethylbenzene to benzene in the case of the large pore zeolite, Y, was found to be 0.9, whereas, in the medium pore zeolite, the observed ratio was less than unity (ZSM-5, the ratio was 0.75). The observations or the criteria are listed below :[157]

1. Large pore molecular sieves exhibit an induction period whereas the medium pore zeolites do not.

2. After the induction period, there is negligible deactivation over zeolites possessing 12 MR, whereas, the zeolites with 10 MR deactivate from the beginning.

3. In large pore zeolites, all isomers are present, whereas, in medium pore zeolites, the bulkiest isomer, the ortho product is absent.

1.7.2.4 Refined Constraint Index (CI*)

Martens et al.[143] have proposed another criterion called the Refined Constraint Index (CI*) based on the hydrocracking of n-decane. It is the ratio of yields of 2-methyl nonane to 5-methyl nonane at a total isomer yield of 5 %.

$$CI^* = \frac{Y_{2-M-N}}{Y_{5-M-N}} \quad \text{at } Y_{isomers} \simeq 5\%.$$

where, Y_{2-M-N}, Y_{5-M-N} and Y_{iso} denote the yields of 2-methyl nonane, 5-methyl nonane and total yield of decane isomers, respectively. The CI* observed over 10 MR and 12 MR molecular sieves are presented in Figure 1.3 (A). The yields of 4-propyl heptane and total mono-branched iso-decanes over large pore molecular sieves are presented in Figure 1.3(B).

The CI* of zeolite Y and ZSM-5 are 1.0 and 4.5, respectively. CI* increases with decreasing pore width. 10 MR zeolites exhibit a broad range of 2.3 - 15.0, whereas for large pore molecular sieves, the range is 1 - 2.3. It was found that crystallite size differences did not influence product selectivities.[158]

1.7.2.5 Spaciousness Index (SI)

C_{10}-naphthenes are used as the probe molecules.[159,160] SI is defined as a ratio of isobutane and n-butane found in the product during the hydrocracking of butyl cyclohexane over bifunctional catalysts.[161] It is mainly used to characterize large pore molecular sieves.

The ratio of iso-butane to n-butane was found to increase with increase in pore width. SI for medium pore zeolites is unity, whereas for the large pore molecular sieves, it has a broad range extending from 3 (for ZSM-12) to 20 (for FAU) thereby making it a useful index for characterizing large pore zeolites. Butyl cyclohexane is preferred over other naphthenes due to its low cost, lack of mass transfer limitations and analytical simplicity. Figure 1.3(C) shows the ordering of zeolites based on SI.

1.7.3   SYNTHESIS OF FINE CHEMICALS AND DRUG INTERMEDIATES

This field has gained attention due to the interesting properties exhibited by zeolites. A variety of reactions such as alkylation, acylation, cyclization, isomerization and cracking have been carried out over zeolites. Dartt and Davis[162] have reviewed the use of zeolites in the synthesis of fine chemicals and Sugi and Toba[163] have discussed the use of zeolites in shape selective alkylation of polynuclear aromatics.
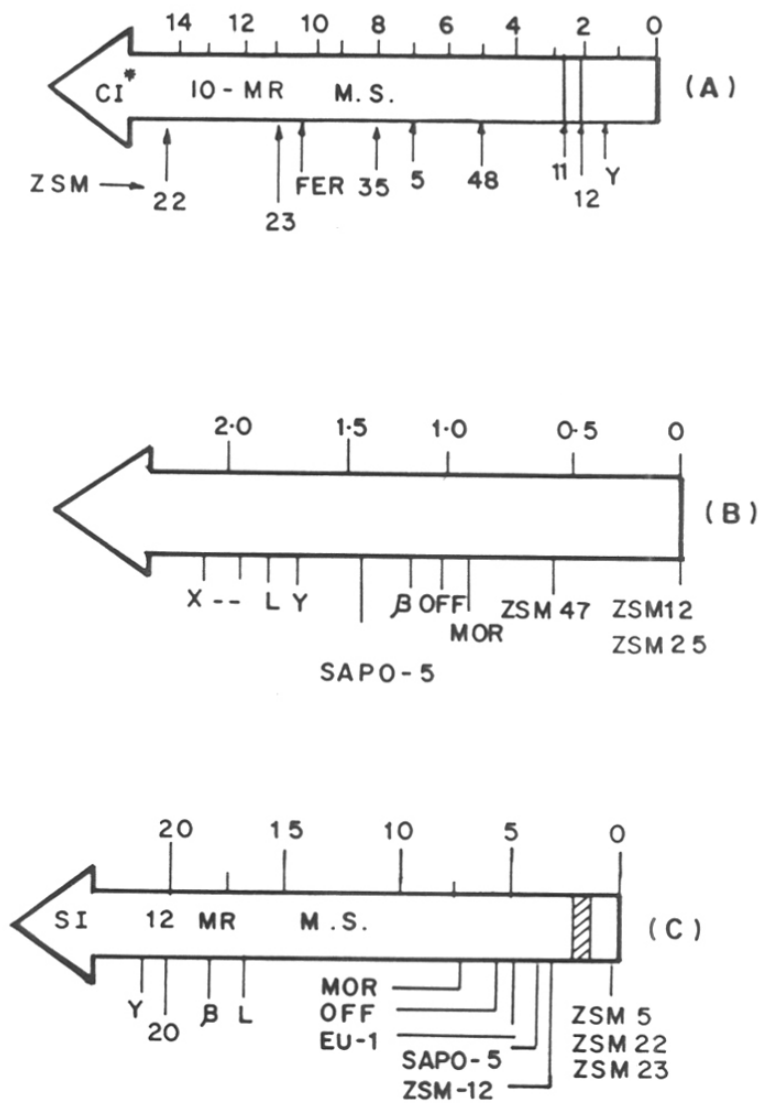
Figure 1.3   Ranking of zeolites based on catalytic test reactions.[143,144]
                (A)   Refined Constraint Index for various zeolites.
                (B)   Yield of 4-propyl heptane and total mono-branched iso-
                        decanes over 12 MR molecular sieves.
                (C)   Spaciousness Index for various zeolites.

34

Isomorphous substitution of Si by transition elements has enabled the applications of zeolite molecular sieves as oxidation catalysts. titanium, vanadium and stanno- silicates have led to major breakthroughs in oxidative catalysis (Table 1.7). Many of the selective oxidation reactions catalyzed by these metallosilicates are difficult to carry out by normal organic synthesis routes.

1.8 ULTRA LARGE PORE MOLECULAR SIEVES

In late 1960s and early 1970s, extensive research was carried out to synthesize materials exhibiting shape selective properties. During 1980s, there was a change in the trend, and the synthesis of new large pore zeolites became the major interest. The synthesis of zeolite beta, a large pore zeolite by Wadlinger et al.[20] led to the synthesis of new materials like ZSM-12 (MTW) and $AlPO_4$-8 (AET). Recently, non-zeolitic large pore molecular sieves such as, VPI-5, cloverite and JDF-20 have been synthesized. The barrier to the synthesis of large and ultra large pore molecular sieves containing pore openings constituted by rings larger than 12 was first overcome by Davis et al.[13,14] in the synthesis of VPI-5 (18 MR with 13 Å pore opening). Cloverite is a gallophosphate molecular sieve[15] with 20-MR pore openings (super cage diameter; 29 Å - 30 Å), the largest pore diameter exhibited by the molecular sieve, while JDF-20 is a 20 MR aluminophosphate molecular sieve with uni-dimensional 20 MR elliptical shaped openings. A mesoporous layered silica polymorph, MCM-41,[166,167] was found to possess pores in the range of 16 Å - 100 Å.

1.9 PORE ARCHITECTURE

The definition of a large pore molecular sieve is based on the accessibility of the pores through the largest member ring system available in the zeolite.[168] The rings that help in the formation of cages are not considered. For example, mordenite has a 12 MR pore system and is called a large pore zeolite while, zeolite A has 8 MR pores and is called a small pore zeolite,

Table 1.7   Some examples of selective oxidation reactions over metallosilicate molecular sieves. [164,165]

Catalyst	Reactants	Products
TS-1 and other titanosilicates	Benzene. Phenol. Carbonyl compounds. Oxime. Olefins. Sulfur compounds. Allyl alcohol. Toluene Aromatic Primary amine n-Alkanes.	Phenol. Catechol and hydroquinone. Oxime. Lactam. Epoxides and diols. Sulfoxides and Sulfones. Propylene oxide Cresols. Azoxy benzene. Alcohols and ketones.
VS-1 and other vanadosilicates	Toluene. Allyl alcohol. Aromatic Primary amine. n-Alkanes.	1° carbon (side chain) oxidation. Acrolein. Nitroso benzene. Alcohols, aldehyde and ketones.
Stannosilicates	Similar to vanadosilicates.	

eventhough, the latter has large cancrinite cages which leads to a larger void volume than mordenite. It has been found that the zeolites with 12 MR have a minimum pore diameter of 6 Å - 7 Å. Higgins[168] has plotted the maximum pore diameter vs minimum pore diameter of the three types of zeolites. He has found that the large pore molecular sieves have nearly equal maximum and minimum pore diameters, whereas, it is not so in the case of zeolites possessing 10 MR. He has attributed it to the presence of higher symmetry (6-fold, 4-fold and 3-fold rotation axes) in the 12 MR zeolites, whereas, a lower symmetry (2-fold rotation axis and mirror planes) is associated with 10 MR zeolites. Pores constituted by 12 MR were found to be more symmetric than those constituted by 10 MR. Higgins[168] has discussed in detail how different ring connectivities lead to different pore systems in zeolites (Table 1.8).

Table 1.8 : Pore topology of large pore molecular sieves.[168]

Type of channel/pores	Connectivity	Examples	Ring constituting the large pore
1 Dimensional tubular pores	Framework connected by 4 & 6 rings.	VFI AET AFI, ATS, CAN	18 MR 14 MR 12 MR
Linear 12 - ring channels	Adjacent 1-D channel is interconnected through 7 & 8 rings apertures in the 12 MR pore wall.	GME, OFF, MOR LTL MAZ, MEI	12 MR, Smooth 12 MR, Sinusoidal stepped lodges and pockets.
Partially intersecting channels	2 Channels intersect perpendicularly giving a 3rd dimension.	BEA BOG, NU-87 and SSZ-26	Two 12 MR intersect. 10 & 12 MR intersect.
Cage structure	Cages are formed by the intersection of 12 MR	FAU, EMT and Cloverite	Possess large void volume.

1.10 REFERENCES

1. (a) McBain, J. W., "The Sorption of Gases and Vapours by Solids", George Rutledge and Sons, London, (1932).

    (b) Cronsted, A. F., *Adak. Handl.* Stockholm, **17**, 120 (1756).

2. Breck, D. W., *J. Chem. Edn.* **41**, 41`(1969).

3. Lowenstein, W., *Am. Minerals.* **39**, 92 (1954).

4. Meier, W. M., and Olson, D. H., "Atlas of Zeolite Structures", Butterworth, London, (1987).

5. Liebau, F., "Structural Chemistry of Silicates: Structure, Bonding and Classification", Springer-Verlag Series, Berlin, (1985).

6. Breck, D. W., "Zeolite Molecular Sieve Structure, Chemistry and Use", Wiley, London (1974).

7. Barrer, R. M., "Hydrothermal Chemistry of Zeolites", London, Academic Press, (1982).

8. Bragg, W. L., "The Atomic Sructure of Minerals", Cornell University Press, Ithaca, New York, (1937).

9. Meier, W. M., "Molecular Sieves", Soc. of Chem. Ind., London, (1968) 10.

10. Flanigen, E. M., "Proceedings of 5th Intern. Conf. on Zeolites", (Rees, L. V. C., Ed.), Naples, Italy, June 2-6, (1980) 760.

11. Sand, L. B., *Econ. Geol.* 191 (1967).

12. Barrer, R. M., "Zeolites and Clay Minerals as Sorbents and Molecular Sieves", Academic Press, New York, London, Ch.2 (1978).

13. Davis, M. E., Saldarriaga, C., Montes, C., Graces, J., and Crowder, C., *Nature.* **331**, 968 (1988).

14. Davis, M. E., Saldarriaga, C., Montes, C., Graces, J., and Crowder, C., *Zeolites.* **8**, 362 (1988).

15. Estermann, M., McCusker, L. B., Baerlocher, Ch., Merrouche, A., and Kessler, H., *Nature.* **352**, 320 (1991).

16. Huo, Q., Xu, R., Li, S., Mu, Z., Thomas, J. M., Jones, R. H., Chippindale, A. M., *J. Chem. Soc. Chem. Commun.* 875 (1992).

17. Kresge, C. T., Leonowicz, M. E., Roth, W. J., and Wartuli, J. C., US Pat. 5,102,643 (1992).

18. Kresge, C. T., Leonowicz, M. E., Roth, W. J., Wartuli, J. C., and Beck, J. S., *Nature.* **359**, 710 (1992).

19. Smith, J. V., Pluth, J. J., Boggs, R. C., and Howard, D. G., *J. Chem. Soc. Chem. Commun.* 363 (1991).

20. Wadlinger, R. L., Kerr, G. T., and Rosinski, E. J., US Pat. 3,308,069 (1967).

21. Treacy, M. M. J., and Newsam, J. M., *Nature.* **332**, 249 (1988).

22. Newsam, J. M., Treacy, M. M. J., Koetsier, W. T., and de Gruyter, C. B., *Proc. Roy, Soc.* London, **A420**, 375 (1988).

23. Higgins, J. B., LaPierre, R. B., Schlender, J. L., Rohrmann, A. C., Wood, J. D., Kerr, G. T., and Rohrbaugh, W. J., *Zeolites.* **8**, 446 (1988).

24. (a) Pluth, J. J., and Smith, J. V., *Am. Minerals.* **75**, 501 (1990).

    (b) Shannon, H. D., *Nature.* **353**, 417 (1991).

    (c) Zones, S. I., Santilli, D. S., Ziemer, J. N., Holtermann, D. L., Pecoraro, T. A., and Innes, R. A., WO 89/109185 (1989) and US Patent. No. 4,910,006 (1990).

25. Breck, D. W., Eeversole, W. G., Milton, R. M., Reed, T. B., and Titomas, T. L., *J. Am. Chem. Soc.* **78**, 5964 (1956).

26. Milton, R. M., US Pat. 2,282,244 (1959).

27. Breck, D. W., US Pat. 3,130,007 (1964).

28. Barrer, R. M., "Molecular Sieves", Society of Chemical Industry, London, p.39 (1968).

29. Barrer, R. M., and Denny, P. J., *J. Chem. Soc.* 971 (1961).

30. Alleilo, R., and Barrer, R. M., *J. Chem. Soc. A.* 1470 (1972).

31. Barrer, R. M., and Mainwaring, D. M., *J. Chem. Soc. A.* 254 (1972).

32. Kerr, G. T., US Pat. 3,247,195 (1966).

33. Kerr, G. T., *Science.* **140**, 1412 (1963).

34. Kerr, G. T., *Inorg. Chem.* **5**, 1539 (1966).

35. Kerr, G. T., US Pat. 3,459,676 (1969).

36. Kerr, G. T., *Inorg. Chem.* **5**, 1537 (1966).

37. Kerr, G. T., and Kokotailo, G. T., *J. Am. Chem. Soc.* **83**, 4675 (1967).

38. Kokotailo, G. T., and Sawruk, S., US Pat. 4,187,283 (1962).

39. Frilette, V. J., Weisz, P. B., and Golden, R. J., *J. Catal.* **1**, 301 (1962).

40. Chen, N. Y., and Degnan, D. F., *Chem. Eng. Progr.* **48(2)**, 32 (1988).

41. Inui, T., and Okazumi, F., *J. Catal.* **90**, 366 (1984).

42. Ono, Y., *Catal. Rev. Sci. Eng.* **34**, 179 (1992).

43. Lukyanov, D. B., Shtral, V. I., and Khadzhiev, S. N., *J. Catal.* **146**, 87 (1944).

44. Flanigen, E. M., and Kellberg, E. B., US Pat. 4,241,036 (1968).

45. Barrer, R. M., Denny, P. J., and Flanigen, E. M., US Pat. 3,306,922 (1967).

46. Baerlochere, C., and Meier, W. M., *Helv. Chem. Acta.* **52**, 1853 (1969).

47. Daniels, R. H., Kerr, G. T., and Rollmann, L .D., *J. Am. Chem. Soc.* **100**, 3097 (1978).

48. Szostak, R., "Molecular Sieves, Principles of Synthesis and Identification", Von Nostrand Reinhold Catalysis Series, New York, (1989).

49. Lok, B. M., Cannan, T. R., and Messina, C. A., *Zeolites.* **3**, 282 (1983).

50. Argauer, R. J., and Landolt, G. R., US Pat. 3,702,886 (1972).

51. Nastro, A., Colella, C., and Aiello, R., "Zeolites: Synthesis, Structure Technology and Applications", Orjaz, B., *et al.* (Eds.), Elsevier, Amsterdam, (1985) p.39.

52. US Pat. 257,885 (1981).

53. Bragin, O. V., Vasina, T. V., Isakova, Y. I., Palishina, N. V., Probrazhensky, A. V., Nefedov, B. K., and Minachev, K H. M.,"Structure and Reactivity of Modified Zeolites", Jacobs, P. A., *et al.* (Eds.), Elsevier, Amsterdam, (1984) p.273.

54. Price, G. D., Pluth, J. J., Smith, J. V., Bennett, J. M., and Patton, R. L., *J. Am. Chem. Soc.* **104**, 5971 (1982).

55. Bennett, J. M., Cohem, J. P., Flanigen, E. M., Pluth, J. J., and Smith, J. V., *ACS Symp. Ser.* **218**, 109 (1983).

56. (a) Kuznicki, S. M., US Pat. 4,853,202 (1989).
    (b) Kuznicki, S. M., US Pat. 4,938,939 (1990).

57. Tapan Kr. Das, Chandwadkar, A. J., Budhkar, A. P., Belhekar, A. A., and Sivasanker, S., *Microporous Materials.* **4**, 195 (1995).

58. Whittam, T. V., Eur. Pat. Appl. 0,054,386 (1982).

59. Planck, C. J., Rosinski, E. J., and Rubin, M. K., US Pat. 4,175,114 (1978).

60. Post, M. F. M., and Manne, J. M., UK Pat. Appln. 2018232 (1979).

61. Araya, A., and Lowe, B. M., *Zeolites.* **6**, 111 (1986).

62. Kaduk, J. A., US Pat. 4,323,481 (1982).

63. (a) Taramasso, M., Perego, G., and Notari, B., Fr. Pat. 2,478,063 (1981).
    (b) Onodera, T., Sakai, T., Yamasaki, Y., and Sumitani, K., US Pat. 4,320,242 (1982).

64. Davis, M. E., and Saldarriagga, C., *J. Chem. Soc. Chem. Commun.* 920 (1988).

65. Szostak, R., US Pat. 4,585,639 (1986).

66. EP Pat. Appln. 174,121 (1986).

67. Kumar, R., Ramesh Reddy, K., and Ratnasamy, P., US Pat. 07/816,211 (1991).

68. Puppe, L., and Weisser, J., US Patent No. 4,439,409 (1984).

69. Rubin, M. K., and Chu, P., US Pat. 4,954,325 (1990).

70. Zones, S. I., Eur. Pat. Appl. EP 231 019 (1987).

71. Absil, R. P. L., Han, S., Marler, D. O., and Shihabi, D. S., US Patent No. 4,962,257 (1990).

72. Chu, C. T. W., Degnan, T. F., and Huh, B. K., US Patent No. 4,982,033 (1991).

73. Kirker, G. W., Mirzahi, S., and Shih, S. S., US Patent No. 5,000,839 (1991).

74. Jacobs, P. A., and Martens, J. A., *Stud. Surf. Sci. Catal.* **33**, 362 (1987).

75. Leonowicz, M. E., Lawton, J. A., Lawton, S. L., and Rubin, M. K., *Science.* **264**, 1910 (1994).

76. (a) Ravishankar, R., Sen, T., Ramaswamy, V., Soni, H. S., Ganapathy, S., and Sivasanker, S., *Stud. Surf. Sci. Catal.* **84(A)**, 331 (1994).

    (b) Corma, A., Corell, C., Martinez, A., and Perez-Pariente, J., *Appl. Catal. A: General.* **115**, 121 (1994).

77. (a) Rubin, M. K., US Patent No. 5,021,141 (1991).

    (b) Dewing, J., Spencer, M. S., and Whittam, T. V., *Catal. Rev. Sci. Eng.* **27(3)**, 461 (1985).

78. Reference 7, Chapter 6.

79. Goldsmith, J. R., *Min. Mag.* **29**, 952 (1952).

80. (a) Taramasso, M., Perego, G., and Notari, B., US Pat. 4,578, 521 (1983).

    (b) Taramasso, M., Perego, G., and Notari, B., "Proc. 5th Intern. Zeolite Conf., Napoli, Rees, L. V. C., (Ed.), Heydon, London, (1980) p.40.

81. Deo, G., Turek, A. M., Wachs, I. E., Huybrechts, D. R. C., and Jacobs, P. A., *Zeolites.* **13**, 365 (1993).

82. (a) Trong On, D., Bonneviot, L., Bittar, A., Sayari, A., and Kaliaguine, S., *J. Mol. Catal.* **74**, 233 (1992).

    (b) Lopez, A., Tuiller, M. H., Guth, J. L., Delmotte, L., and Popa, J. M., *J. Solid State Chemistry.* **812**, 480 (1992).

83. (a) Trong On, D., Bittar, A., Sayari, A., Kaliaguine, S., and Bonneviot, L., *Catal. Lett.* **16**, 85 (1992) 85.

(b)   Bittar, A., Adnot, A., Sayari, A., and Kaliaguine, S., *Research on Chemical Intermediates.* **18**, 49 (1992).

84.   De Castro-Martins, S., Khouzami, S., Tuel, A., Ben Taarit, Y., El Murr, N., and Sellami, A., *J. Electroanal. Chem.* **250**, 15 (1993).

85.   Ione, K. G., Vostrikova, L. A., and Masthikin, V. M., *J. Mol. Catal.* **31**, 355 (1985).

86.   Wilson, S. T., Lok, B. M., Messina, C. A., Cannan, T. R., and Flanigen, E. M., *J. Am. Chem. Soc.* **104**, 1146 (1982).

87.   Wilson, S. T., and Flanigen, E. M., *ACS Symp. Ser.* **298**, 329 (1988).

88.   Han, S., Schmitt, K. D., Shihabi, D. S., and Chang, C. D., *J. Chem. Soc. Chem. Commun.* 1287 **(1993)**.

89.   Reddy, J. S., and Sayari, A., *J. Chem. Soc. Chem. Commun.* 23 (1995).

90.   Barrer, R. M., and Meier, W. M., *Trans. Faraday Soc.* **55**, 130 (1959).

91.   Dizdar, Z., *J. Inorg. Nucl. Chem.* **34**, 1069 (1972).

92.   Kucherov, A. V., and Slinkin, A. A., *Zeolites.* **7**, 43 and 583 (1987).

93.   Niwa, M., Itoh, H., Kato, M., Hattori, T., and Murakami, Y., *J. Chem. Soc. Chem. Commun.* 819 (1982).

94.   Farneth, W. E., and Gorte, R. J., *Chem. Rev.* **95**, 615 (1995).

95.   (a)   van Hoof., J. H. C., and Roelofsen, J. W., *Stud. Surf. Sci. Catal.* **58**, 242 (1991).

         (b)   Karge, H., *Stud. Surf. Sci. Catal.* **65**, 133 (1991).

96.   (a)   Yashima, T., Sato, K., Hayasaka, T., and Hara, N., *J. Catal.* **26**, 303 (1972).

         (b)   Ono, Y., *Stud. Surf. Sci. Catal.* **5**, 19 (1980).

         (c)   Unland, M. L., and Warker, G. E., "Catalysis of Organic Reactions", Moser, W. R., (Ed.), Chem. Ind. Ser., Marcel and Dekker Inc., New York, 5 (1981) p.51.

97.   Barthomoeuf, D., *Stud. Surf. Sci. Catal.* **65**, 157 (1991).

98.   Szostak, R., "Handbook of Molecular Sieves", Von Nostrand Reinhold, New York, (1992).

99.   (a)   Visser, J., *J. Appl. Cryst.* **2**, 89 (1969).

         (b)   Bibby, D. M., Aldridge, L. P., and Milestone, N. B., *J. Catal.* **72**, 72 (1971).

100.   (a)   Rietveld, H.M. *J. Appl. Cryst.* **2**, 65 (1969).

         (b)   Rudolf, P. R., Saldarriaga, C., and Clearfield, A., *J. Phys. Chem.* **90**, 6122 (1986).

101. Pluth, J. J., Smith, J. V., Bennet, J. M., *Acta Crystallog.* **42**, 283 (1986).

102. Charnell, J. F., *J. Cryst. Growth.* **8**, 291 (1971).

103. Chao, K .J., Lin, J. C., Wang, Y., and Lee, G. H., *Zeolites.* **6**, 35 (1986).

104. Mahller, B., *Z. Kristallogr.* **174**, 141 (1986).

105. Anderson, M. W., Terasaki, O., Ohsuna, T., Phillippou, A., Mackay, S. P., Ferrierra, A., Rochea, J., and Lindin, S., *Nature.* **367**, 347 (1994).

106. Kemp, W., "Spectroscopy of Organic Compounds", ELBS, (1987) p.47.

107. Flanigen, E. M., "Zeolite Chemistry and Catalysis", *ACS Monograph.* Rabo, J. A., (Ed.), **171**, 80 (1976).

108. Ward, J. W., ibid, p.118.

109. Maroni, V. A., Martin, K. A., and Johnson, S. A., *ACS Symp. Ser.* **368**, 85 (1988).

110. Janin, A., Lavalley, J. C., Macedo, A., and Raatz, F., *ACS Symp. Ser.* **368**, 117 (1988).

111. Baker, M. D., Bodber, J., and Ozin, G. A., ibid, p.136.

112. Camblor, M. A., Corma, A., and Perez-Parientie, J., *J. Chem. Soc. Chem. Commun.* 557 (1993).

113. Kosslick, H., Tunan, V. A., Fricke, R., Peuker, Ch., Pilz, W., and Storek, W., *J. Phys. Chem.* **97(21)**, 5678 (1993).

114. Kutz, N., "Heterogeneous Catalysis-II", (Shapiro, B. L., Ed.), p.121.

115. Jansen, J. C., van Der Gaag, F. J., and Van Bekkum, H., *Zeolites.* **4**, 369 (1984).

116. Jacobs, P. A., Beyer, H. K., and Valiyan, J., *Zeolites.* **1**, 161 (1981).

117. Coudurier, G., Naccache, C., and Vedrine, J. C., *J. Chem. Soc. Chem. Commun.* 1413 (1982).

118. Jacobs, P. A., "Carboniogenic Activity of Zeolites", Elsevier, Amsterdam, 39 (1977).

119. Lippmaa, E., Magi, M., Samson, A., Engelhardt, G., and Grimmer, A. R., *J. Am. Chem. Soc.* **102**, 4889 (1980).

120. Nagy, J. B., and Derouance, E. G., *ACS Symp. Ser.* **368**, 2 (1988).

121. Engelhardt, G., and Michel, D., "Higher Resolution Solid State NMR of Silicates and Zeolites", Wiley, Chichester, (1987).

122. (a)   Fyfe, C. A., Gobbi, G. C., Klinowski, J., Thomas, J. M., and Ramdas, S., *Nature.* **296**, 530 (1982).

     (b)   Fyfe, C. A., Gobbi, G. C., Klinowski, J., and Thomas, J. M., *J. Phys. Chem.*

86, 1247 (1982).

123. Engelhardt, G., Lohose, U., Lippmaa, E., Tarmak, M., and Magi, A. M., *Z. Anarg. Allg. Chem.* **482**, 49 (1981).

124. Fyfe, C. A., Grondey, H., Feng, Y., and Kokotailo, G. T., *Chem. Phys. Lett.* **173**, 211 (1990).

125. Fyfe, C. A., Feng, Y., Grondey, H., Kokotailo, G. T., and Mar, A., *J. Phys. Chem.* **95**, 3747 (1991).

126. Fyfe, C. A., Feng, Y., Gies, H., Grondey, H., and Kokotailo, G. T., *J. Am. Chem. Soc.* **112**, 3264 (1990).

127. Fyfe, C. A., Gies, H., and Fend, Y., *J. Am. Chem. Soc.* **111**, 7702 (1989).

128. Thomas, J. M., Fyfe, C. A., Ramdas, S., Klinowski, J., and Gobbi, G. C., *J. Phys. Chem.* **86**, 3061 (1982).

129. Ramdas, S., and Klinowski, J., *Nature.* **308**, 521 (1984).

130. (a) Klinowski, J., *Chem. Rev.* **91**, 1459 (1991).

    (b) Anderson, M. W., and Klinowski, J., *J. Am. Chem. Soc.* **112**, 10 (1990).

131. Kumar, R., Thangaraj, A., and Rajmohanan, P., *Ind. J. Chem.* **29A**, 1083 (1990).

132. (a) Buhl, J. Ch., Engelhardt, G., Felsche, J., Luger, S., and Foerster, H., *Ber. Bunsenges. Phys. Chem.* **92**, 176 (1988).

    (b) Lin, C. F., and Chao, K. J., *J. Phys. Chem.* **95(23)**, 9411 (1991).

    (c) Man, P. P., and Klinowski, J., *Chem. Phys. Lett.* **147(6)**, 581 (1988).

133. Thangaraj, A., and Sivasanker, S., *J. Chem. Soc. Chem. Commun.* 123 (1992).

134. (a) Satterfield, C. N., "Heterogeneous Catalysis in Practice", 2nd edition, McGraw Hill, New York, (1993).

    (b) Satterfield, C. N., and Sherwood, T. K., "The Role of Diffusion in Catalysis", Addison-Wesley Publishing Company, Inc., New York, (1963).

135. Weisz, P. B., *Chem. Tech.* **3**, 498 (1973).

136. (a) Weisz, P. B., and Frilette, V. J., *J. Phys. Chem.* **64**, 173 (1960).

    (b) Weisz, P. B., *Pure Appl. Chem.* **52**, 2091 (1980).

137. (a) Csicsery, S. M., *J. Catal.* **23**, 124 (1971).

    (b) Csicsery, S. M., *Zeolites.* **4**, 202 (1984).

    (c) Csicsery, S. M., "Zeolite Chemistry and Catalysis", (J.A. Rabo, Ed.), Am. Chem. Soc., Monograph, **171** 680 (1976).

138. Csicsery, S. M., *J. Catal.* **19**, 394 (1970).

139. Chen, N. Y., and Degnan, T. F., *Chem. Engg. Prog.* 32 (1988).

140. Miale, J. N., Chen, N. Y., and Weisz, P. B., *J. Catal.* 6, 278 (1966).

141. Derouane, E. G., and Gabelica, Z., *J. Catal.* 65, 486 (1980).

142. (a) Kaeding, W. W., Young, L. B., and Chu, C. C., *J. Catal.* 89, 267 (1984).

    (b) Lónyi, F., Engelhardt, J., and Kalló, D., *Zeolites.* 11, 169 (1991).

143. (a) Martens, J. A., Tielen, M., Jacobs, P. A., and Weitkamp, J., *Zeolites.* 4, 98 (1984).

    (b) Jacobs, P. A., and Martens, J. A., *Pure Appl. Chem.* 58, 1329 (1986).

    (c) Martens, J. A., and Jacobs, P. A., *Zeolites.* 6, 334 (1986).

144. Weitkamp, J., and Ernst, S., *Catal. Today.* 19, 107 (1994).

145. Frilette, V. J., Haag, W. O., and Lago, R. M., *J. Catal.* 67, 218 (1981).

146. Haag, W. O., Lago, R. M., and Weisz, P. B., *Faraday Discuss. Chem. Soc.* 72, 317 (1982).

147. Hölderich, W., and Riekert, L., *Chem. Ing. Tech.* 58, 412 (1986).

148. Voogd, P., and Van Bekkum, H., *Appl. Catal.* 59, 311 (1990).

149. Haag, W. O., and Dessau, R. M., "Proc. 8th Intern. Cong. Catal.", Verlag Chemie, Weinheim, Deerfield Beach, Basel, Vol.2 (1984).

150. Haag, W. O., Dessau, R. M., and Lago, R. M., *Stud. Surf. Sci. Catal.* 60, 255 (1991).

151. Csicsery, S. M., *J. Org. Chem.* 34, 3338 (1969).

152. Corma, A., and Sastre, E., *J. Catal.* 129, 177 (1991).

153. Gnep, N. S., Teda, J., and Guisnet, M., *Bull. Soc. Chem. Fr.* II, 5 (1982).

154. Martens, J. A., Perez-Pariente, J., Sastre, E., Corma, A., and Jacobs, P. A., *Appl. Catal.* 45, 85 (1988).

155. Dewing, J., *J. Mol. Catal.* 27, 25 (1984).

156. Joensen, F., Blom, N., Tapp, N. J., Derouane, E. G., and Fernandez, C., *Stud. Surf. Sci. Catal.* 49B, 65 (1989).

157. (a) Karge, H. G., Ladebeck, J., Sarbak, Z., and Hatada, K., *Zeolites.* 2, 94 (1982).

    (b) Karge, H. G., Hatada, K., Zhang, Y., and Fiedorow, R., *Zeolites.* 3, 13 (1983).

158. Martens, J. A., and Jacobs, P. A., *Zeolites.* 6, 334 (1986).

159. Egan, C. J., Langlois, G. E., and White, R. J., *J. Am. Chem. Soc.* 84, 1204 (1962).

160. Ernst, S., and Weitkamp, J., "Proc. Intern. Symp. On Zeolite Catalysis", Siofok, Hungary, May 13-16, 457 (1985).

161. Weitkamp, J., Ernst, S., and Kumar, R., *Appl. Catal.* **27**, 207 (1986).

162. Dartt, C. B., and Davis, M. E., *Catal. Today.* **19**, 151 (1994).

163. Sugi, Y., and Toba, M., ibid, p.187.

164. (a)   Thangaraj, A., Ph. D. Thesis, University of Pune, Oct. (1991).

     (b)   Reddy, J. S., Ph. D. Thesis, University of Pune, (1992).

165. Rao, P. R. H. P., Ph. D. Thesis, University of Pune, (1993).

166. Beck, J. S., Chu, C. T. W., Johnson, I. D., Kresge, C. T., Leonowicz, M. E., Roth, W. J., and Wartuli, J. C., WO 91/11390 (1990).

167. Kresge, C. T., Leonowicz, M. E., Roth, W. J., Wartuli, J. C., and Beck, J. S., *Nature.* **359**, 710 (1992).

168. Higgins, J. B., *Catal. Today.* **19**, 7 (1994).

CHAPTER II

SYNTHESIS AND CRYSTALLIZATION

KINETICS OF MCM-22

2.1 INTRODUCTION

The high silica zeolite, MCM-22, was first reported by Rubin and Chu (Mobil).[1] This is believed to be iso-structural to PSH-3, synthesized by Puppe and Weisser (Bayer) in 1984,[2] and SSZ-25 synthesized by Zones (Chevron)[3] in 1987. During the last five years, numerous patents, describing the use of MCM-22 as a catalyst for a variety of reactions, have been filed.[4-10]

This chapter recounts the synthesis of the zeolite MCM-22[11] and the optimization of the synthesis parameters such as temperature, SiO_2/Al_2O_3, OH^-/SiO_2 and R/SiO_2 ratios (where, R is the organic templating agent) of the synthesis gels to obtain highly crystalline samples. Modification of various zeolite samples was carried out to use these materials in different reactions. The procedures used for dealumination of the samples[12-15] are also discussed in this chapter.

2.2 EXPERIMENTAL

2.2.1 SYNTHESIS

Hydrothermal syntheses of MCM-22 samples were carried out in a stainless steel, high-pressure stirred reactor [Parr Instruments, USA] of 300 ml capacity. Before use, the reactor vessel was washed thoroughly with a dilute HF solution to avoid seeding effects during synthesis.

The raw materials used for the synthesis were sodium silicate (Lona Industries, Bombay; 26.69% SiO_2, 9.10% Na_2O, 64.21 % H_2O), hexamethyleneimine (Aldrich; 99%), aluminum sulphate (E. Merck (India) Ltd., Bombay; $Al_2(SO_4)_3 . 18 H_2O$) and concentrated sulphuric acid (Ranbaxy Laboratories, Punjab; 98%). Other sources of silica, namely, fumed silica (Sigma; S-

5130; 99.8 % SiO_2, surface area = 390 ± 40 m^2/g) and SiO_2 sol (30 % SiO_2 and 70 % H_2O), were also used for the syntheses of MCM-22.

Syntheses of MCM-22 with SiO_2/Al_2O_3 ratios of 30, 45, 60, 88, 100 and 150 were carried out with the following ratios in the synthesis gels held constant: R/SiO_2 = 0.46, R/Na_2O = 1.39, H_2O/SiO_2 = 49 and OH^-/SiO_2 = 0.10. The samples with higher silica contents were prepared by adding excess sulphuric acid to maintain OH^-/SiO_2 = 0.10. A typical synthesis procedure for obtaining MCM-22 with SiO_2/Al_2O_3 = 30 is described below.

Sodium silicate [43.58 g] was mixed with distilled water [20 g] in a polypropylene beaker (250 ml capacity). The mixture was stirred for 5 minutes. Hexamethyleneimine [8.81 g], the organic templating agent, was added over a period of 30 minutes to the solution. The pale yellow mixture was further stirred for 15 minutes. A solution of aluminum sulphate [4.33 g], distilled water [110 g] and concentrated sulphuric acid [3.52 g] was added dropwise, slowly over a period of 15 minutes with continuous stirring. The mixture was left undisturbed for 1 hour. The final mixture was pale yellow and its pH was 11.4.

The above mixture had the following composition in terms of oxide mole ratios:

$$9.83 \ Na_2O \ : \ 29.78 \ SiO_2 \ : \ Al_2O_3 \ : \ 13.7 \ R \ : \ 1367.9 \ H_2O.$$

The mixture was autoclaved and allowed to crystallize at 423 K. Crystallization periods for samples with SiO_2/Al_2O_3 ratios, 30, 45, 60, 88, 100 and 150 were 80, 90, 95, 105, 120 and 135 hours, respectively. The crystalline white products were filtered and the mother liquor was found to have a pH = 12.4. The sample was washed thoroughly with distilled water and dried at 393 K for 6 hours.

The as-synthesized material was calcined to remove the occluded organic template molecules within the channels and cages of the zeolite. Though, complete removal of the template could be achieved in 3 h at 1023 K, a crystallinity loss of about 20 % was noticed at this high temperature. It was found that prolonged heating (> 24 h) in air was necessary for

complete removal of the template at 773 or 823 K. The best method for the template removal was heating first in a flow of nitrogen at 723 K for 4 hours and then in dry air at 873 K for 6 hours. In all the syntheses, the yields were between 86% to 92%.

$$Yield = \frac{Wt. \ of \ the \ calcined \ material}{Wt. \ of \ (SiO_2 + Al_2O_3) \ in \ the \ silica \ and \ alumina \ sources} \times 100.$$

2.2.2 MODIFICATION OF ZEOLITE SAMPLES

2.2.2.1 Ion-exchange

The calcined samples were converted into a catalytically active protonic form by standard ion-exchange techniques. The samples were converted into the protonic form by three exchanges with 1M ammonium acetate solution at 360 K (10 ml solution/g of zeolite sample; duration of each exchange was 6 hours). After the first and second exchanges, the samples were washed and dried at 393 K for 2 h. The final samples (after the 3rd exchange) were washed thoroughly with distilled water, dried at 393 K for 6 hours and calcined in dry air at 773 K for 6 hours, to get the catalytically active H$^+$-forms.

2.2.2.2 Impregnation method

The catalytically active H-forms of the zeolites were modified by impregnation techniques to obtain supported noble metal catalysts.

A solution of Pt[(NH$_3$)$_4$ (NO$_3$)$_2$] was used for impregnation. 5 g of the H-form of the zeolite sample was made into a paste with a known amount of a solution of the platinum complex. The slurry was thoroughly mixed and dried at 358 K. The dried sample was made into a paste again by adding distilled water and dried again. Finally, the samples were dried at 383 K for 2 hours and calcined in a flow of dry air at 823 K for 6 hours. Thus, samples with 0.1, 0.2, 0.3, 0.5 and 0.75 wt. % Pt-loadings were prepared.

The catalyst (Pt-loaded H-MCM-22) was pressed into pellets, crushed and sieved into (-12 +18) mesh particles. The sieved catalyst was loaded into the reactor and catalytic reactions were carried out (Chapter V).

2.2.2.3 Dealumination of zeolite MCM-22

The high-silica form of the MCM-22 sample ($SiO_2/Al_2O_3 = 80$) was dealuminated using the procedures described below. The extraction of aluminum was carried out by two methods, namely, by (I) ammonium fluorosilicate treatment[12,13] and (ii) ethylene diammine tetraacetic acid [EDTA] method.[14,15]

(i) Ammonium fluorosilicate [NH_4SiF_6] method:

1.6 g of calcined Na-MCM-22 ($SiO_2/Al_2O_3 = 80$) was added to 3.5 ml of (1M) ammonium acetate solution and the mixture was refluxed at 358 K for 6 h. The material was filtered, washed thoroughly with distilled water and dried at 383 K for 2 h. This exchange procedure was repeated thrice. To the exchanged sample, 10 ml of distilled water was added and the slurry was stirred vigorously at 358 K. 1 ml of NH_4SiF_6 solution (0.4 M) containing sufficient Si^{4+} ions to replace all the Al^{3+} ions in the sample, was introduced slowly using a syringe pump (Sage Instruments, USA) into the slurry of the catalyst over a period of 6 h. The pH was maintained at 6.2. The mixture was stirred vigorously for 8 h.

The sample was filtered, washed with boiling water and finally dried at 383 K for 2 h. The dried material was calcined at 723 K in flowing air for 6 h. The filtrate was analyzed for aluminum by atomic absorption spectroscopy [AAS]. Solutions containing ammonium fluorosilicate and Al^{3+} ions dissolved in distilled water were used as standards. The results obtained from the AAS analysis indicated that the filtrate contained 2.5 % of the total aluminum content of the parent zeolite sample.

(ii) EDTA method :

To 2 g of the zeolite sample, 10 ml of distilled water was added and made into a slurry. An aqueous solution of (H_4-EDTA) [1 g in 16 ml] was added to the zeolite slurry over a period of 16 h using a syringe pump at 373 K. The mixture was refluxed at 373 K for 16 h. The final mixture was filtered, washed with boiling water and dried at 393 K for 2 h. The zeolite sample

was calcined at 723 K in flowing air for 6 h. 7.6 % of aluminum was found, by analysis, to be leached out of the zeolite. The entire leaching procedure was repeated thrice. The final sample was found to contain 14 % less aluminum than the parent sample. Method (ii), the EDTA method, was found to be more effective for the dealumination of MCM-22 samples.

After dealumination, minor changes in XRD peak positions were observed when compared to the parent sample. This slight shifting of peaks indicated the removal of framework aluminum. The XRD patterns of the parent (calcined) and the dealuminated (calcined) samples are presented in Figure 2.1. The larger peak intensities of some lines noticed in the XRD profile of the dealuminated sample is probably due to the leaching out of amorphous impurities which may have been present in the channels. Chumbale *et al.* have observed regular increase in XRD peak intensities during the dealumination of mordenite.[16] The as-synthesized, calcined and dealuminated materials were characterized by ^{27}Al and ^{29}Si MAS NMR techniques and the results are discussed in Chapter III.

2.2.3 KINETIC EXPERIMENTS

Eventhough, a detailed study of the kinetics of crystallization has not been carried out, the influence of few important parameters on the crystallization was investigated.[17]

The kinetic experiments were carried out by stopping the reaction at regular time intervals and rapidly cooling the reactor with cold water (~ 10° C). Before the withdrawal of the sample, the synthesis mixture was stirred in order to homogenize the solution. After withdrawal of the sample, the reactor was heated again and the crystallization continued. The percentage crystallinity of the solid materials were calculated based on the ratios of the sum of the areas of peaks with 2θ values between 25° and 30° with the areas of the peaks in the same range for a standard sample. The best sample with no impurity phases and maximum crystallinity was chosen as the reference or standard sample. The physico-chemical properties of
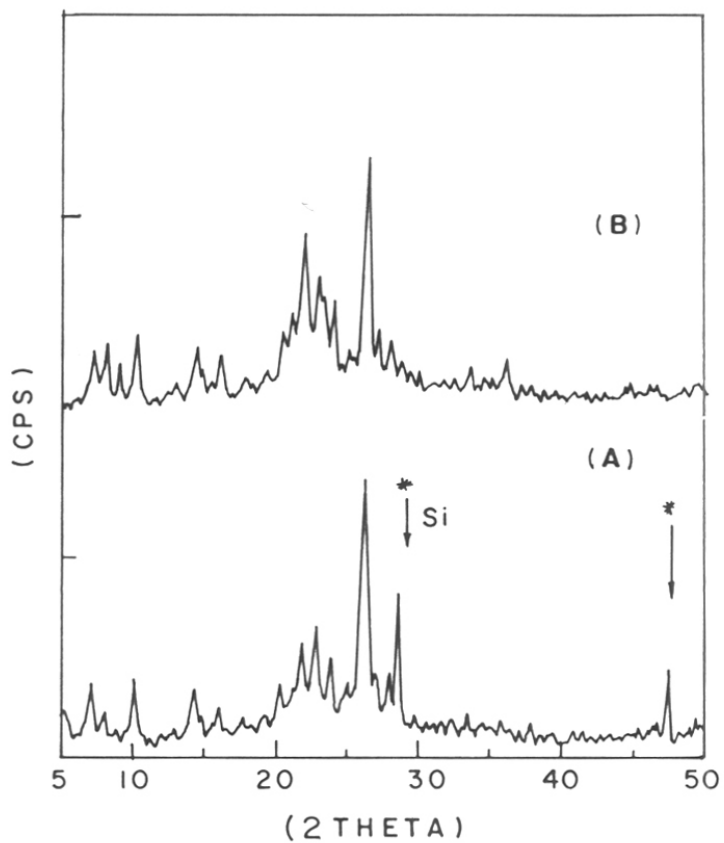
Figure 2.1   XRD profiles of zeolite MCM-22 samples.

    (A) :   Parent sample.
    (B) :   After dealumination and successive calcination.
    (*)   Silicon - Internal standard.

53

the standard sample were determined (Chapter III and IV). The same sample was also used in a variety of catalytic reactions (Chapter V).

The results of the preliminary characterization of the reference sample are described below. The as-synthesized sample had platelet morphology with no change in crystal morphology upon calcination. The platelets were 4 - 5 μm in diameter, 0.1 - 0.2 μm thick and were bundled into large crystals. XRD analyses indicated that the sample was free from other phases such as ZSM-12 and FU-1. The lines were indexed to an orthorhombic symmetry and unit cell parameters were determined ('a' = 24.606 $\pm$ 0.005 Å, 'b' = 14.395 $\pm$ 0.005 Å and 'c' = 24.753 $\pm$ 0.005). I.R. spectrum of the sample indicated the presence of bands at 555 cm^{-1} and 402 cm^{-1}, attributable to pentasil rings and 12 MRs, respectively. The sorption of probe molecules, namely, water, n-hexane, cyclohexane, m-xylene and mesitylene were found to be 15.11 %, 11.5 %, 9.5 %, 9.8 % and 8.9 %, respectively.

2.3 RESULTS AND DISCUSSIONS

2.3.1 CHARACTERIZATION

2.3.1.1 Chemical Analysis

The chemical compositions of the materials with different SiO_2/Al_2O_3 ratios are presented in Table 2.1. As seen in Table 2.1, there is a regular difference in the ratio between the input gel and the output product composition.

The sodium contents of the as-synthesized samples were found to be lower than the calculated amounts. Since the framework charge is balanced by the extra-framework sodium ions, the number of sodium ions must be approximately equal to number of framework aluminum ions. But, the observations suggest this was not so in our case. Corma *et al.* have suggested that this imbalance is due to charge balancing by the template cations.[18]

Table 2.1   Chemical Composition of MCM-22 samples.

| Samples | SiO_2/Al_2O_3 | | Na_2O/Al_2O_3 | |
	Input	Product	Input	Product
A	30	28	9.85	0.11
B	45	40	9.83	0.14
C	60	56	9.85	0.18
D	88	80	9.84	0.19
E	100	96	9.84	0.25
F	150	140	9.85	0.97

2.3.1.2 X-Ray Diffraction [XRD]

The kinetics of crystallization was followed by XRD. The XRD patterns of the samples collected at different intervals of time (0 h, 30 h, 50 h and 80 h) are depicted in Figure 2.2. The samples were found to be 0, 4 %, 68.5 % and 100 % crystalline, respectively, which were confirmed by other studies discussed in the following sections. From the Figure 2.2, it could be seen that the crystallization started at about the 30th hour and was complete between 80 - 90 hours.

2.3.1.3 I.R. Spectroscopy

The I.R. spectra of the samples collected at different time intervals are presented in Figure 2.3. The observed I.R. bands were assigned tentatively based on the work of Flanigen *et al.*[19] The bands were assigned to internal symmetric stretching, external asymmetric stretching, external symmetric stretching, double rings, T-O bending vibrations and pore opening. The intensities of the bands at 550 cm^{-1} and 1080 cm^{-1} were found to increase as the time of crystallization increased and was found to be maximum for the sample with 100 % crystallinity.

2.3.1.4 Scanning Electron Microscopy [SEM]

Figure 2.4 presents the SEM pictures of the samples obtained after different crystallization times, namely, 0, 30, 50 and 80 hours. The sample collected at the 80th hour was found to be fully crystalline free from other amorphous impurties. XRD data revealed that the samples collected at 0, 30, 50 and 80 hours were 0, 4, 68.5 and 100 % crystalline with respect to the reference sample. The presence of a few platelets in the SEM picture (Figure 2.4 (B)), confirmed the start of crystallization started at about 30 h. The crystallization was complete at about 80 hours (Figure 2.4 (D)). No changes occurred in crystal size or the shape between 80 and 100 hours.
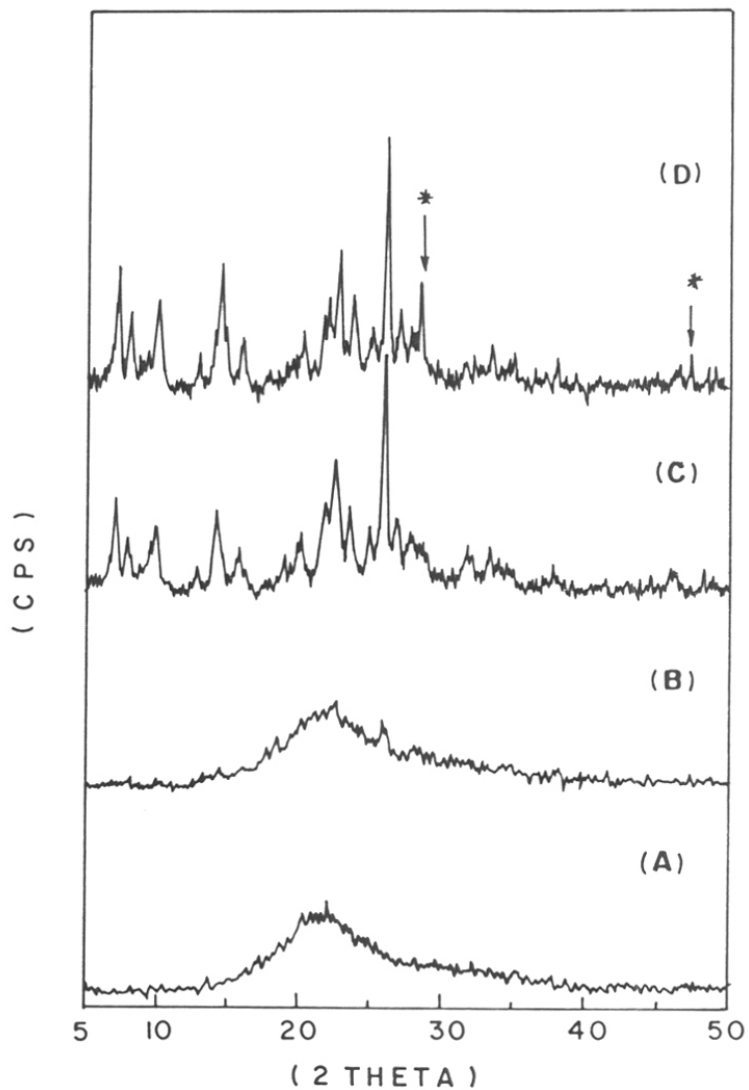
Figure 2.2   XRD profiles of samples collected at different intervals of time.
$SiO_2/Al_2O_3 = 28$, $R/SiO_2 = 0.46$, $OH^-/SiO_2 = 0.1$, $Na_2O/Al_2O_3 = 9.83$ and
$H_2O/SiO_2 = 45$. Temp. = 423 K and stirring rate = 200 rpm.

(A) 0 h, (B) 30 h, (C) 60 h and (D) 80 h.
(∗) : Silicon - Internal standard.
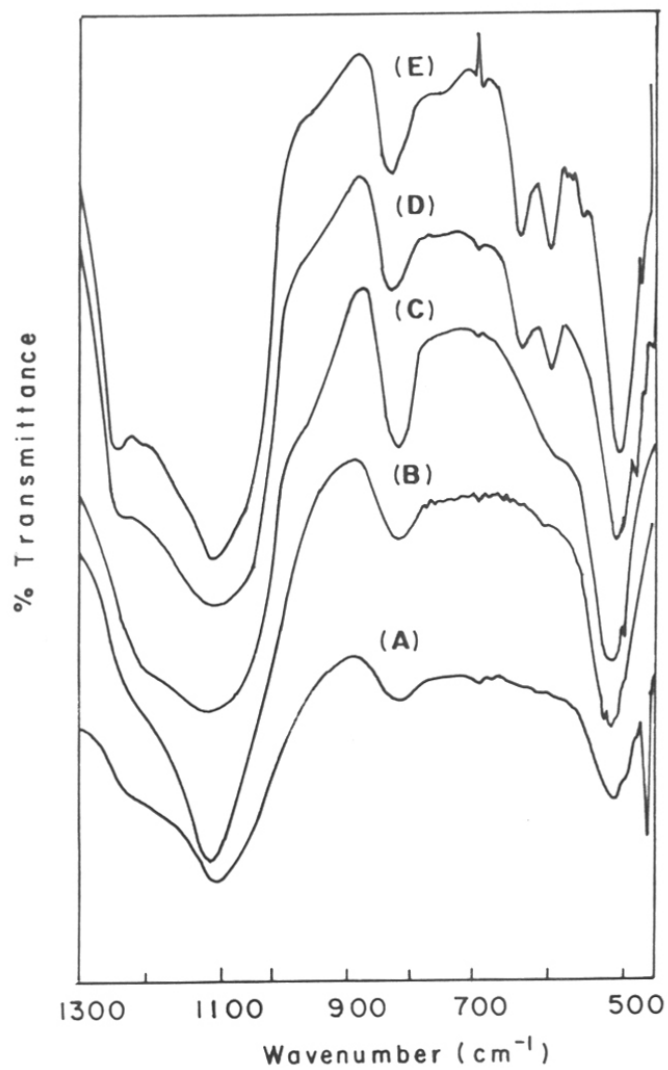
Figure 2.3   I.R. spectra of samples collected at different time intervals.

(A) 0 h, (B) 24 h, (C) 30 h, (D) 60 h and (E) 80 h.
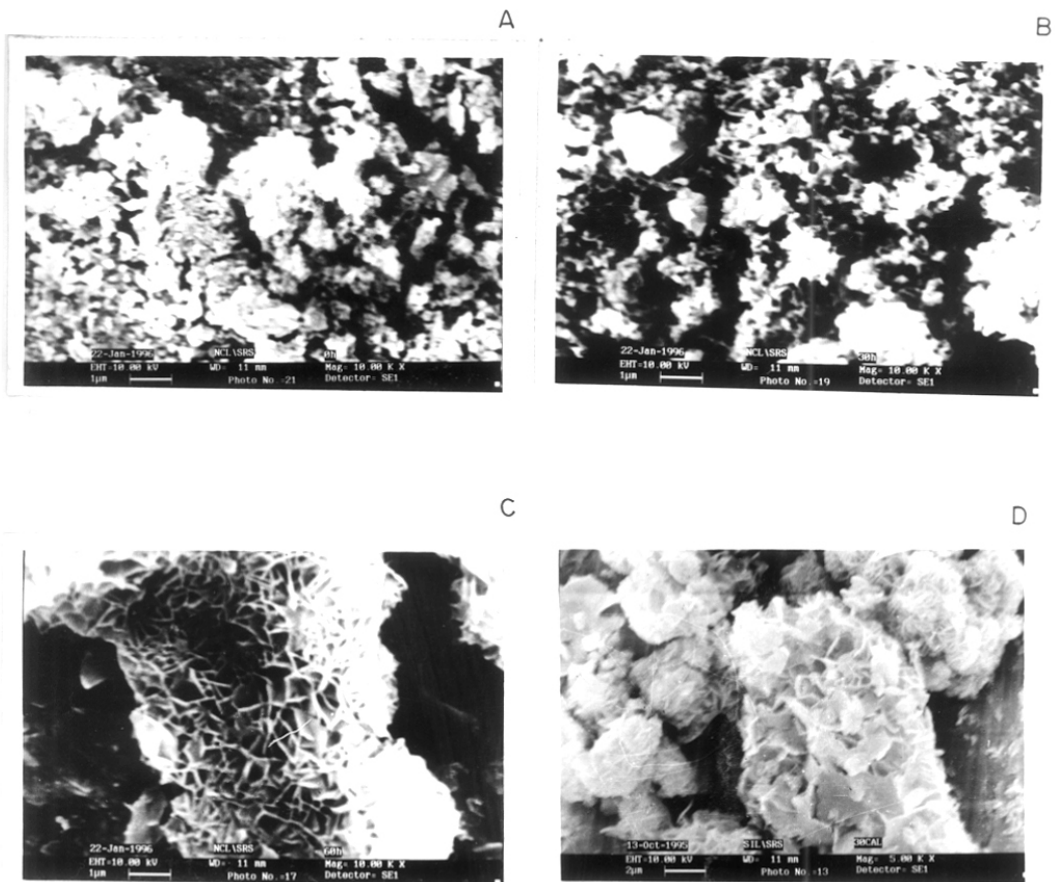
Figure 2.4   Scanning electron micrographs of MCM-22 samples collected at different intervals of time representing different percentages of crystallinity.

(A) 0 %, (B) 4 %, (C) 68.25 % and (D) 100 %.

2.3.2 KINETICS OF CRYSTALLIZATION

2.3.2.1 The effect of Si/Al ratios

Three types of silica sources, namely, sodium silicate, silica sol (30 % SiO_2) and fumed silica, were used in the synthesis of MCM-22. It was found that, the crystallization time was shortest when sodium silicate was used as the silica source (80 - 90 h). When silica sol and fumed silica were used, 7 and 10 days were required for crystallization of pure MCM-22, respectively.

The effect of SiO_2/Al_2O_3 ratios is depicted in Figure 2.5. It can be seen that, as the aluminum content decreased, a longer crystallization time was required. Normally, the reverse phenomenon is observed during the synthesis of other molecular sieves.[20-22] However, the substitution of heavier metal ions such as Ti and V has been reported to decrease the rate of crystallization.[23] For example, during the studies on the synthesis of TS-2, Reddy et al.[23] observed a decrease in the rate of crystallization of samples with higher titanium content. Similar observations have also been reported during the incorporation of titanium in the MFI system[24] and vanadium in MEL-type and NCL-1 zeolites.[25,26] Crea et al.[27] have reported an increase in the rate of crystallization during the synthesis of aluminum free silica polymorph of ZSM-5. However, faujasite type zeolites, X and Y, synthesized with higher aluminum contents[27] (SiO_2/Al_2O_3 = 1.5 - 3) require lower crystallization time than that required for the synthesis of silicalite-1. The crystallization of faujasite type zeolites occurs at 353 K - 373 K in about 8 h, whereas, silicalite-1 requires atleast one day at 413 K.[24] The apparent reason is that, the incorporation of aluminum is more favored for the stabilization of the faujasite structure. In the case of MCM-22, the exact reason for the increase in crystallization time with the increase in SiO_2/Al_2O_3 ratio is not known. It may possibly be due to the strong requirement of aluminum for the stability of the MCM-22 framework, the absence of Al probably leading to the destruction of the zeolite structure. The fact that, the sample (SiO_2/Al_2O_3 = 80) could not
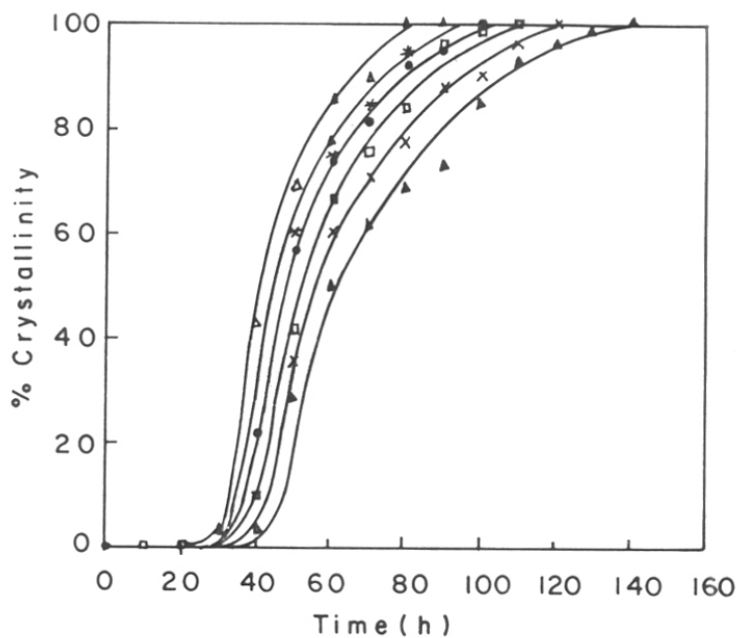
Figure 2.5   The effect of SiO_2/Al_2O_3 ratios over crystallization.
R/SiO_2 = 0.46, OH⁻/SiO_2 = 0.1, Na_2O/Al_2O_3 = 9.83, H_2O/SiO_2 = 45.
Temp. = 423 K and stirring rate = 200 rpm.

SiO_2/Al_2O_3 ratios : (Δ) 28, (+) 40, (*) 56, (□) 80, (x) 96 and (▲) 140.

be dealuminated beyond a certain limit (maximum of 14 %) supports the belief that aluminum stabilizes the framework.

Also, the Si/Al ratios in the products were lower than that of the input gel. Beyond, SiO_2/Al_2O_3 ratio = 100, the time required for complete crystallization was greater than 100 hours and co-crystallization of other impurity phases was found to occur. Figure 2.6 presents the XRD patterns of MCM-22 samples with SiO_2/Al_2O_3 = 28, 96 and 140. It can be seen from the figure that the intensities of the peaks except the one at $2\theta = 26°$ (100 %) for samples with higher SiO_2/Al_2O_3 ratios were low. Beyond SiO_2/Al_2O_3 = 150, impurity phases (more stable phases) such as, ZSM-5 (see Figure 2.7 (A)) and quartz crystallized as a single phase. Synthesis of samples with higher aluminum contents (SiO_2/Al_2O_3 < 30) led to the formation of dense phases such as crystobalite and magadite and the zeolite mordenite. Similar observations have also been reported by Corma et al.[18] These authors have observed that as the SiO_2/Al_2O_3 ratio was increased, the time of crystallization also increased and for the samples with higher Si/Al ratios, extra moles of OH⁻ were necessary. They have also reported that carrying out the synthesis of MCM-22 under a static condition led to impurity phases such as ferrierite or ZSM-5 without any MCM-22 phase.[18]

Synthesis of samples with Si/Al $\simeq \infty$ were attempted. This led to the formation of an entirely different phase, a clathrate, designated as "nonasil".[28] The synthesis of this silica-polymorph has already been reported by Marler et al. using hexamethyleneimine as one of the organic templating agents.[28]

Thus, the optimum range of SiO_2/Al_2O_3, in which the zeolite MCM-22 could be synthesized, was found to be SiO_2/Al_2O_3 = 30 to 150.[11,18] Lower SiO_2/Al_2O_3 ratios led to the formation of dense phases, while higher ratios led to the formation of other zeolites and a clathrate (nonasil).
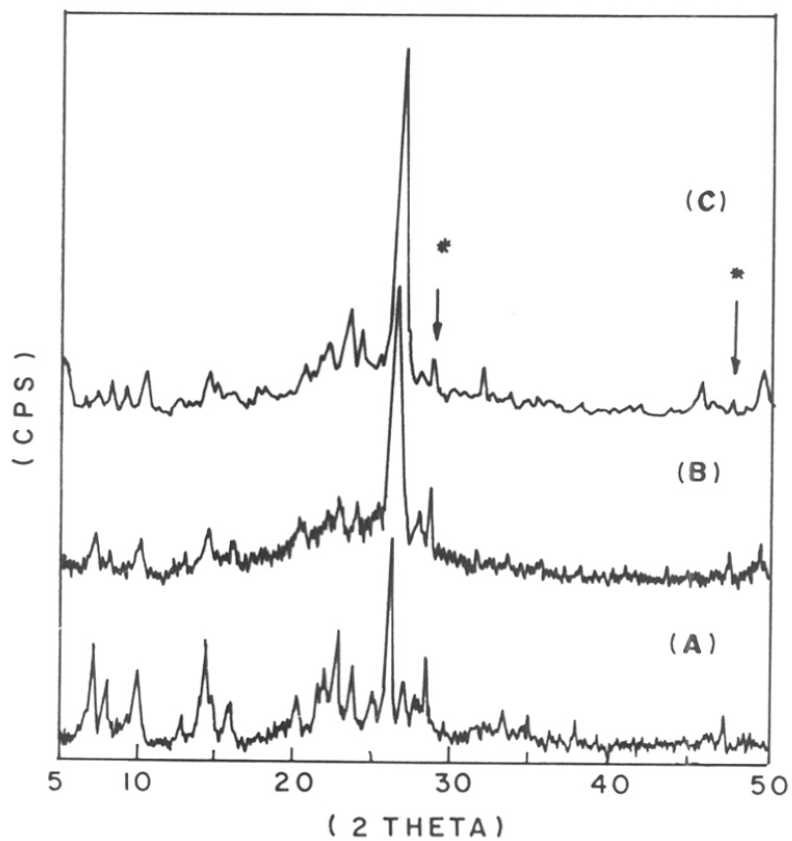
Figure 2.6   XRD patterns of samples with high SiO_2/Al_2O_3 ratios along with the standard
sample for comparison.

SiO_2/Al_2O_3 ratios : (A) 28, (B) 96 and (C) 140.
(*) : Silicon - Internal standard.
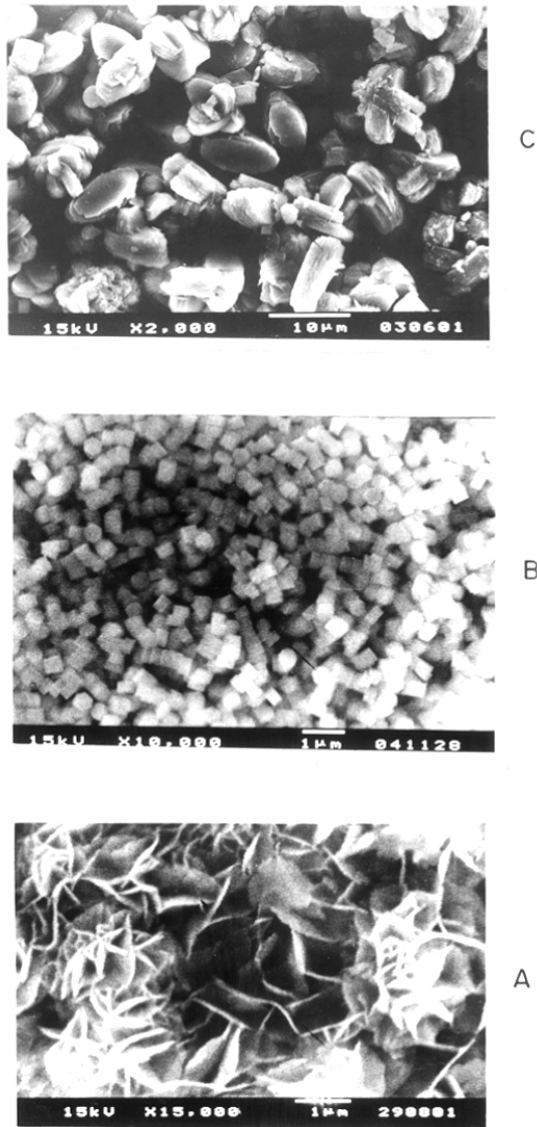
Figure 2.7   Scanning electron micrographs of impurity phases along with the standard sample.

(A) MCM-22 (standard), (B) ZSM-5 and (C) Ferrierite phases..

2.3.2.2 The effect of Temperature

The crystallization temperature was varied from 403 K - 448 K. The zeolite syntheses were carried out keeping other parameters constant. The results are presented in Figure 2.8. The increase in temperature led to an increase in the rates of nucleation and crystallization.

The crystallization curves could be distinctly demarcated into three regions, (I) induction, (II) nucleation and (III) crystallization (Figure 2.8). It can be seen from the figure that the nucleation and crystallization period is very short for higher temperatures, whereas, both, nucleation and crystallization periods are short at higher temperatures (> 403 K).

The most suitable temperature for the synthesis of MCM-22 without impurity phases and with minimum crystallization period was found to be 423 K. Below 423 K, crystallization was prolonged, the crystallization requiring 9 - 10 days. At temperatures above 423 K, the rate of crystallization was faster, but co-crystallization of other impurity phases such as mordenite, ZSM-5 and ferrierite occurred.

The studies reveal that a very narrow temperature window exists for the effective crystallization of MCM-22.

2.3.2.3 The effect of R/SiO$_2$ ratios and template structure

The effect of R/SiO$_2$ ratios was studied by changing the template concentration. The effective R/SiO$_2$ ratio at which MCM-22 samples crystallized without impurity phases was found to be 0.50. (See Figure 2.9).

When the synthesis was attempted without using a template, only amorphous material resulted after 15 days. The effect of a slight variation in the structure of the organic template on the synthesis of MCM-22 was investigated by substituting the hydrogen attached to the nitrogen by an ethyl chloride group, (2-(Hexamethyleneimino)ethylchloride monohydrochloride) (see Figure 2.10). It was found that the gel remained amorphous even after 10 days. The above results indicate the sensitivity of the crystallization to the size (shape) and structures of the
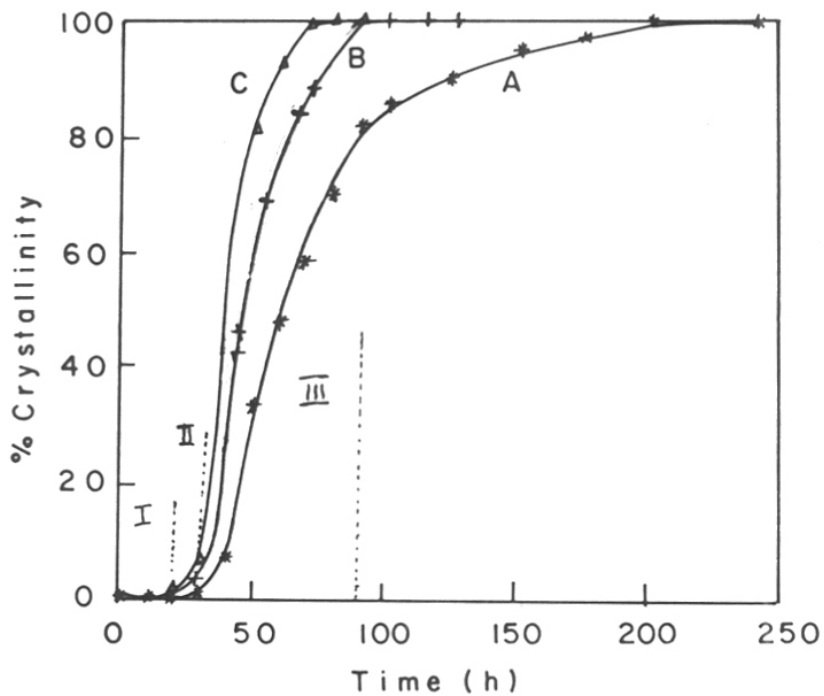
Figure 2.8   The effect of temperature upon the crystallization of MCM-22 sample.
$SiO_2/Al_2O_3 = 28$, $R/SiO_2 = 0.46$, $OH^-/SiO_2 = 0.1$, $Na_2O/Al_2O_3 = 9.83$ and
$H_2O/SiO_2 = 45$ and stirring rate = 200 rpm.

(A) 403 K, (B) 423 K and (C) 448 K.
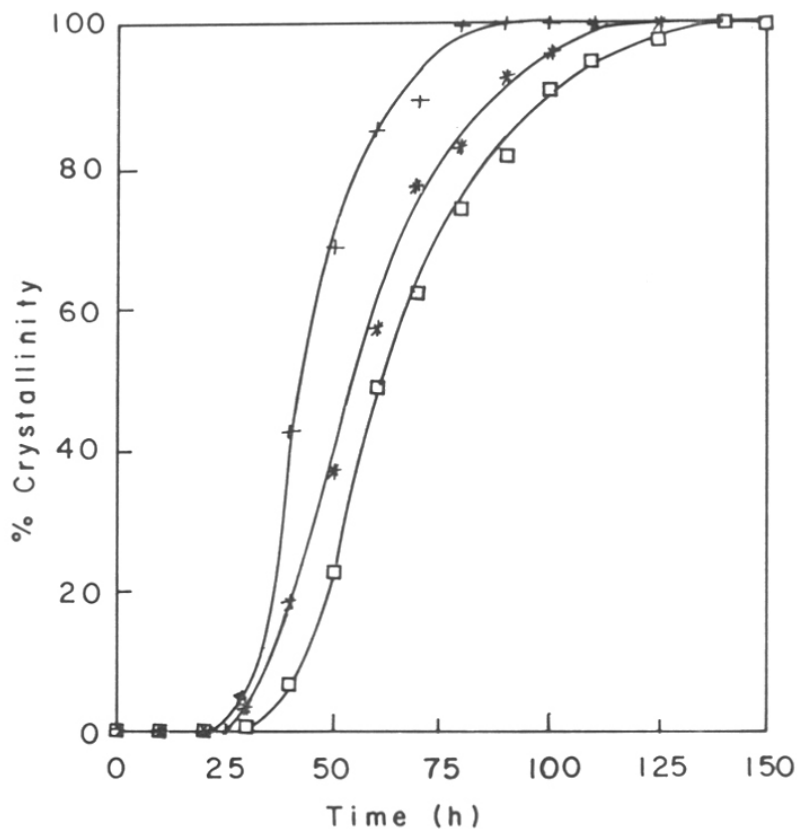
Figure 2.9   The influence of template concentration upon the crystallization of
               MCM-22.
               $SiO_2/Al_2O_3 = 28$, $OH^-/SiO_2 = 0.1$, $Na_2O/Al_2O_3 = 9.83$, $H_2O/SiO_2 = 45$,
               Temp. $= 423$ K and stirring rate $= 200$ rpm.

               R/SiO_2 ratios : (+) 0.46, (∗) 0.3 and (□) 0.15.
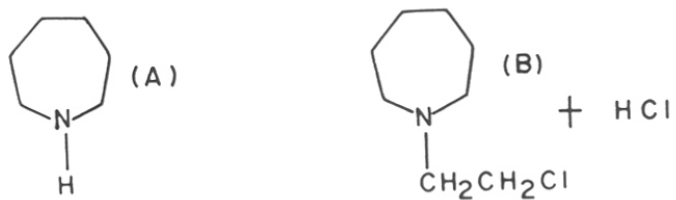
Figure 2.10   The structure of the organic molecules used in the synthesis of MCM-22.

(A) : Hexamethyleneimine and (B) : 2-(Hexamethyleneimino)ethyl chloride monohydrochloride.

template. So far, there have been no reports on the use of other templates in the synthesis of the zeolite MCM-22.

Eapen et al.[29] have studied the effect of template concentration and different templates on the rate of crystallization of zeolite ß. These authors have observed that the rate of crystallization and nucleation were enhanced by tetraethyl ammonium hydroxide (TEAOH), but only negligible changes were observed when tetraethyl bromide (TEABr) was used as the template. Reddy et al.[30] have carried out kinetic studies over NCL-1 using hexamethylene bis(triethylammonium bromide). They have reported that even minor variations of the template structure resulted in amorphous materials.

Otake[31] has carried out the crystallization of MFI type zeolites without the organic template. He has observed that the SiO_2/Al_2O_3 range within which the MFI samples could be synthesized without the aid of templates was 30 - 50, beyond which amorphous phase resulted. He also studied the effect of the addition of a small dosage of TPA cations to the template free synthesis mixture and found that the resultant product was much similar to the original MFI material than the product obtained by employing template free synthesis. He has suggested that the TPA template was an unique structure directing agent of MFI type zeolites and can be used as a supplementary to the synthesis of MFI type zeolites in the presence of other templates.[32] Shiralkar and Clearfield[33] have shown that the template free synthesis of MFI resulted in materials predominantly containing mordenite.

Thus, it appears that MCM-22 can be synthesized only with hexamethyleneimine as the template, the template acting as a structure directing agent.

2.3.2.4 The effect of OH^-/SiO_2 ratios

The synthesis of zeolites is generally carried out in alkaline medium. However, excess basicity may cause redissolution of the zeolite phase back into the solution, leading to a

decrease in yield. The influence of OH^-/SiO_2 was investigated by varying the amount of sulphuric acid which is governed by the relation as follows :

Moles of free OH^- = [moles of [OH^-] from the base] − [{sum of the moles of H^+ obtained from acid (H_2SO_4)} and {3 x moles of H^+ obtained from aluminum source}].

The effect of OH^- concentration is presented in Figure 2.11. The OH^-/SiO_2 mole ratio was varied from 0.075 to 0.30. As observed in the synthesis of other high silica zeolites,[20-22,34,35] the rate of crystallization was found to increase when OH^-/SiO_2 was increased. However, above a critical pH, the redissolution of zeolitic phase back into solution leads to supersaturation in the mother liquor. Thus, yield and crystallinity decrease beyond an optimum range of OH^- concentration. The increase in pH (from 11.4 to 12.4) of the mother liquor during crystallization is attributed to the formation of the crystalline material which is similar to the observations of Casci and Lowe.[36] The increase in pH is due to the incorporation of SiO_2 units from the gel phase into the crystalline phase leaving behind the highly alkaline mother liquor. But, the incorporation of alumina units is independent of the concentration of the free base and have negligible effects.

2.3.2.5 The effect of agitation

Three syntheses under different agitation rates were carried out using the same synthesis gel. They were, (i) in Parr reactor, at autogeneous pressure with a stirrer speed of 200 rpm, (ii) in a tumbling stainless steel reactor with a tumbling rate of 60 rpm and (iii) in a static condition. The other synthesis parameters were the same in all these cases.

It was found that the synthesis carried out in the Parr reactor yielded a good crystalline material after 3.5 days (crystallinity = 100 %). The samples obtained by employing synthesis
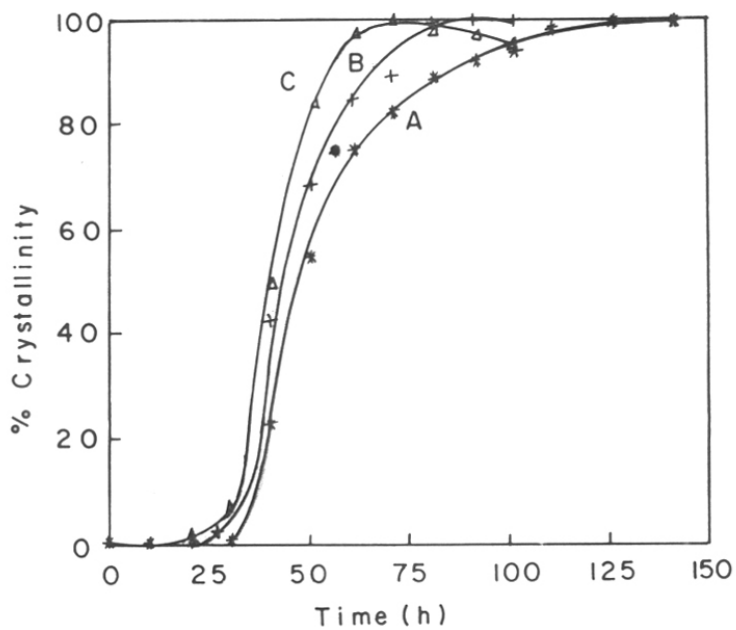
Figure 2.11   The effect of OH⁻/SiO$_2$ mole ratios upon the crystallization period. SiO$_2$/Al$_2$O$_3$ = 28, R/SiO$_2$ = 0.46, Na$_2$O/Al$_2$O$_3$ = 9.83 and H$_2$O/SiO$_2$ = 45. Temp. = 423 K and stirring rate = 200 rpm.

OH⁻/SiO$_2$ mole ratios : (A) 0.075, (B) 0.10 and (C) 0.30.

method (ii) were found to be 60 % crystalline after 3.5 days, the maximum crystallinity being ~ 80 % after 10 days. The products obtained by using method (iii) were found to be amorphous after 3.5 days and contained ZSM-5 after 20 days; there was no indication of the formation of MCM-22 phase. Thus, the samples were synthesized in a Parr reactor at a stirrer speed of 200 r.p.m. at 423 K and were used for characterization and catalytic studies.

2.4 REFERENCES

1. Rubin, M. K., and Chu, P., US Patent No. 4,954,325 (1990).

2. Puppe, L., and Weisser, J., US Patent No. 4,439,409 (1984).

3. Zones, S. I., Eur. Patent Appln. EP 231 019 (1987).

4. Absil, R. P. L., Marler, D. O., and Shihabi, D. S., US Patent No. 4,962,257 (1990).

5. Huss, A., Kirker, G. W., Keville, K. M., and Thomson, R. T., US Patent No. 4,992,615 (1991).

6. Morrison, R. A., US Patent No. 4,992,611 (1991).

7. Chu, P., Kirker, G. W., Kushnerick, J. D., and Marler, D. O., US Patent No. 5,043,512 (1991).

8. Kushernick, J. D., Marler, D. O., McWilliams, J. P., and Smith, C. M., US Patent No. 4,992,606 (1991).

9. Del Rossi, K. J., and Shih, S. S., US Patent No. 5,043,503 (1991).

10. Angevine, P. J., Degnan, T. F., and Marler, D. O., US Patent No. 4,982,040 (1991).

11. Ravishankar, R., Tapas Sen, Veda Ramaswamy, Soni, H. S., Ganapathy, S., and Sivasanker, S., *Stud. Surf. Sci. Catal.* **84(A)**, 331 (1994).

12. Breck, D. W., Blass, H., and Skeels, G. W., US Patent No. 4,503,023 (1985).

13. Garralón, G., Fornés, V., and Corma, A., *Zeolites.* **8**, 268 (1988).

14. Barthomeuf, D., and Beaumount, R., *J. Catal.* **30**, 288 (1973).

15. Kerr, G. T., *J. Phys. Chem.* **72**, 2594 (1968).

16. Chumbale, V. R., Chandwadkar, A. J., and Rao, B. S., *Zeolites.* **12**, 62 (1992).

17. Szostak, R., "Molecular Sieves, Principles of Synthesis and Identification", Van Nostrand Reinhold Catalysis Series, New York, (1989).

18. Corma, A., Corell, C., and Pérez-Pariente, J., *Zeolites.* **15**, 2 (1995).

19. Flanigen, E. M., Khatami, H., and Szymanski, H. A., *Adv. Chem. Ser.* **101**, 201 (1971).

20. Ghamami, L., and Sand, L. B., *Zeolites.* **3**, 155 (1983).

21. Barrer, R. M., *Zeolites.* **1**, 130 (1981).

22. (a) Ernst, S., Jacobs, P. A., Martens, J. A., and Weitkamp, J., *Zeolites.* **7**, 7 (1987).

    (b) Kotasthane, A. N., Shiralkar, V. P., Hegde, S. G., and Kulkarni, S. B., *Zeolites.* **6**, 253 (1986).

23. Reddy, J. S., and Kumar, R., *Zeolites.* **12**, 45 (1992).

24. Thangaraj, A., Ph.D. Thesis, University of Pune, (1991).

25. (a) Rao, P. R. H. P., Ph.D. Thesis, University of Pune, (1992).

    (b) Ramesh Reddy, K., Ph.D. Thesis, University of Pune, (1993).

26. Crea, F., Nastro, A., Nagy, J. B., and Aiello, R., *Zeolites*, **8**, 262 (1988).

27. Ratnasamy, P., Kotasthane, A. N., Shiralkar, V. P., Thangaraj, A., and Ganapathy, S., *ACS Symposium Series*, Occelli, M. L., and Robson, H. E., (Eds.,) **398**, Ch. 28 (1989).

28. Marler, B., Dehnbostel, N., Eulert, H. H., Gies, H., and Liebau, F., *J. Incl. Phenom.* **4**, 339 (1986).

29. Eapen, M. J., Reddy, K. S. N., and Shiralkar, V. P., *Zeolites.* **14**, 295 (1994).

30. Ramesh Reddy, K., Kumar, R., Veda Ramaswamy, and Ramaswamy, A. V., *Zeolites.* **14**, 326 (1994).

31. Otake, M., *Zeolites.* **14**, 142 (1994).

32. Otake, M., JPN Kokai. Pat. 285 813 (1991).

33. Shiralkar, V. P., and Clearfield, A., *Zeolites.* **9**, 363 (1989).

34. Bhat, R. N., and Kumar, R., *J. Chem. Technol. Bio. Technol.* **48**, 458 (1990).

35. Jacobs, P. A., and Martens, J. A., *Stud. Surf. Sci. Catal.* **33**, 58 (1987).

36. Casci, J. L., and Lowe, B. M., *Zeolites.* **3**, 186 (1983).

Chapter III

Physico - Chemical Characterization of MCM-22

3.1 INTRODUCTION

Samples of MCM-22, synthesized[1,2] as described in chapter II, have been characterized using various physico-chemical techniques. MCM-22 samples were synthesized in a wide range of SiO_2/Al_2O_3 ratios of 30 - 150. Representative samples from this range were chosen for characterization. The high silica, as-synthesized sample (SiO_2/Al_2O_3 = 80) was used for the high resolution solid state MAS NMR spectroscopic studies. The sample exhibited well resolved ^{29}Si NMR spectrum. Other as-synthesized and calcined samples were characterized by techniques, such as, FT-IR, thermal analyses, XRD and scanning electron microscopy. The characterization results confirmed that there was no phase change after the calcination of the samples.

This chapter summarizes the results of the physico-chemical characterization of the MCM-22 samples. The discussion focuses on XRD, SEM, framework I.R., MAS NMR and thermal analyses of these materials.

3.2 EXPERIMENTAL

3.2.1 CHEMICAL ANALYSIS

Wet chemical analyses were carried out in order to determine the chemical composition of the gels and the crystalline materials. The typical analysis of a synthetic sample is as follows. A clean, dried and previously weighed [W_o] Pt crucible was used. Approximately 200 mg of the calcined sample was taken in this crucible [W_1]. The sample was heated in the Bunsen flame for 3 hours and cooled in a descicator. The heating, cooling and weighing were repeated to get concordant values. The final weight was recorded as [W_2] . The difference between the weights before and after ignition provides the weight loss of the sample on ignition [LOI]. The dry weight was noted. To the sample in the crucible, 2 drops of concentrated sulphuric acid and 10

ml of concentrated HF [48 %] were added. The contents were heated over a hot plate till most of the silica had been expelled. Again, 10 ml of HF was added and the contents were heated. This procedure was further repeated twice to ensure that all the silicon species had been expelled as H_2SiF_6. The crucible was then heated over a Bunsen flame to red heat for 2 hours. It was then cooled in a descicator. Concordant weight was noted [W_3].

Approximately 200 mg of potassium pyrosulphate was added to the contents in the crucible and the mixture was fused. This fused mixture was dissolved in hot water and diluted to a known volume. A blank was also prepared in each case without using the any solid, repeating the same procedures. The solutions were analyzed for aluminium and sodium by an atomic absorption spectrophotometer.

$[W_1 - W_o]$ = W_i gives the weight of sample taken initially.

$[W_i - W_2]$ = W_{LOI} gives the weight loss after ignition [LOI].

$[W_{LOI} - W_3]$ = W_{Si} gives the weight loss due to silicon.

From these weights and the results obtained from atomic absorption spectroscopy, SiO_2/Al_2O_3 ratios of the samples were determined.

3.2.2 X-RAY DIFFRACTION

Powder X-Ray diffraction patterns of all MCM-22 (both as-synthesized and calcined) samples were recorded using a computer-automated X-Ray diffractometer (Rigaku, Model D MAX III VC, Japan). The samples were first ground and dried at 383 K for 2 h. The samples were equilibrated over a saturated $CaCl_2$ solution at room temperature for 6 hours prior to measurements. They were packed on a glass sample holder and subjected to nickel filtered Cu $K\alpha$ radiation through a graphite monochromator. Data were collected in the 2θ range of 4° to 50° in steps of 0.02° and a step time of 10 sec with continuous rotation of the sample during the scan. Silicon was used as the internal standard.

The relative intensities (I/I_o x 100) of the observed peaks were obtained after smoothing, background correction and subsequent $K\alpha_2$ stripping. The observed interplanar "d" spacings were used for indexing the diffraction lines by trial and error methods using PDP-11 software (University of Trieste, Italy) and automated indexing programs like VISSER[3] and TAUPIN. The patterns were indexed based on an orthorhombic unit cell.[4,5] The unit cell parameters obtained were refined using least square fitting of the indexed lines of the different samples.

3.2.3 SCANNING ELECTRON MICROSCOPY [SEM]

Crystallite size and morphology of the as-synthesized and calcined zeolite samples were determined by SEM (Model JSM, 5200, JEOL, Japan) equipped with energy dispersive X-ray analysis (EDX). The samples were sputtered with gold to prevent surface charging and to protect from thermal damage due to the electron beam.

3.2.4 INFRARED SPECTROSCOPY

Self-supported KBr pellets containing MCM-22 samples (1 mg) and KBr (300 mg) were used for framework I.R. analysis. The FT-IR spectra were recorded in a Nicolet SXB FT-IR spectrometer. The framework region between 400 cm^{-1} to 1350 cm^{-1} and the hydroxyl region between 3500 cm^{-1} - 3800 cm^{-1} were studied.

Self-supported wafers of the samples ($\sim$ 6 mg/cm^2) were prepared and loaded in the cell for studying the hydroxyl region. Each sample was evacuated at 673 K for 4 h to a pressure of 10^{-6} Torr. The sample was then cooled to 373 K. Pyridine (vapour pressure = 10 mm of Hg) was adsorbed for 1 h and was desorbed for 1 h at the same temperature and pressure. Each spectrum was averaged over 1000 scans and had a spectral resolution of 4 cm^{-1}.

3.2.5 THERMAL ANALYSIS

Simultaneous TGA-DTA analyses of the as-synthesized samples were carried out in a computer-controlled thermal analyzer (Setaram, France, Mode TG-DTA 92-12), in air and

helium atmospheres in the temperature range of 298 - 1173 K with a linear heating rate of 10 K min^{-1}.

The temperature-programmed decomposition/desorption (TPD) of the template molecules in the as-synthesized samples under an inert atmosphere (Argon) was carried out in a separate apparatus (Sorbstar, Institute of Isotopes, Hungary). The desorbates were analyzed with a thermal conductivity detector (TCD) cell coupled with a quadrupole mass spectrometer (Hilden, UK).

3.2.6 SOLID STATE MULTINUCLEAR MAS NMR SPECTROSCOPY

Multinuclear Solid State MAS NMR spectroscopy was used to characterize the as-synthesized, calcined and dealuminated samples with higher SiO_2/Al_2O_3 ratios. Solid state ^1H, ^{27}Al and ^{29}Si MAS NMR spectra were recorded at ambient probe temperature (298 K) on a Bruker MSL-300 FT NMR spectrometer at Larmor frequencies of 300.13, 78.17 and 59.60 MHz, respectively. ^1H - ^{29}Si Cross-Polarization (CP-MAS) experiments were performed using single contact Hartmann-Hahn match at an applied radio frequency field of 45 kHz. The spinning speed was maintained at approximately 2.9 - 3.3 kHz. Bloch Decay spectra were obtained using a 45° flip angle pulse (2 μ s) followed by acquisition. The standards used for the calibration of ^{29}Si, ^{27}Al, ^{13}C and ^1H spectra are given below :

Isotope	Calibration Standards
^{29}Si	Tetramethyl silane [TMS]
^{27}Al	Hexaaquo aluminium III complex, $[Al(H_2O)_6]^{3+}$
^{13}C	Adamantane
^1H	Tetramethyl silane [TMS]

78

3.3 RESULTS AND DISCUSSIONS

3.3.1 CHEMICAL ANALYSIS

The chemical composition of the samples have been presented in Chapter II (Table 2.1). It can be seen that the products have SiO_2/Al_2O_3 ratios less than those of the input values.

3.3.2 X-RAY DIFFRACTION

Zeolite samples with SiO_2/Al_2O_3 ratios of 28, 40, 56, 80, 96 and 146 (Figure 3.1) were prepared[1,2] and characterized by powder X-Ray diffraction methods to determine the phase purity, to estimate the crystal symmetry and unit cell parameters.[5] Rubin and Chu,[1] and Puppe and Weisser[6] have found that the zeolite samples could be crystallized in a SiO_2/Al_2O_3 range of 30 - 150. Samples with SiO_2/Al_2O_3 ratios up to 100 were found to be highly crystalline beyond which the crystallinity was found to decrease. The samples with higher SiO_2/Al_2O_3 ratios were found to require more crystallization time than the samples with lower SiO_2/Al_2O_3 ratios. Corma et al.[7a] have reported similar observations. When the crystallization time was decreased by increasing the hydroxide concentration, it was found that, samples were contaminated with other zeolitic phases namely, ZSM-5, mordenite and ferrierite. Synthesis of samples with SiO_2/Al_2O_3 ratios higher than 1000 lead to the formation of "Nonasil".[8,9] This material has already been reported in the literature to crystallize in the presence of the same template (hexamethyleneimine).[8,9] The XRD profiles of the as-synthesized and calcined samples (SiO_2/Al_2O_3 = 28) are given in Figure 3.2. It is seen from the figure that the calcined samples have slightly higher peak intensities than the as-synthesized samples, though in general, the XRD patterns are similar. The general broadness of the peaks (see Figure 3.2) can be attributed to the presence of stacking faults or defects. MCM-22[1] has been proposed to be isostructural with PSH-3,[6] SSZ-25[10] and FU-1.[11,12] PSH-3 was first synthesized in 1984 by Puppe and Weisser[6] using hexamethyleneimine as the organic templating agent. Zones[10] and Dewing et al.[12]
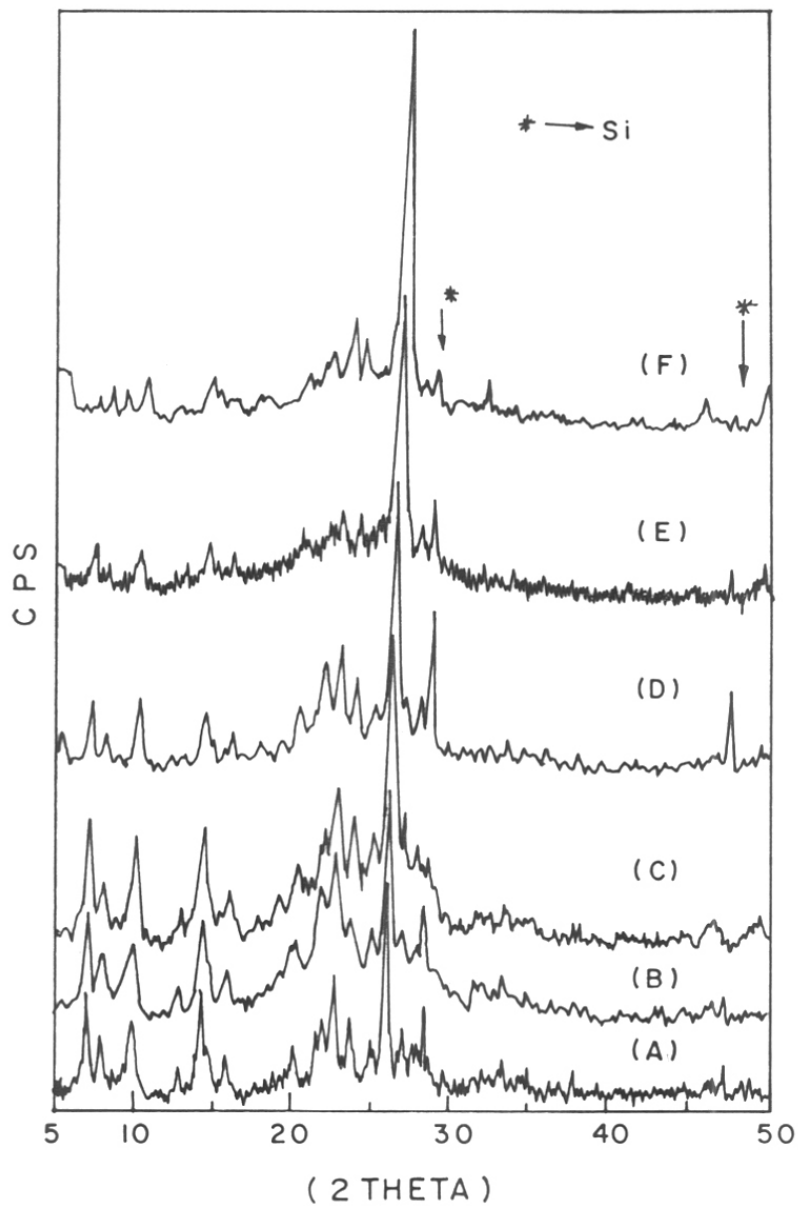
Figure 3.1   XRD profiles of calcined MCM-22 samples with different
SiO$_2$/Al$_2$O$_3$ ratios.

SiO$_2$/Al$_2$O$_3$ ratios : (A) 28, (B) 40, (C) 56, (D) 80, (E) 96 and
(F) 140. (*) Peak position of silicon (used as internal standard).
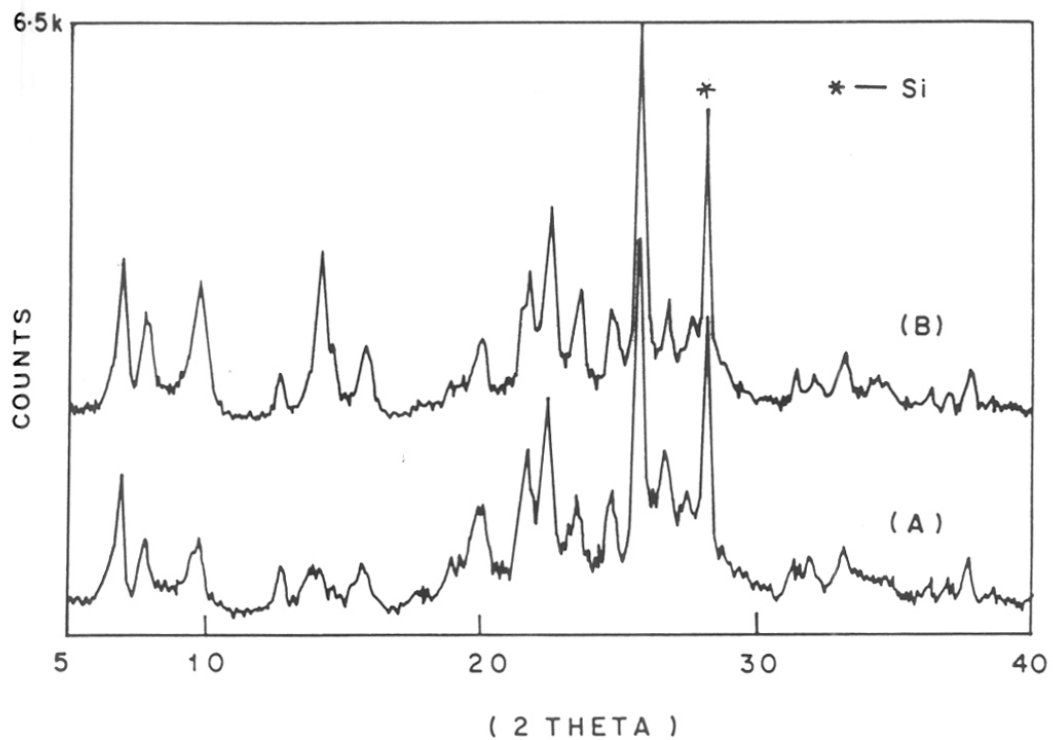
Figure 3.2   X-Ray diffraction patterns of sample (A; SiO_2/Al_2O_3 = 28)

(A) As-synthesized and (B) calcined forms.

(*) Peak position of silicon (used as internal standard).

used, respectively, 1,1,1-trimethyl admantammonium hydroxide and tetramethyl ammonium salt as the templates in the synthesis of SSZ-25 and FU-1. The XRD lines of the MCM-22 sample with SiO_2/Al_2O_3 = 28 along with the reported values[13] for MCM-22,[1] PSH-3,[6] SSZ-25[10] and FU-1,[12] are presented in Table 3.1. The data demonstrate that the MCM-22 synthesized, in this work, shows close structural correspondence to materials reported by several other research groups.[6, 10-12] The ranking in the agreement of our data with the earlier reported materials is as follows : MCM-22 > PSH-3 > SSZ-25 > FU-1. The following empirical method[14] was used in the matching of the patterns. Three regions having intense peaks common to the zeolites being compared corresponding to "d" values between (i) 1.3 nm - 0.85 nm, (ii) 0.41 nm - 0.345 nm and (iii) 0.343 nm - 0.320 nm were chosen. Each region had two reasonably intense peaks. The separation between the two peaks in each region was compared between the different zeolites. The peak separation ("Δd") values in the 3 regions for the different zeolites are listed in Table 3.2. The values match in the following order:

Range I: MCM-22 (SiO_2/Al_2O_3 = 28) ("Δd" = 0.347) < MCM-22 (0.350) < SSZ-25 (0.352) < PSH-3 (0.379) > FU-1 (0.116).

Range II: MCM-22 (SiO_2/Al_2O_3 = 28) ("Δd" = 0.056) > MCM-22 (0.054) > PSH-3 (0.053) > SSZ-25 (0.043) > FU-1 (0.034).

Range III: MCM-22 (SiO_2/Al_2O_3 = 28) ("Δd" = 0.022) = MCM-22 (0.022) = PSH-3 (0.022); (in the cases of SSZ-25 and FU-1, lines were absent in this region).

Eventhough the intensities of the major peaks are similar for the different zeolites, there are significant differences in the intensities of the others. It is noticed that, generally, the deviations are too large in the case of SSZ-25 and FU-1. It is appears that the material (MCM-22; SiO_2/Al_2O_3 = 28) is probably structurally similar to PSH-3 and not SSZ-25[10] and FU-1.[12] PSH-3[6] matches well in ranges II and III, but has a large deviation in range I. The lines of MCM-22 (Mobil) match well with our samples and only minor deviations are noted.

Table 3.1 Comparison of X-Ray powder diffraction data of the synthesized sample with MCM-22,[1] PSH-3,[9] SSZ-25[13] and FU-1.[15]

| MCM-22 | | Values from Literature[16] | | | | | | | |
| $SiO_2/Al_2O_3 = 28$ | | MCM-22 | | PSH-3 | | SSZ-25 | | FU-1 | |
`d' (nm)	I/I$_o$ x 100	`d' (nm)	I/I$_o$ x 100	`d' (nm)	I/I$_o$ x 100	`d' (nm)	I/I$_o$ x 100	`d' (nm)	I/I$_o$ x 100
-	-	3.000	25	-	-	-	-	-	-
-	-	2.210	10	-	-	2.550	17	-	-
1.229	40	1.236	96	1.263	100	1.230	100	-	-
1.106	26	1.103	47	1.092	30	1.100	55	-	-
-	-	-	-	-	-	-	-	0.951	31
0.882	34	0.886	51	0.884	60	0.878	63	0.835	8
0.691	-	0.686	11	0.686	5	-	-	0.692	28
0.685	11	-	-	-	-	-	-	0.661	9
0.615	44	0.618	42	0.615	40	0.617	40	0.626	9
0.603	17	0.600	15	-	-	-	-	-	-
0.555	17	0.554	20	0.550	15	0.551	17	0.525	16
-	-	0.495	5	0.492	5	0.491	5		
0.455	5	0.464	5	0.460	1	-	-	0.461	63

0.440	16	0.441	20	0.439	15	-	-	0.448	6
-	-	0.425	5	-	-	-	-	0.435	13
0.408	23	0.410	20	0.409	20	-	-	0.407	19
0.405	32	0.406	13	-	-	-	-	0.400	9.4
0.391	48	0.391	30	0.391	30	0.390	38	0.389	13
0.373	24	0.375	13	0.375	5	-	-	0.373	23
0.356	20	0.356	20	0.356	3	-	-	-	-
0.354	13	-	-	-	-	0.347	20	-	-
0.352	13	-	-	-	-	-	-	-	-
0.342	100	0.342	100	0.341	100	0.342	65	0.344	100
0.330	24	0.330	14	0.330	2	-	-	-	-
0.320	20	0.320	15	0.319	3	-	-	-	-
-	-	0.314	10	0.311	2	-	-	-	-
-	-	0.299	5	-	-	-	-	-	-
0.283	7	-	-	0.283	2	-	-	-	-
0.282	7	0.282	5	-	-	-	-	-	-
0.277	7	0.278	5	-	-	-	-	-	-
0.276	7	-	-	-	-	-	-	-	-
0.268	13	0.268	5	0.269	3	-	-	0.268	34

Table 3.2   An analysis of peak separations[17] in 3 empirical regions.

	"Δd" Range		
	Region I	Region II	Region II
Zeolites	1.30 - 0.85 (nm)	0.41 - 0.345 (nm)	0.343 - 0.320 (nm)
MCM-22	$(1.229 - 0.882) =$ 0.347	$(0.408 - 0.352) =$ 0.056	$(0.342 - 0.320) =$ 0.022
MCM-22[1]	$(1.236 - 0.886) =$ 0.350	$(0.410 - 0.356) =$ 0.054	$(0.342 - 0.320) =$ 0.022
PSH-3[9]	$(1.263 - 0.884) =$ 0.376	$(0.409 - 0.356) =$ 0.053	$(0.341 - 0.319) =$ 0.023)
SSZ-25[13]	$(1.230 - 0.878) =$ 0.352	$(0.390 - 0.347) =$ 0.043	-
FU-1[15]	$(0.951 - 0.835) =$ 0.116	$(0.407 - 0.373) =$ 0.034	-

Thus, the material synthesized in our laboratory corresponds to MCM-22 reported earlier by the Mobil workers.

The XRD lines of the sample with $SiO_2/Al_2O_3 = 28$ along with their relative intensities $(I/I_o \times 100)$ and "h k l" values are presented in Table 3.3. As the SiO_2/Al_2O_3 ratio decreases, the amount of the larger Al^{3+} ions (Al^{3+} ionic radius = 0.039 nm; Si^{4+}, ionic radius = 0.026 nm) in the framework positions increases. This leads to increase in the unit cell parameters and the unit cell volume.

The unit cell parameters (Table 3.4) were calculated based on an orthorhombic unit cell.[2,4,5] The indexing was performed by trial and error methods using PDP-11 software (University of Trieste, Italy). The system with least deviation and maximum figure of merit was chosen as the crystal symmetry of the zeolite. Only "Orthorhombic" symmetry could be fitted satisfactorily and all the lines have been indexed. The unit cell parameters calculated based on orthorhombic symmetry were latter refined using other software such as, VISSER[3] and HOCT.

The structure of zeolite MCM-22 was reported by Leonowicz et al.[4] Boron-MCM-22 has been reported to crystallize in a hexagonal symmetry with 8 distinct T sites, whereas, the corresponding aluminum form (Al-MCM-22) exhibited orthorhombic symmetry with 13 crystallographically non-equivalent T sites. The unit cell parameters of B-MCM-22 and Al-MCM-22 reported by Leonowicz et al.[4] are given in Table 3.4 for comparison. The calculated unit cell parameters[8] (Table 3.4) agree well with the reported values.[4]

Recently, Corma et al.[7a] have reported the synthesis and characterization of zeolite MCM-22. The XRD patterns agree well with that reported by Corma et al.[7a] Unvericht et al.[16] have also reported the synthesis of zeolite MCM-22 and have carried out characterization of the samples by various techniques. Our results match their data.[7,16]

Table 3.3   Index planes along with the unit cell parameters with least square fitting for zeolite MCM-22 sample with $SiO_2/Al_2O_3 = 28$ based on orthorhombic unit cell.

"h"	"k"	"l"	"d" Obs.	"d" Cal.	ΔD	I/I_o x 100
2	0	0	12.285	12.303	−0.018	40
2	0	1	11.056	11.017	0.039	26
1	1	2	8.820	8.769	0.052	34
0	2	1	6.905	6.911	−0.007	11
3	1	1	6.852	6.848	0.004	19
4	0	0	6.150	6.151	−0.001	44
2	2	1	6.025	6.026	−0.001	17
4	0	1	6.001	5.970	0.031	17
2	2	2	5.552	5.552	0.000	17
5	1	1	4.553	4.576	−0.023	5
1	3	2	4.395	4.402	−0.007	16
0	2	5	4.083	4.079	0.004	23
6	0	1	4.050	4.046	0.004	32
1	1	6	3.912	3.915	−0.003	48
1	3	4	3.746	3.748	−0.001	24

"h"	"k"	"l"	"d" Obs.	"d" Cal.	ΔD	I/I$_o$ x 100
4	2	4	3.731	3.731	0.000	25
0	4	1	3.555	3.561	−0.007	20
0	0	7	3.541	3.536	0.005	19
6	2	1	3.519	3.527	−0.008	13
6	0	4	3.418	3.418	0.000	100
0	4	3	3.300	3.299	0.001	24
2	4	3	3.196	3.186	0.010	20
8	2	0	2.828	2.828	0.000	7
7	3	1	2.819	2.817	0.002	7
4	4	4	2.773	2.776	−0.003	7
2	2	8	2.768	2.770	−0.002	7
8	0	4	2.755	2.754	0.001	7
3	5	1	2.700	2.700	0.000	7
7	3	3	2.683	2.682	0.001	13

"a" Å	"b" Å	"c" Å
24.606 ± 0.005	14.395 ± 0.005	24.753 ± 0.005

Table 3.4 Lattice parameters of the zeolite samples based on an orthorhombic symmetry.

SiO₂/Al₂O₃	Unit cell parameters (Å)			Unit cell volume[@]
	"a"	"b"	"c"	(Å)³
28	24.606	14.395	24.753	8767.596
40	24.618	14.360	24.794	8763.614
56	24.620	14.343	24.821	8764.907
80	24.635	14.289	24.875	8756.237
96	24.642	14.275	24.811	8726.630
140	24.653	14.197	24.929	8725.116
[+]B-MCM-22[7]	14.115	14.115	24.882	4293.040
Al-MCM-22[7]	24.447	14.115	24.882	8586.017

[@]Unit cell volume : Orthorhombic symmetry.
[+]B-MCM-22   : Hexagonal symmetry.

89

3.3.3 SCANNING ELECTRON MICROSCOPY [SEM]

SEM pictures of the as-synthesized and calcined samples with varying SiO_2/Al_2O_3 ratios are presented in Figures 3.3 and 3.4, respectively. The samples were found to be free from amorphous materials and had uniform platelet morphology (approximately 1 - 2 μm diameter and 0.1 - 0.2 μm thick) bunched into 4 - 5 μm particles. Some fine needles/fibres of 1.5 - 2 1 μm length with an aspect ratio of approximately 5 were also observed. Both the as-synthesized (Figure 3.3) and calcined samples (Figure 3.4) have similar morphologies.

3.3.4 INFRARED SPECTROSCOPY

FT-IR spectroscopy is an useful technique to determine the secondary building units (SBUs) present in a zeolite system.[17,18] Each zeolite has its own characteristic bands apart from some common bands. For example, metallosilicates[19-23] such as TS-1, VS-1 and their MEL analogs (TS-2 and VS-2, respectively) have characteristic bands at 950 cm^{-1} - 970 cm^{-1}. The two regions that provide useful informations about the structure of zeolites are : (a) framework region extending from 200 cm^{-1} to 1400 cm^{-1} and (b) the hydroxyl region extending from 3500 cm^{-1} to 3700 cm^{-1}.

Though it is generally difficult to identify the structure of the zeolite from its infrared spectrum, the characteristic double ring and T - O bending frequencies at 555 cm^{-1} and 445 cm^{-1} are attributed to the presence of 5 MR in MCM-22 samples. The framework infrared spectra of samples (A) - (F) are given in Figure 3.5. I.R. spectrum of sample (A) is depicted in Figure 3.6(A). The prominent bands highlighted in Figure 3.6(A) are attributed to the different internal tetrahedral and external linkage vibrations and have been assigned based on the I.R. analysis reported by Flanigen et al.[17,18] These assignments are summarized in Table 3.5 (A).

Corma et al.[7] have observed a similar type of spectrum and the two shoulders at 1187 cm^{-1} and 1090 cm^{-1} were attributed to assymetric stretching T - O vibrations and external vibrations of TO_4 tetrahedra respectively. In the case of dealuminated zeolite Y, Flanigen et
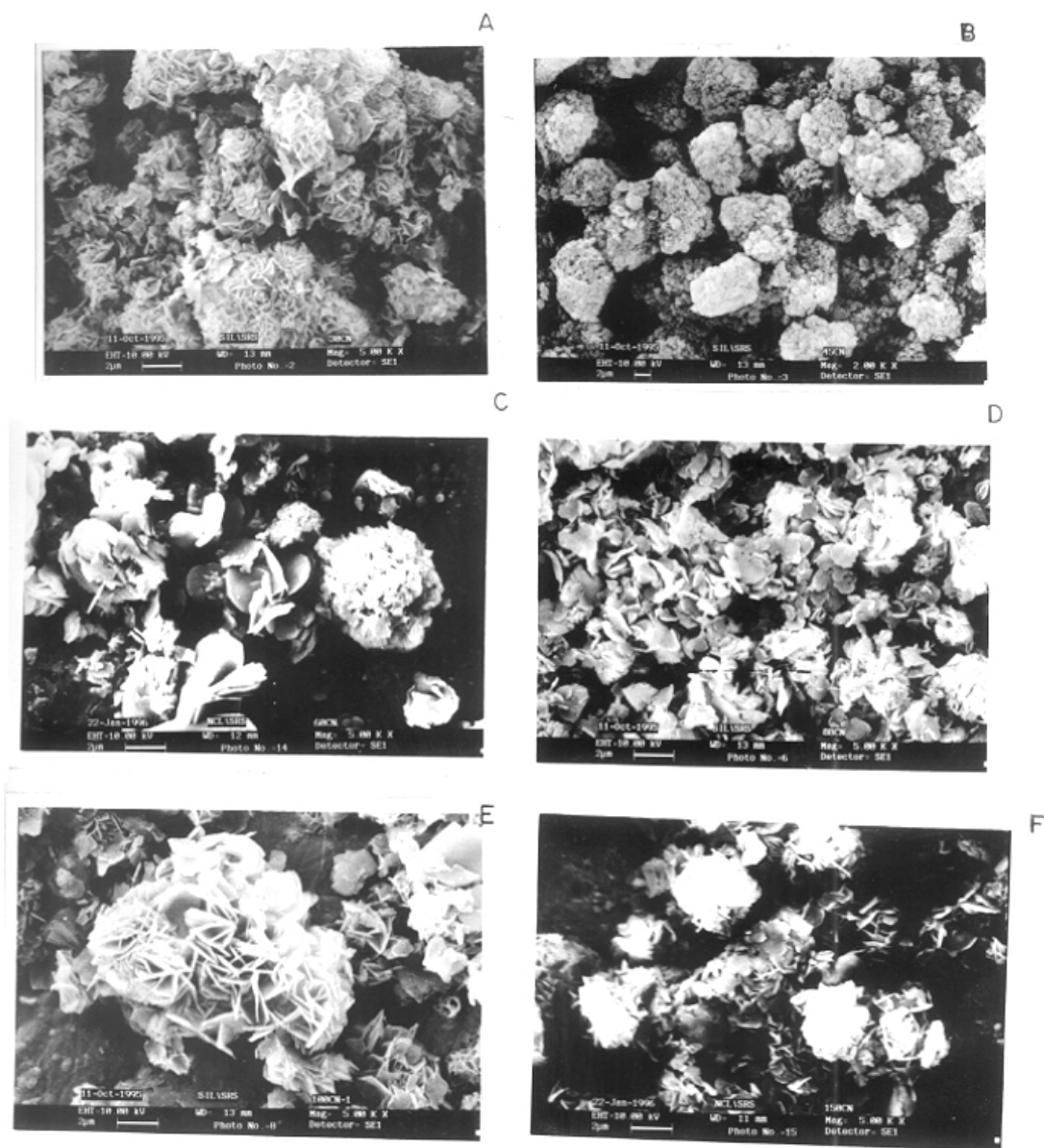
Figure 3.3 Scanning Electron Micrograph (SEM) pictures of uncalcined MCM-22 samples with different SiO_2/Al_2O_3 ratios.

SiO_2/Al_2O_3 ratios : (A) 28, (B) 40, (C) 56, (D) 80, (E) 96 and (F) 140.
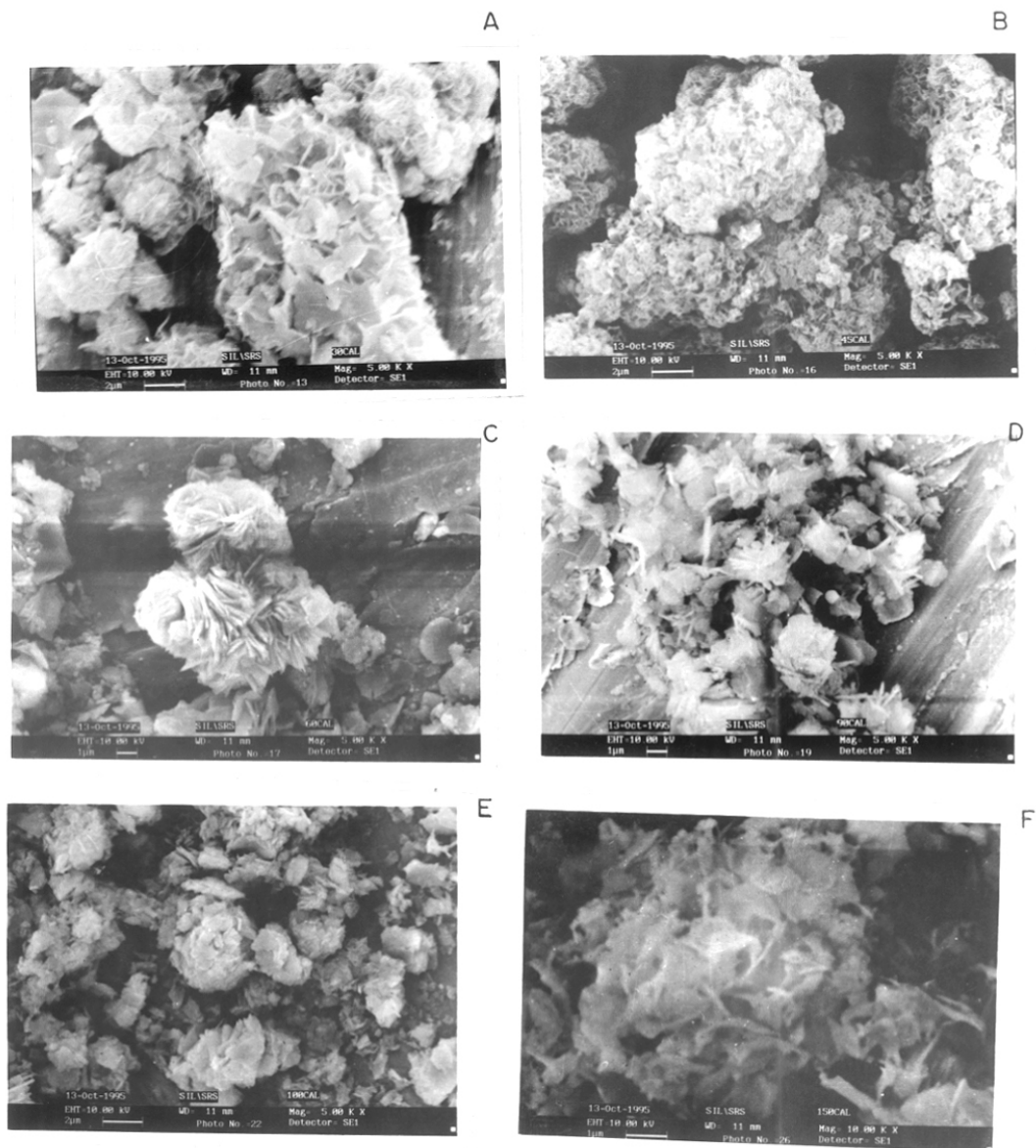
Figure 3.4   SEM pictures of calcined MCM-22 samples with different
SiO$_2$/Al$_2$O$_3$ ratios.
SiO$_2$/Al$_2$O$_3$ ratios : (A) 28, (B) 40, (C) 56, (D) 80, (E) 96 and
(F) 140.
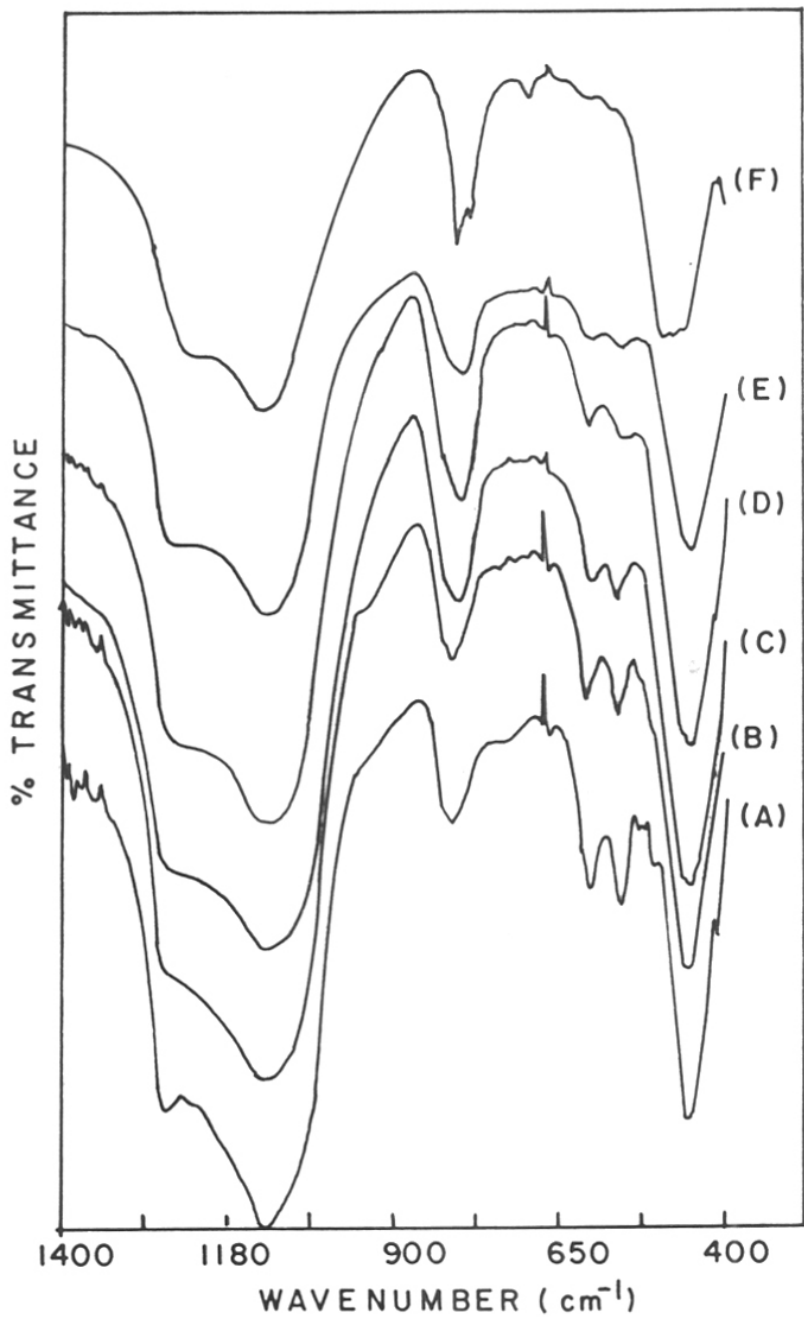
Figure 3.5   Framework I.R. spectra of MCM-22 samples with varying

SiO$_2$/Al$_2$O$_3$ ratios.

SiO$_2$/Al$_2$O$_3$ ratios : (A) 28, (B) 40, (C) 40, (D) 80, (E) 96

and (F) 140.
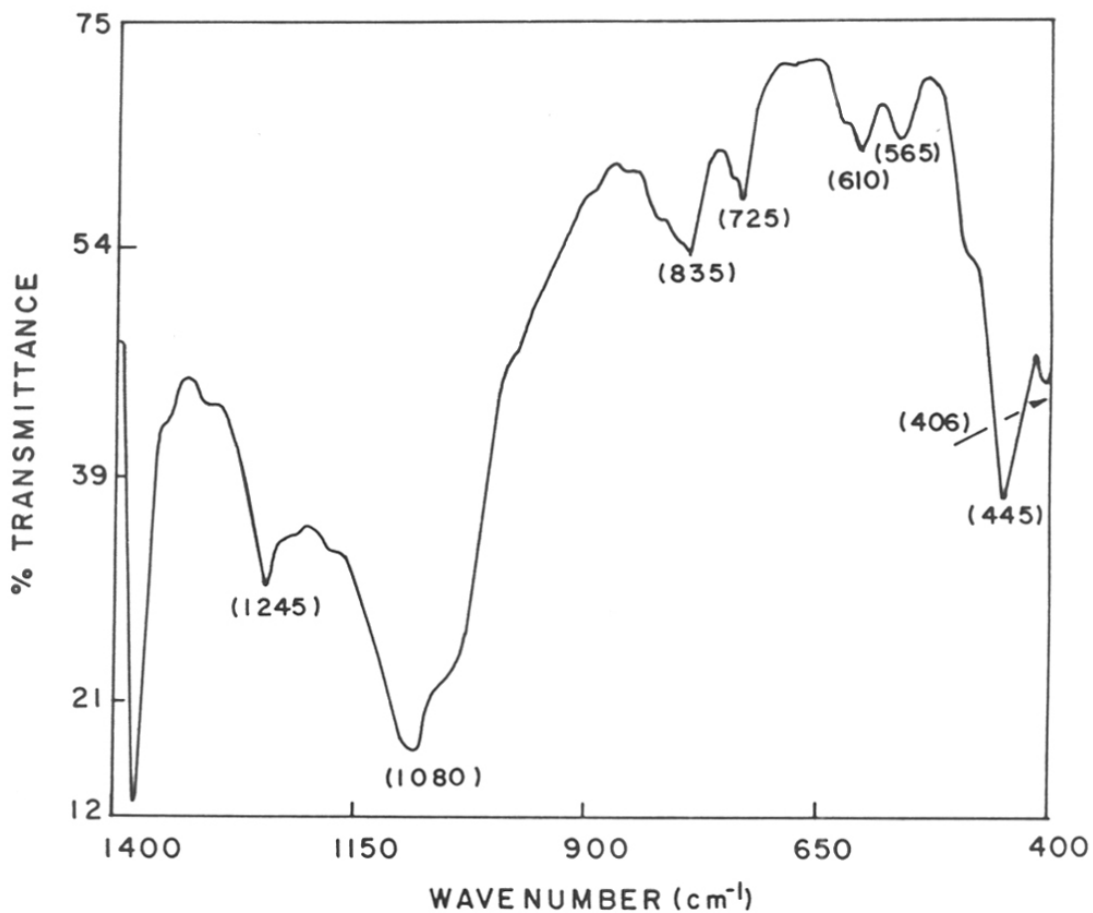
Figure 3.6 (A)   Framework infrared spectrum of MCM-22 sample with

SiO$_2$/Al$_2$O$_3$ = 28.

Table 3.5 (A)   Tentative assignments[17] of infrared bands in the framework region

obtained over sample A ($SiO_2/Al_2O_3 = 28$).

$\bar{\nu}$ cm^{-1}	Assignments
1245	External linkages : Asymmetric stretching
1080	Internal tetrahedra : Asymmetric stretching
835	External linkages : Symmetric stretching
725	Internal tetrahedra : Symmetric stretching
610 and 555	External linkages : Double ring (Pentasil)
445	Internal tetrahedra : T-O bend
406	Pore openings (12 MR)

Table 3.5 (B)   Tentative assignments of infrared bands in the hydroxyl region
obtained over sample A ($SiO_2/Al_2O_3 = 28$).[24-26]

$\bar{\nu}$ cm^{-1}	Assignments
3747	External silanol groups at the crystal surface..
3700 and 3500	Internal silanols in defects.
3700	Internal silanols observed in zeolite Y.[24,25]
3500	Internal silanols observed in ZSM-5.[26]

al.[17,18] have assigned the bands in the region of 402 cm^{-1} - 408 cm^{-1} to 12 MR pore openings. The occurrence of a weak band at 406 cm^{-1} in MCM-22 suggests the probable presence of 12 MR.

The infrared spectrum of the hydroxyl region has been recorded for sample (A) (Figure 3.6(B)). The assignments of the bands observed in the hydroxyl region are presented in Table 3.5(B). Bands at 3744 cm^{-1}, 3725 cm^{-1} to 3672 cm^{-1} and 3625 cm^{-1} to 3615 cm^{-1} are attributed to external silanol groups, defect sites, hydroxyl (OH) groups associated with non-framework aluminum species and bridging hydroxyl groups, respectively. A very weak shoulder at around 3700 cm^{-1} was assigned to internal silanols. The external silanols reside at the crystal surface (3747 cm^{-1}) and the internal silanols (3700 cm^{-1} and 3500 cm^{-1}) in defects. They are involved in molecular interactions with cavity walls.[7b] The internal silanols in zeolite Y occur at 3700 cm^{-1}, while those in ZSM-5 occur at 3500 cm^{-1}.[24-26] It should be noted that the samples with SiO$_2$/Al$_2$O$_3$ ~ 30 and 45 exhibited NMR signals due to non-framework aluminium species (discussed in the following sections) and the absorption at 3725 cm^{-1} may be attributed to hydroxyl (-OH) groups associated with these species.

A self-supported wafer of sample A (~6 mg/cm^2) was prepared. This sample was evacuated at 673 K for 4 h to a pressure of 10^{-6} Torr. It was then cooled to 373 K. Pyridine (vapour pressure = 10 mm of Hg) was adsorbed for 1 hr and was desorbed again for 1 h. The sample was scanned and the results were averaged over 1000 scans with a spectral resolution of 4 cm^{-1}. I.R. spectrum of the pyridine sorbed sample is presented in Figure 3.6(C). Sorption of bases such as ammonia, pyridine and pyrole are used to determine the nature of the acid sites present in zeolites. The bands at 1454 cm^{-1} and 1540 cm^{-1} are due to the Lewis and Brönsted acid centres, respectively.[27] The existence of pyridinium ion is indicated by the presence of a band at 1541 cm^{-1}. Corma *et al.*[7b] have also observed a similar type of infrared spectrum upon adsorption of pyridine and the observation of an I.R. band at 1450 cm^{-1} has been attributed to
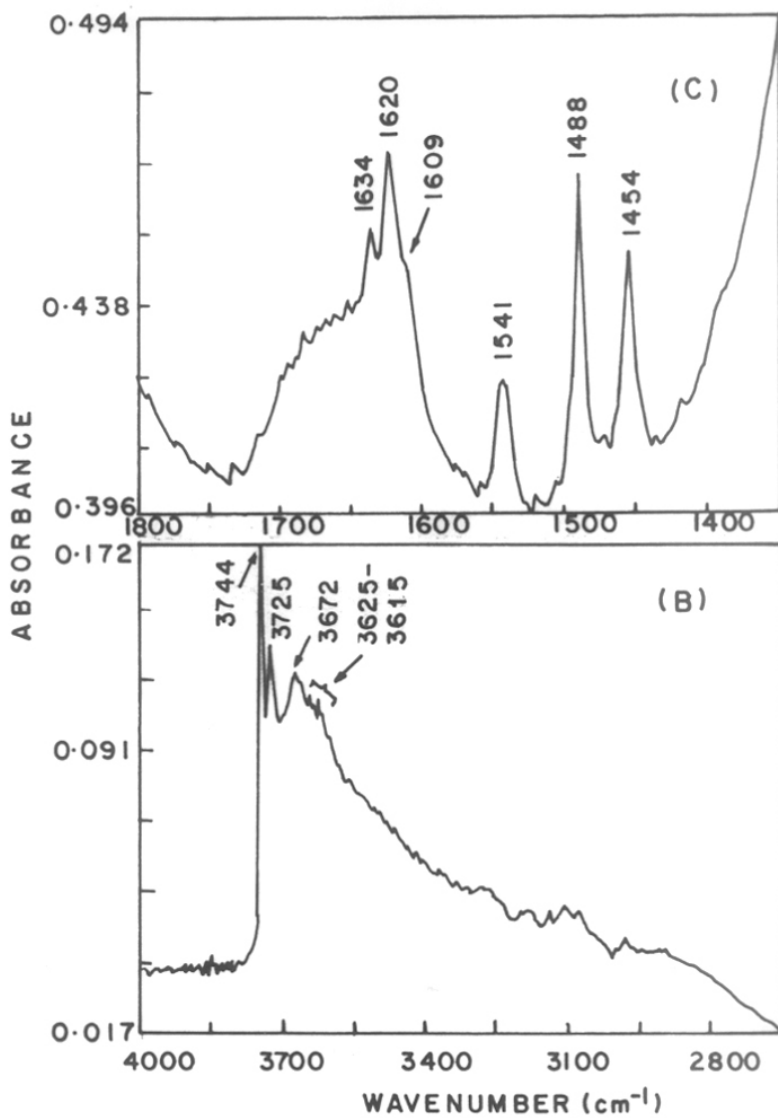
Figure 3.6 (B) Infrared spectrum of the hydroxyl region ($SiO_2/Al_2O_3 = 28$).

(C) Pyridine adsorbed over MCM-22 sample with

$SiO_2/Al_2O_3 = 28$ at 373 K for 1 h.

the presence of extra-framework aluminium species, which originated upon calcination and subsequent dealumination from the framework.

3.3.5 THERMAL ANALYSES

The simultaneous TGA-DTA thermograms are presented in Figure 3.7. From Figure 3.7 (B), it is clear that there are three stages of mass loss when the zeolite sample is heated from 298 K to 1000 K. Water desorbs from the zeolite up to about 423 K. The template decomposes in two steps in both inert atmosphere (in helium, Figure 3.7(C)) and air (Figure 3.7(B)). These stages occur below and above 753 K. In the case of helium, the weight loss amounts to a total of 10.8 % in two steps of 6.9 and 3.9 %. In air, the template weight loss is 8.9 % in steps of 3.2 % and 5.7 %. The decomposition of the template (hexamethyleneimine) in inert atmosphere occurs at temperatures below 753 K into small fragments like CH_4, C_2H_4, C_3H_6 and NH_3. This has been confirmed during temperature programmed decomposition studies using quadrupole mass spectrometer. The mass spectrum (Figure 3.7(A)) also reveals that a negligible amount of undecomposed template is desorbed. As these fragments (especially NH_3 and CH_4) are richer in H_2 than the parent compound, a C-rich skeleton remains on the zeolite.

The intriguing aspect of the TGA-DTA experiments is the exothermic decomposition of the template in the helium atmosphere. A similar exotherm was not observed in the case of two other molecular sieves ($AlPO_4$-5 and $AlPO_4$-22) synthesized using the same template hexamethyleneimine. Approximate calculations suggest that the exothermicity of the peak cannot be explained based upon the differences in the heats of formations of the template and hydrocarbon fragments. Both the exothermicity and greater weight loss in helium can be explained if we assume that partial oxidation of the template (especially the hydrogen component) by the surface hydroxyl (OH) groups occurs during its decomposition. In air, the combustion of the H part of the template is rapid, so loss of most of the H and N atoms occurs below 753 K, the rest of the C-skeleton burning at a higher temperature (850 K).[5] The
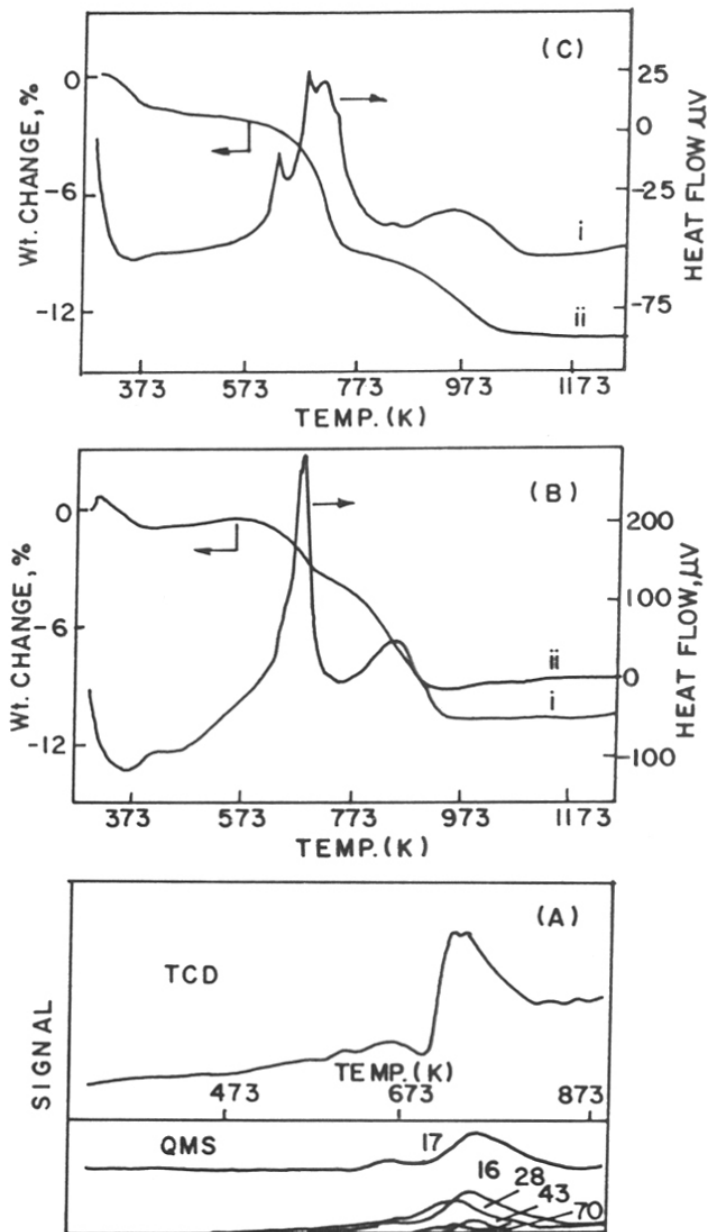
Figure 3.7   TGA/DTA/TPD of as-synthesized MCM-22 (SiO_2/Al_2O_3 = 28).

(A)   Temperature programmed decomposition (TPD) of template.

(B)   TGA/DTA in air.

(C)   TGA/DTA in helium.

fragmentation of the template during desorption in an inert atmosphere and the two-step combustion of the molecule in air indicate that the template is very strongly held inside the zeolite pores. The C, H and N microanalyses of the sample indicated that the template constitutes ~ 10 % of the as-synthesized material.

The above results suggest that at least a part of the template is more strongly adsorbed than the rest. The template could be present in two types of locations: (i) inside the 10-MR channels (stronger interactions) and (ii) inside the 12-membered ring cages (weaker interactions). Souverrijns et al.[28] have concluded that, stronger acid sites are present in 10 MR channels while weaker acid sites are present in the 12 MR cages. Corma et al.[7] have confirmed that, the template plays two roles, namely, charge compensation (hexamethyleiminium ion) and a structure directing role. Since, the strength of acid sites is higher in 10 MR channels, the template ions are more likely to act as charge compensating cations in the 10 MR channels. This might lead to a stronger interaction of the template with the framework.

3.3.6 STRUCTURAL OVERVIEW OF THE ZEOLITE

The structure of the zeolite MCM-22 was reported recently by Leonowicz et al.[4] The zeolite samples of both Al- and B- analogs were used for the structure determination. Since the borosilicate analogs had well defined large crystals and sharp powder diffraction patterns compared to the Al-analogs, B- analogs had been chosen for detailed structural characterization by Leonowicz et al.[4]

The B-MCM-22 was found to exhibit hexagonal crystal symmetry, with the P6/mmm space group. There are 72 T atoms per unit cell. The framework connectivities of dodecasil-H (DOH)[29,30] and MCM-22[4] were found to be similar. The framework connectivities of DOH and MCM-22 are depicted in Figure 3.8. In DOH,[29,30] the hexagonal sheets of $[4^2 5^6 6^3]$ cages share 4-ring faces with adjacent cages within the sheet. The 12 MR cavities are bordered by six cages joined within those sheets. The sheets join along the unit cell `c' direction through single
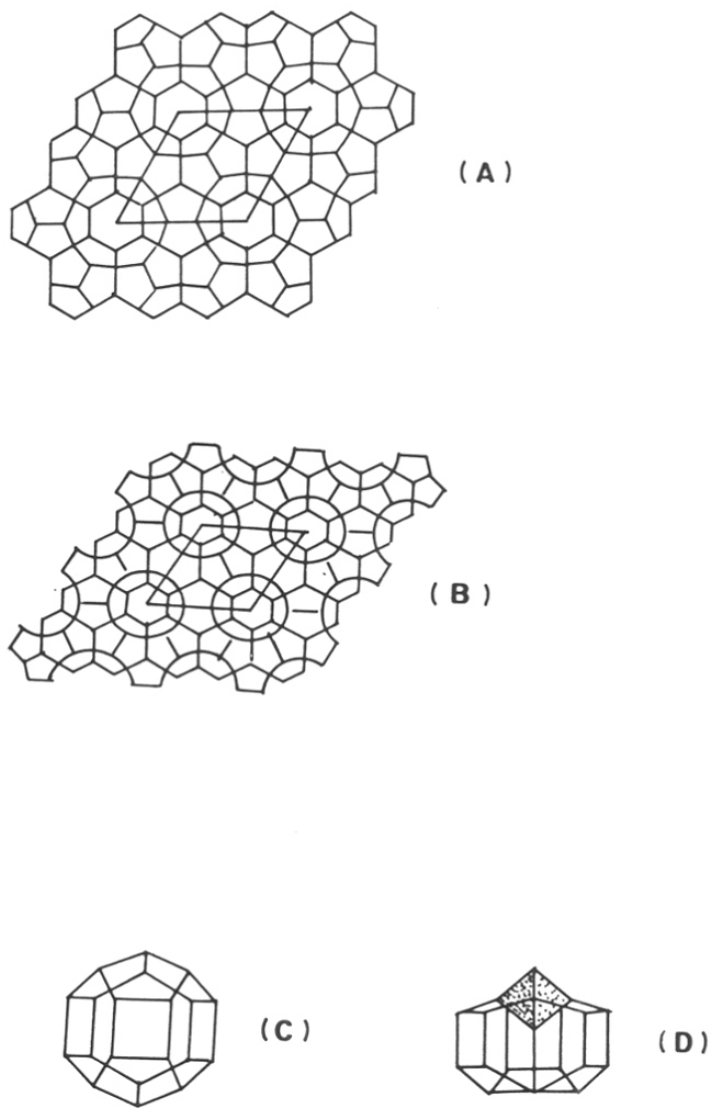
Figure 3.8 Framework connectivities of :

(A) Dodecasil-H [DOH] and (B) MCM-22, (C) $[4^3 5^6 6^3]$ cage in DOH and (D) $[4^3 5^6 6^3 [4^3]]$ cage in MCM-22 (highlighted unit is an unusual unit present in MCM-22).

6-rings that cap the 12 MR cavities at either end. The adjacent sheets were found to be connected directly through bonds between the apical T atoms on the three fold axes of $[4^2 5^6 6^3]$. But in the case of MCM-22,[4] the cage is slightly different. There is an unusual TO_3 cap on the top of the cage over the reversed three fold axis leading to the formation of a small $[4^3]$ unit. This small $[4^3]$ unit has been found only in three zeolites belonging to natrolite group,[31] viz., edingtonite, natrolite and thomsonite. The T atom located on the top of the $[4^3]$ unit links the two identical layers through a shared oxygen atom. Thus, the elliptical 10-membered ring aperture formed is distinct from the usual ones found in medium pore zeolites, viz., MEL system.[32-34] A large super cage with $[4^2 5^8 10^2]$ topology with dimensions inside the cage of 7.1 Å x 7.1 Å x 18.1 Å was found to be present. The super cages were found to stack one above the other by D6R units. Leonowicz *et al.*[4] have reported that there is no connection between the interlayer supercage and the intralayer sinusoidal channel formed by the 10 membered rings. The averaged crystal geometry parameters such as bond lengths and non-symmetry constrained T-O-T angles are 1.61 Å and 136° - 164°, respectively.[35] Some bonds have unusual lengths of 1.49 Å, 1.52 Å and 1.72 Å. By DLS refinement of the MCM-22 model in orthorhombic symmetry with Cmmm space group,[35] reasonable results were obtained with T-O-T bond angles within the range of 157° - 161°. Thus, orthorhombic crystal symmetry was found to be energetically favoured with Cmmm space group having 13 distinct, crystallographically non-equivalent T sites.[35,36]

3.3.7 SOLID STATE MULTINUCLEAR MAS NMR SPECTROSCOPY

The as-synthesized MCM-22 sample (containing nitrogen, CN form) has been characterized by ^1H, ^{13}C, ^{27}Al and ^{29}Si MAS NMR and cross-polarization (CP) techniques. The results obtained are discussed below and compared with the earlier reports.

3.3.7.1 Background

Kennedy *et al.*[35] have used the H-forms of B-MCM-22 and Al-MCM-22 for spectroscopic studies. Deboronation and dealumination were carried out by usual hydrothermal treatments. The resulting highly siliceous materials were characterized by ^{29}Si MAS NMR and spin-lattice relaxation time measurements. Both B- and (Al-) MCM-22 samples were found to exhibit the same type of spectra. 7 distinct peaks with better resolution in the case of the highly siliceous material were identified. The calcined sample gave a broad spectrum which was attributed to smearing and overlapping of silicon resonances. The improved resolution, in the case of the dealuminated sample, has been attributed to the removal of framework aluminum (a quadrupolar nucleus) and the corresponding effect of this dealumination on the distribution of nearest neighbour atoms.

The hexagonal symmetry[35] of MCM-22 has 8 distinct T sites in the ratio of 1 : 3 : 3 : 1 : 1 : 3 : 3 : 3, whereas, the orthorhombic form has 13 T sites in the ratio of 1 : 1 : 1 : 1 : 2 : 2 : 1 : 1: 2 : 2 : 1 : 1 : 2. The seven resonances of the dealuminated samples are in the ratio 3 : 2: 2 : 2 : 3 : 4 : 2. From NMR peak intensities, it is concluded that the orthorhombic form is more favoured.

Progressive saturation techniques[35] were carried out to probe the difference in the spin-lattice relaxation characteristics of the silicon atoms. Kennedy *et al.*[35] have found that a "T" site is "buried" well inside the lattice and is not situated near the channels. They have assigned this slowly relaxing T site as T_3 and T_4 in orthorhombic and hexagonal forms, respectively. Tentative peak assignments have been made on the basis of the observed peak intensities, spin-lattice relaxation time behaviour and the relationship between T-O-T angles and ^{29}Si chemical shifts. A similar situation was observed in the case of highly siliceous ZSM-12, where a "**buried T site**"[37] was found to exist and was assigned as T_5. The tentative assignments[35,36] are given in Table 3.6.

Table 3.6. Tentative assignments[35] of T sites based on NMR chemical shifts

(Orthorhombic form).

Chemical shift (ppm)	T site distribution
−105.5	$T_2 + T_6$
−110.8	$T_3 + T_1$
−111.5	T_{13}
−112.4	T_5
−113.7	$T_4 + T_7 + T_{12}$
−115.8	$T_9 + T_{10}$
−119.9	$T_8 + T_{11}$

Hunger et al.[38] have characterized MCM-22 samples with high aluminum content (Si/Al = 11) and the corresponding dealuminated sample (Si/Al = 20) by ^{29}Si and ^{27}Al MAS NMR techniques. A similar observation has been made in the case of the calcined sample, where a broad spectrum is observed, which may be due to smearing of the overlapping signals and also may be due to a fairly high aluminum content (Si/Al = 11). The dealuminated sample did not exhibit a well resolved spectrum.[38] The observed spectrum was deconvoluted and was found to comprise of five lines (ca. −118.5 ppm, −115.3 ppm, −112.3 ppm, −110.3 ppm and −104.0 ppm). The signal at −98.0 ppm was attributed to Si(1Al) species.

^{1}H - ^{29}Si CP/MAS experiments were carried out over the H-form of MCM-22 samples.[38] It was concluded that the hydroxyl protons of the bridging OH groups are bonded via oxygen bridges to Si(1Al) atoms located on five crystallographically non-equivalent T sites. The observations of Hunger et al.[38] support the hexagonal symmetry proposed by Kennedy et al.[35] and Leonowicz et al.[4] with T-O-T angles ranging from 136° - 164° with 8 crystallographically distinct T sites.

^{27}Al MAS NMR spectra of calcined and dealuminated samples were found to exhibit signals corresponding to both framework and non-framework aluminum, respectively.[36,38] The non-framework aluminum corresponds to 5% of the framework aluminum species.[38] The signals have been deconvoluted into 5 lines. The overall intensity ratio of two samples were almost same except for the signal at 49 ppm. This has been attributed to the framework site with the highest aluminum population.

The ^{1}H MAS NMR spectrum of the ammonium-ion-exchanged sample exhibited signals at 1.9, 2,8, 4.2 and a broad hump at 6.2 ppm. These were attributed to silanol (defect sites), OH groups due to extraframework aluminum, acidic bridging OH groups and residual ammonium ions present in the sample, respectively.

Kolodziejski *et al.*[36] have carried out ^{27}Al and ^{29}Si MAS NMR experiments over the zeolite samples with different Si/Al ratios. A multiline ^{29}Si spectrum consisting of signals at $\delta = -98$ ppm and $\delta = -105$ ppm were assigned to defect sites and the interference of resonances from both defect sites and Si(1Al) sites, respectively.[39] In the case of the as-synthesized samples, the signal at $\delta = -99$ ppm was mainly attributed to Si(1Al) due to the decrease in its intensity on calcination. The signal at $\delta = -98$ ppm, exhibited by highly siliceous samples, was exclusively attributed to Si-OH sites. The observed chemical shift of Si(0Al) sites had a range extending from $\delta = -104$ ppm to -120 ppm and the T-O-T bond angles, from $138°$ - $164°$ and the results were found to support[37] the hexagonal P6/mmm spacegroup based on the fitting of their experimental spectra.

Kolodziejski *et al.* have studied ^{27}Al MAS NMR of the as-synthesized and calcined MCM-22 samples.[36] They have suggested that atleast two types (each) of Al species exist in the framework and in extra-framework positions.

3.3.7.2 Discussions

The multinuclear NMR studies[40] carried out over sample D (SiO$_2$/Al$_2$O$_3$ = 80) are now discussed taking into account the earlier reports. Tentative assignments of ^{29}Si resonances to crystallographically different tetrahedral (T) lattice sites are made based on spin-lattice relaxation time measurements and T-site geometry considerations.[40] Sharper signals were exhibited by the as-synthesized sample than by the calcined or dealuminated samples. The results are discussed in detail in the following sections.

3.3.7.3 ^{27}Al MAS NMR Experiments

The ^{27}Al MAS NMR spectra of the MCM-22 samples are given in Figure 3.9. From the Figure 3.9(A & B), it can be seen that, there is no extra-framework aluminum in the case of as-synthesized and calcined materials, but a signal at $\delta = 0$ - 1 ppm, characteristic of non-framework octahedral aluminum species is found to be present only in the dealuminated sample,
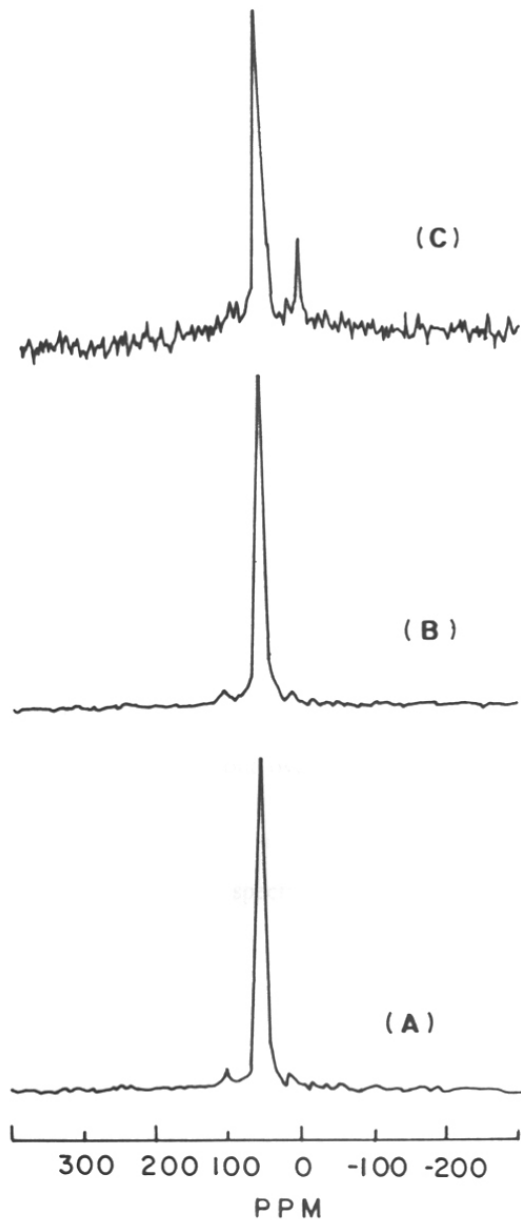
Figure 3.9   78.17 MHz ^{27}Al MAS NMR spectra of sample (D) (SiO$_2$/Al$_2$O$_3$ = 80).

(A) As-synthesized, (B) calcined and (C) dealuminated samples.

Figure 3.9(C). This is in contrast to the results obtained by Corma et al.,[7b] where the authors have found that dealumination was found to occur even while grinding the sample and also during calcination. Hunger et al.[38] have correlated the crystallographic T-site multiplicity through ^{27}Al MAS NMR experiments over MCM-22 sample with Si/Al = 11 recorded at a high magnetic field (17.6 Tesla). Our observations are based on results obtained over samples with lower aluminum content and at lower magnetic field (7.05 Tesla). Splittings of the tetrahedral and octahedral aluminum signals are not observed unlike the observations by Kolodziejski et al.[36] The line broadening associated with the observed ($\frac{1}{2} \leftrightarrow -\frac{1}{2}$) central transition of the spin 5/2 ^{27}Al nucleus generally obscures fine structural features to be discerned from our ^{27}Al spectra.

3.3.7.4 ^{29}Si MAS NMR Experiments

^{29}Si NMR experiments were carried out over the as-synthesized (containing nitrogen, CN), calcined and dealuminated samples.

Figure 3.10 shows the ^{29}Si MAS NMR spectrum of sample D. The spectrum consists of 5 distinct signals which occur at δ = $-$ 99.39 ppm, $-$ 104.3 ppm, $-$ 110.69 ppm, $-$ 113.28 ppm and $-$ 119.71 ppm.

The signal at δ = $-$ 99.39 ppm (Figure 3.10 (A)) has been attributed to different species by different researchers.[35,36,38,40] It has been attributed to Si(OSi)$_x$(OH)$_y$, (where x + y = 4 and 4 > x ≥ 2), terminal silanol groups or defect sites. Evidence for assigning this signal to terminal silanol species is obtained from ^{1}H - ^{29}Si Cross-Polarization (CP) MAS experiments. ^{1}H MAS NMR experiments over the samples also support the results and confirm our assignment of the signal at δ = $-$99.39 ppm to terminal silanol groups.

The resonances of the ^{29}Si MAS NMR spectrum of the as-synthesized sample (Si/Al = 40) have been assigned to three regions (see Figure 3.10). The resonance marked (II) in Figure 3.10, at δ = $-$104.3 ppm occurs in the overlap region of the resonances due to both Q^4(1Al)
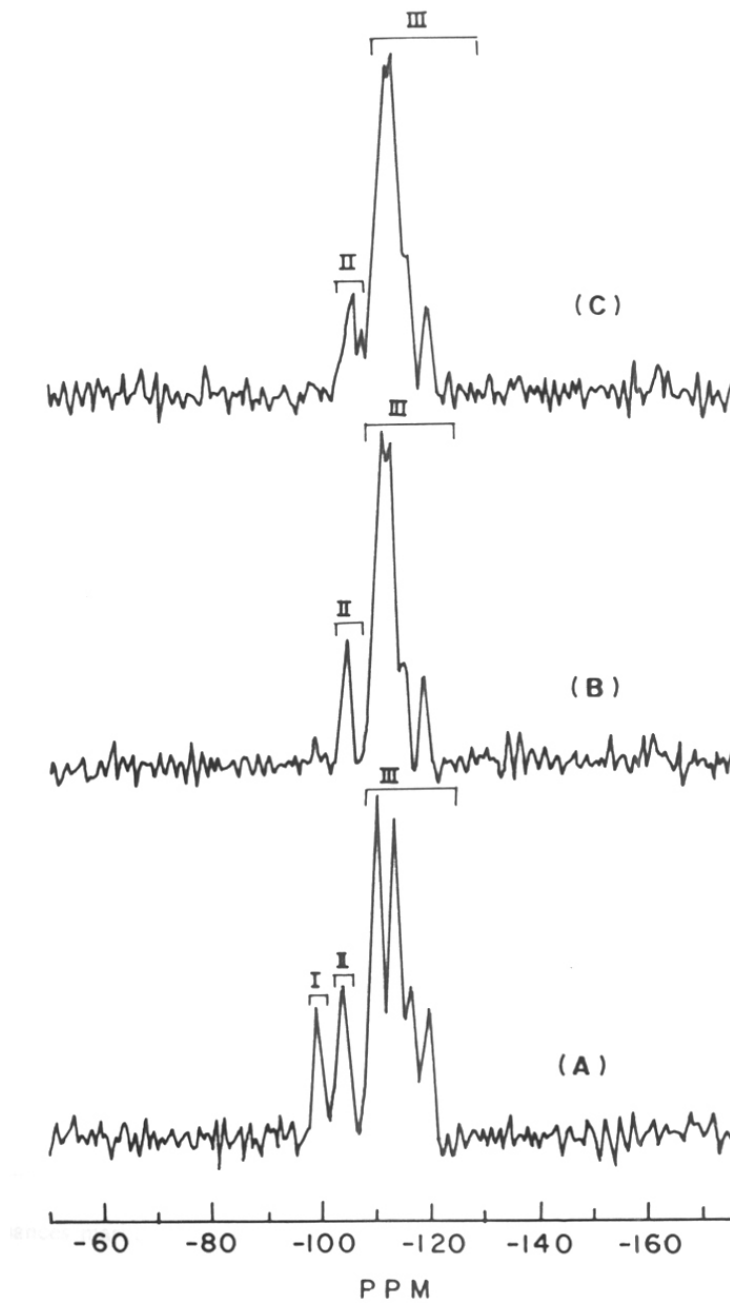
Figure 3.10   59.60 MHz ^{29}Si MAS NMR spectra of sample (D) (SiO$_2$/Al$_2$O$_3$ = 80).

(A) As-synthesized, (B) calcined and (C) dealuminated samples.

[I] : δ = −99.39 ppm, [II] : δ = −104.3 ppm and

[III] : δ = −110 ppm to - 122 ppm.

and $Q^4(0Al)$ species.[39] The dealuminated sample exhibited a similar type of spectrum with a decreased intensity of this peak. Further, successive dealumination of the samples revealed a decrease in the intensity of the signal. The signal at $\delta = -104.3$ ppm has therefore been assigned to $Q^4(1Al)$ species. This assignment is consistent with the decreased population of $Q^4(1Al)$ species at increased aluminum content and the corresponding appearance of a signal at $\delta = -105$ ppm as observed in other zeolite systems.[41] Based on the assignment of the resonance at $\delta = -104.3$ ppm to $Q^4(1Al)$ species and since there is no extraframework aluminum as confirmed by ^{27}Al MAS NMR spectrum (see Figure 3.9(B)), the framework Si/Al ratio was calculated from the deconvoluted signal intensities of the spectrum (Figure 3.11) to be 21.4. There is a marked discrepancy between the framework Si/Al ratio (21.4) calculated from the deconvoluted signal intensities of the spectrum and the value (Si/Al = 40) obtained from chemical analysis of the as-synthesized sample. Since, as mentioned above, there was no octahedral aluminum species in the sample (both as-synthesized and calcined), all the aluminum atoms occupy framework positions, and this difference can be explained only by assuming that the signal at $\delta = -104.3$ ppm is due to the overlapping of the resonances of both $Q^4(1Al)$ and $Q^4(0Al)$ species. Calculations reveal that the Si/Al ratio based on the NMR spectra will match the analytical value (Si/Al = 44) if $Q^4(1Al)$ species contribute 48.6% to the signal intensity of $\delta = -104.3$ ppm signal

The resonances marked (III) (see Figure 3.10(A)) occur in the region characteristic of highly siliceous environments devoid of any Si-O-Al linkages. These resonances occur exclusively in the range of Si(0Al) species. Thus, they correspond to the crystallographically non-equivalent T sites of zeolite MCM-22. The deconvoluted silicon spectrum of the as-synthesized and calcined samples are presented in Figure 3.11. For the calcined sample, the resonance positions of $Q^4(0Al)$ species, occur in the same chemical shift range as those reported for a highly siliceous MCM-22 at a higher magnetic field (11.45 Tesla). This multiline spectrum
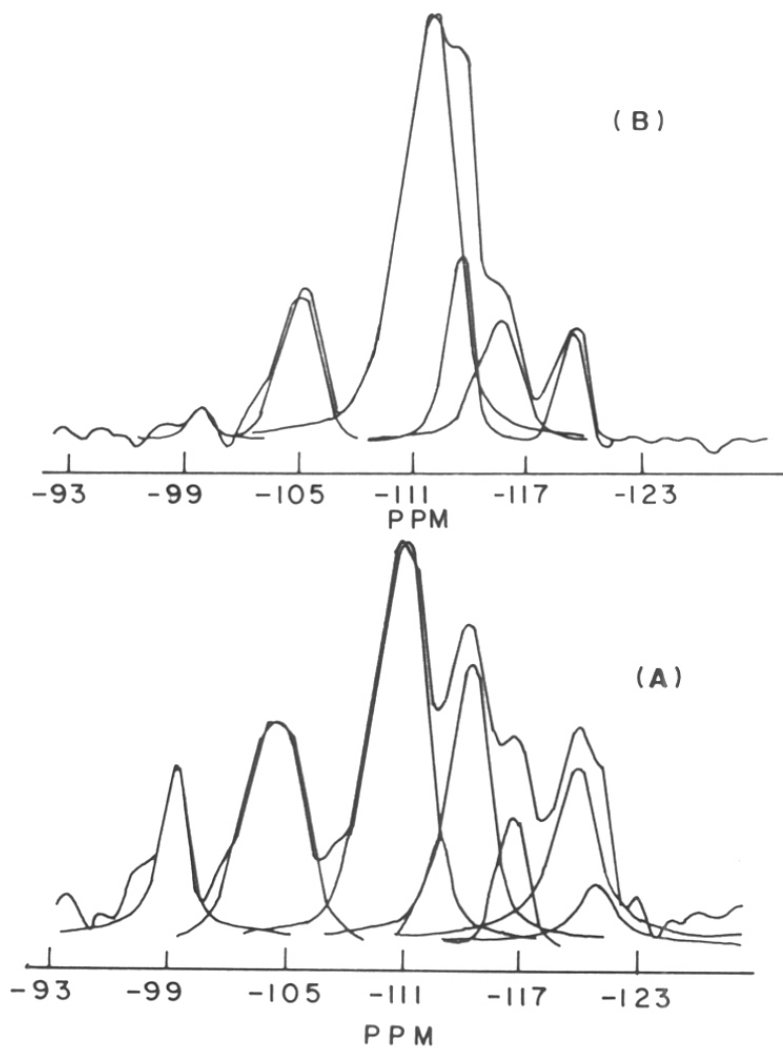
Figure 3.11   Deconvoluted ^{29}Si MAS NMR spectra of sample (D) with

SiO$_2$/Al$_2$O$_3$ = 80 showing Q^4(0Al) and Q^4(1Al) species.

(A) As-synthesized **and (B)** calcined samples.

is known to originate from differences in the T-site geometry.[42]   Since, there is a reduced chemical shift dispersion at 7.05 Tesla field used in our studies, there is a significant spectal overlap, especially in the chemical shift range, $\delta = -110$ ppm to -116 ppm, owing to the very small variation of (2°) of T-O-T angles.[7,35]   We find that the dispersion of $Q^4(0Al)$ species occurs over a slightly larger frequency range ($\delta = -99.39$ ppm to -121 ppm) excluding the signal at $\delta = -104.3$ ppm, assigned to $Q^4(1\ Al)$ species, for the as-synthesized sample when compared to the calcined sample ($\delta = -110$ ppm to -121 ppm). Further, the overlap of silicon resonances due to the various T sites was less severe in the as-synthesized form. Since, the XRD patterns of the as-synthesized and calcined samples (see Figure 3.2(A & B)) are similar and conform to the orthorhombic structure,[35,36] our experimental observations[40] suggest that while no structural phase transformation occurs upon calcination, there could be significant alterations in the T-O-T geometry.

3.3.7.5 ^{1}H MAS NMR Experiments

The ^{1}H MAS NMR spectra of the as-synthesized sample are shown in Figure 3.12. The observed proton spectrum comprises a slightly broad water resonance at $\delta = 4.8$ ppm, flanked by a partially resolved line at $\delta = 1.6$ ppm. The latter, due to the defect hydroxy groups, is unmistakably revealed in the spectrum of the dehydrated material (Figure 3.12(C)), in which, the water component has been eliminated. The proton line due to the template molecules is too broad (line width > 30 kHz) to be observed within the spectral range of the Figure 3.12. This observation also confirms the steric hindrance of the template, suggesting a tight fit of the template molecules within the pores of the MCM-22, as the protons of the hexamethyleneimine constitute a tightly dipolar coupled spin system. The intensity of ^{29}Si resonance of the silanol groups (at $\delta = -99.39$ ppm) is extremely small in the calcined and dealuminated samples (refer to Figure 3.10(B & C), respectively). The reduction in the intensity of the above signal is attributed to the loss of hydroxyl groups upon heat treatments, and the formation of the Si-O-
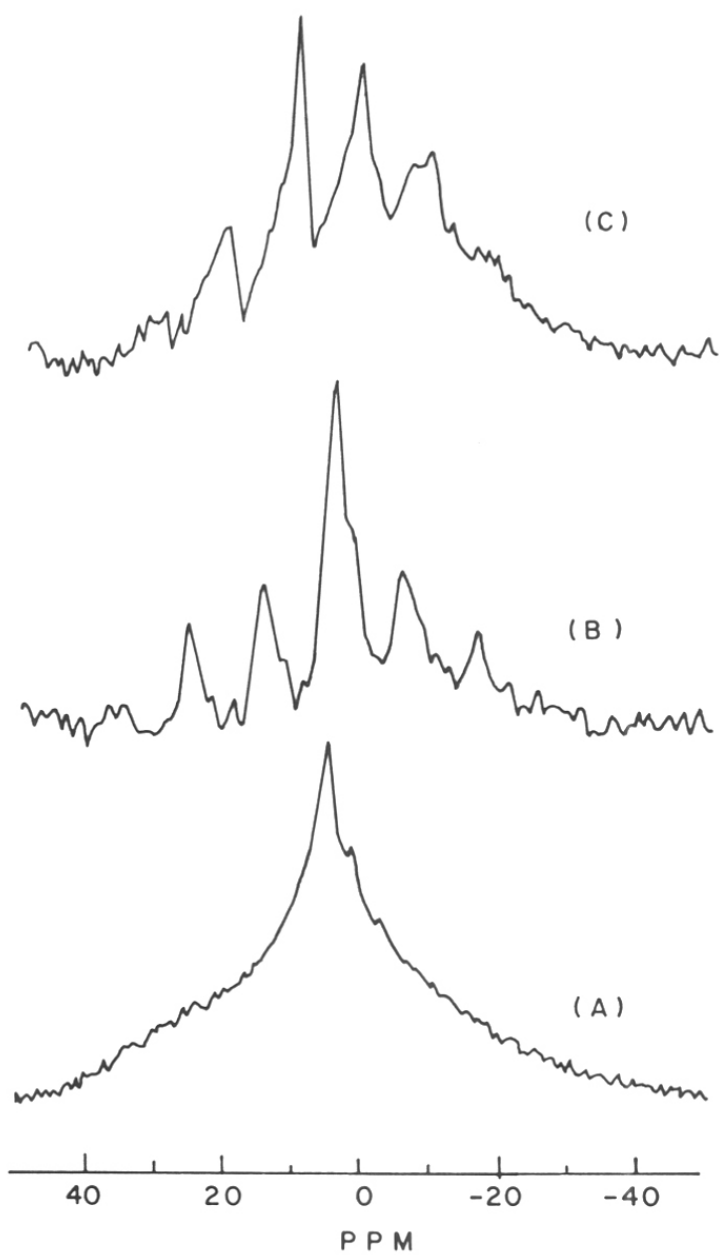
Figure 3.12   300 13 **MHz** ¹H MAS NMR spectra of MCM-22 sample (D).

(A) As-synthesized sample at slow spinning rate, *ca.*, 550 Hz.

(B) Spinning rate = 2.9 KHz.

(C) Dehydrated **as-synthesized** sample with spinning rate = 2.9 KHz.

Si bridges. The assignment of the signal and the above explanations also support the assumption in section 3.3.5, of the oxidation of the template (especially H) by the surface hydroxyl groups during template decomposition/calcination.

3.3.7.6 ^{1}H - ^{29}Si Cross-Polarization (CP) MAS NMR Experiments

The cross-polarization (^{1}H - ^{29}Si) MAS NMR experiments[40] have been carried out to learn about the interaction of protons attached directly to silicon atoms or the protons that are in the vicinity of the co-ordination of the silicon atoms. The Bloch decay spectrum of the as-synthesized sample along with the ^{1}H - ^{29}Si CP-MAS NMR spectrum are presented in Figure 3.13(B). The CP experiments were carried out using an optimally chosen mixing time of 2.5 ms. From the Figure 3.13(B), it is seen that there is a selective CP enhancement of the resonance corresponding to signal assigned to terminal silanol (Si-OH) groups. Also, the absence of resonances at δ = -104.3 ppm and -120.9 ppm corresponding to Q^4(1Al) and Q^4(0Al) species,[39] respectively, are noted from Figure 3.13(B). The dynamics of cross-polarization has been studied in an effort to probe the interaction between the ^{1}H - ^{29}Si nuclei. The observed contact time variations for the silicon resonances at δ = -99.2 ppm and -120.9 ppm (see Figure 3.10(A) (I) and (III)) are shown in Figure 3.14. Cross-polarization time (T_{1S}) of 1.3 and 1.6 ms and proton rotating frame spin-lattice relaxation time ($T_{1\rho S}$) of 3.4 and 8.6 ms have been estimated from a computer fitting of the data for the above signals. There is only a marginal difference in the T_{1S} value of (I) and (III), whereas, the $T_{1\rho S}$ values are markedly different. From this difference in $T_{1\rho S}$ values and our ^{1}H MAS spectral observations, we identify two distinct ^{1}H - ^{29}Si magnetization transfer mechanisms, one involving the hydroxyl protons at the defect sites and the other involving the template protons. Since the Q^4(0Al) resonances, in (II) and (III) (refer Figure 3.10(A)) are exclusively cross-polarized by the template protons, and in view of the inverse sixth power dependence of inter-nuclear distance on the cross-polarization rate, the observed disappearance of the silicon resonances at δ = $-$
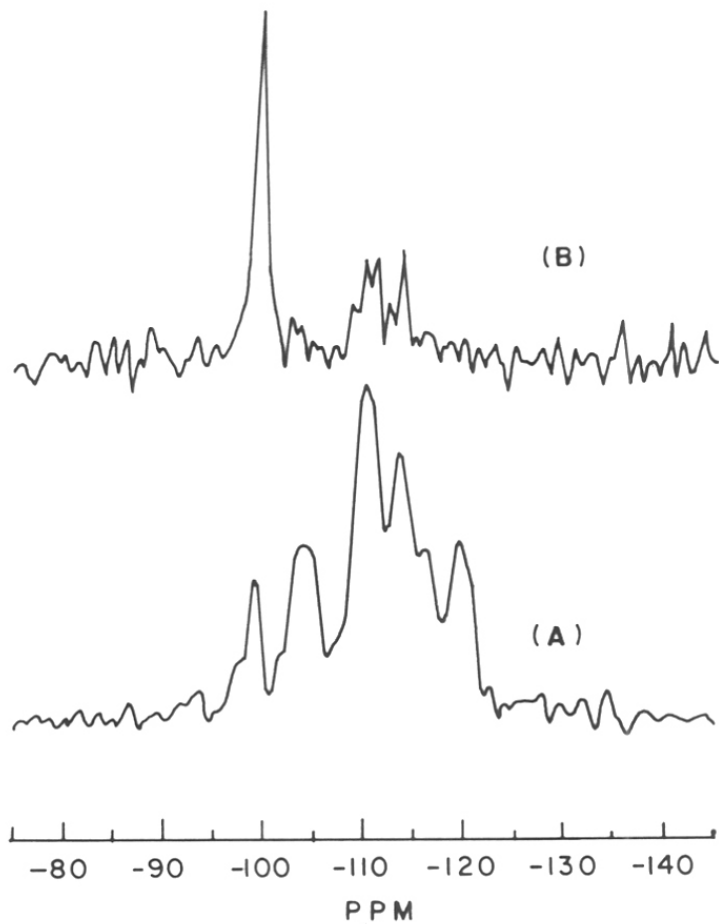
Figure 3.13   The Bloch Decay spectra of sample (D) ($SiO_2/Al_2O_3 = 80$).

(A) ^{29}SI MAS NMR spectrum of **as-**synthesized sample and (B)

^1H - ^{29}Si CP-MAS NMR spectrum.
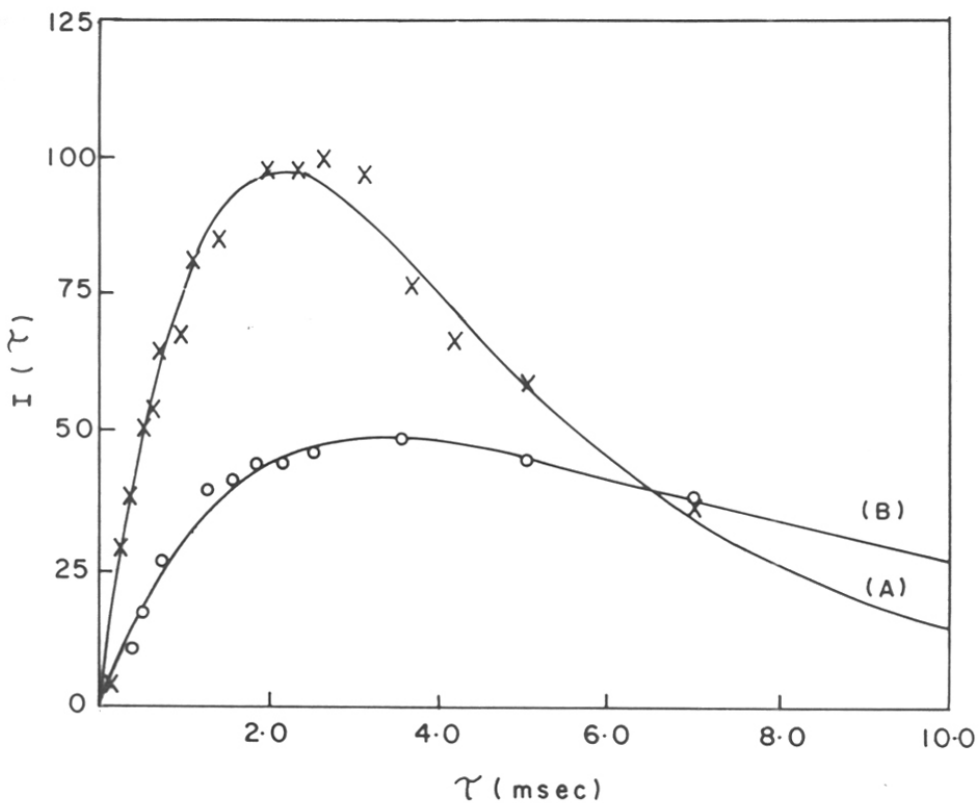
Figure 3.14   Variation of cross-polarization intensity of silicon resonances in Figure 3.10(A).

Region (I)   in Figure 3.10(A) : (X) δ = - 99.2 ppm.

Region (III) in Figure 3.10(A) : (O) δ = - 110.5 ppm.

The solid lines through experimental points deplot a fitting of the data points to the cross-polarization equation :

$$I_{(\gamma)} = I_o (1-\lambda)^{-1} \{1-\exp[-(1-\lambda)\gamma/T_{1S}] \times \exp[-\gamma/]; \lambda = T_{1S}/T_{1\rho}^{H}.$$

99.2 ppm and -110.5 ppm (Figure 3.13(B)) point to a distant location of these T sites from the template molecule present in the zeolite channel. The CP-MAS observations also suggests that in this zeolite, aluminum preferably occupies the distant or buried T site, which supports the earlier report by Kennedy et al.[35]

3.3.7.7 ^{13}C MAS NMR Experiments

^{13}C MAS NMR experiments were carried out over the as-synthesized samples to learn about the extent of the interaction of the template and the zeolite lattice. The organic template, hexamethyleneimine, as neat liquid, the template adsorbed over silica gel (9 wt.%; SiO_2, S5505 Sigma) and the as-synthesized samples were used for ^{13}C NMR studies (Figure 3.15). The spectrum of the neat liquid (Figure 3.15(B)) exhibits three sharp lines at $\delta = 27.60$ ppm, 31.95 ppm and 49.74 ppm for the three non-equivalent pairs of protons (in Figure 3.15(A) mentioned as a, b and c, respectively). Two broad lines are observed for the template adsorbed over SiO_2 gel at $\delta = 27.6$ ppm and 56.26 ppm (Figure 3.15(C)). The ^{13}C MAS NMR spectrum of the as-synthesized sample is similar to that of the spectrum obtained in the case of template adsorbed over SiO_2 gel, except that the low-field signal (which corresponds to $\delta = 56.26$ ppm in the case of the template adsorbed over SiO_2 gel) is split into a doublet with $\delta = 47.53$ ppm and 55.62 ppm (Figure 3.15(D)). These results indicate the non-equivalence in the magnetic environment of protons of C1 and C6 (figure 3.15(A)). The template may be sterically hindered/having a tight fit in the 10 membered ring channels. Thus, these results confirm the strong interaction of the template with the zeolite framework.

3.3.7.8 ^{29}Si NMR of the Synthesis gel

^{29}Si NMR spectrum of the final synthesis gel was recorded. The synthesis gel was prepared according to the procedure described in Chapter II. Figure 3.16 represents the ^{29}Si NMR spectrum of the final synthesis gel. The spectrum consists of 5 distinct signals which can be attributed to silicon atoms in different environments,[39] namely, Si(2Al), Si(1Al), Si(OH)$_x$ and Si(0Al). The total chemical shift range extends from $\delta = -74.0$ ppm to -120.0 ppm, including
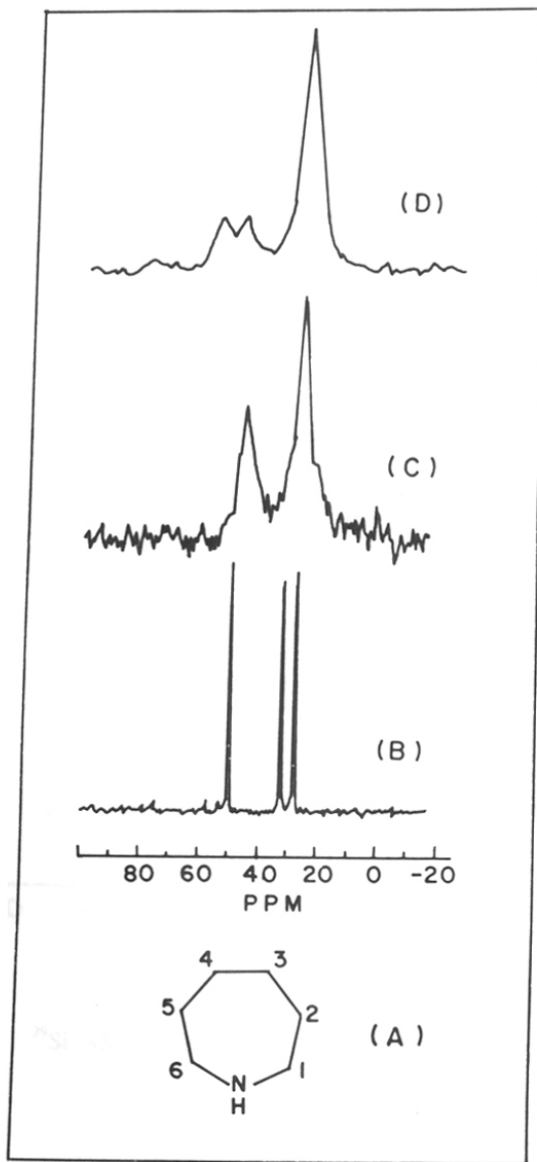
Figure 3.15 ^{13}C NMR spectra of the template molecule in different environments.

(A)   Structure of the template molecule (Hexamethyleneimine) with different sets of protons (marked by 1-6).

(B)   Neat template - (Liquid).

(C)   Template adsorbed over SiO_2 gel.

(D)   Spectrum of the as-synthesized sample with SiO_2/Al_2O_3 ratio = 40, calibrated with reference to signals of C-H groups ($\delta = 37.8$ ppm) of admantane.
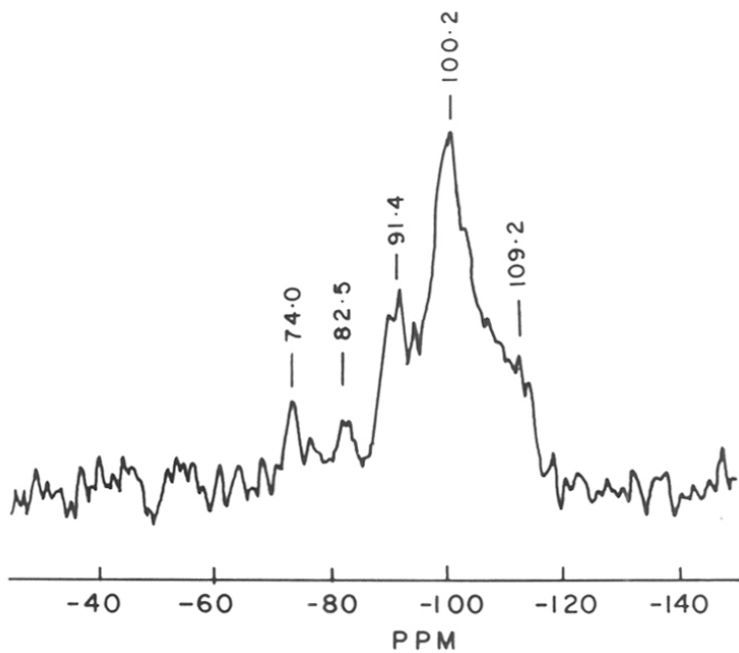
Figure 3.16 ^{29}Si NMR spectra of synthesis gel with SiO_2/Al_2O_3 ratio = 88.

Si(2Al), Si(1Al), Si(OH)$_x$ species. The resonance at $\delta = -74.0$ ppm corresponds to Q^4(2 Al) species. Thus, during synthesis, all possible species exist, which then transform into Q^4(1 Al) species during crystallization.

3.4 REFERENCES

1.   Rubin, M. K., and Chu, P., US Patent No. 4,954,325 (1990).

2.   Ravishankar, R., Tapas Sen., Veda Ramaswamy., Soni, H. S., Ganapathy, S., and Sivasanker, S., *Stud. Surf. Sci. Catal.* **84(A)**, 331 (1994).

3.   Visser, J. W., *J. Appl. Cryst.* **2**, 89 (1969).

4.   Leonowicz, M. E., Lawton, J. A., Lawton, S. L., and Rubin, M. K., *Science.* **269**, 1910 (1994).

5.   Ravishankar, R., Bhattacharya, D., Jacob, N. E., and Sivasanker, S., *Microporous Materials.* **4**, 83 (1995).

6.   Puppe, L., and Weisser, J., US Patent No. 4,439,409 (1984).

7.   (a)   Corma, A., Corell, C., and Pérez-Pariente, J., *Zeolites.* **15**, 2(1995).

        (b)   Corma, A., Corell, C., Kolodziejski, W., and Pérez-Pariente, J., *Zeolites.* **15**, 575 (1995).

8.   Rubin, M. K., US Patent No. 5,021,141 (1991).

9.   Marler, B., Dehnbostel, N., Eulert, H. H., Gies, H., and Liebau, F., *J. Incl. Phenom.* **4**, 339 (1986).

10.   Zones, S. I., Eur. Pat. Appln., EP 231,019 (1987).

11.   Whittam, T. V., US Patent No. 4,209,498 (1980).

12.   Dewing, J., Spencer, M. S., and Whittam, T. V., *Catal. Rev. Sci. Eng.* **27(2)**, 461 (1985).

13.   Szostak, R., "Handbook of Molecular Sieves", Van Nostran Reinhold, New York, (1992).

14.   Ramesh Reddy, K., Ph. D. Thesis, University of Poona, (1993).

15.   Shannon, R. D., *Acta. Cryst. A* **32**, 751 (1976).

16.   Unvericht, S., Hunger, M., Ernst, S., Karge, H. G., and Weitkamp, J., *Stud. Surf. Sci. Catal.* **84(A)**, 37 (1994).

17.   Flanigen, E. M., *Am. Chem. Soc. Monogr.* **171**, Ch. 2 (1976).

18.   Flanigen, E. M., Khatami,H., and Szymanski, H. A., *Adv. Chem. Ser.* **101**, 201 (1971).

19.   Thangaraj, A., Ph. D. Thesis, University of Poona, (1991).

20. Boccuti, M. R., Rao, K .M., Zecchina, A., Leofanti, G., and Petrini, G., *Stud. Surf. Sci. Catal.* **48**, 133 (1988).

21. Sudhakar Reddy, J., Ph. D. Thesis, University of Poona, (1992).

22. Hari Prasad Rao, P. R., Ph. D. Thesis, University of Poona, (1993).

23. Camblor, M. A., Corma, A., and Pérez-Pariente, J., *J. Chem. Soc. Chem. Commun.* 557 (1993).

24. Jacobs, P. A., and Uytterhoeven, J. B., *J. Catal.* **22**, 193 (1971).

25. Scherze, J., and Bass, J. L., *J. Catal.* **28**, 101 (1973).

26. Woolery, G. L., Alemany, L. B., Dessau, R. M., and Chester, A. W., *Zeolites.* **6**, 14 (1984).

27. Emeis, C. A., *J. Catal.* **141**, 347 (1993).

28. Souverrijns, W., Verrelst, W., Vanbutsele, G., Martens, J. A., and Jacobs, P. A., *J. Chem. Soc. Chem. Commun.* 1671 (1994).

29. Gerke, H., and Gies, H., *Z. Kristallogr.* **116**, 11 (1984).

30. Gunawardane, R. P., *Ind. J. Chem.* **27 A**, 380 (1988).

31. Breck, D. W., "Zeolite Molecular Sieves: Structure, Chemistry and Use", Wiley, New York, (1974).

32. Kokotailo, G. T., Chu, P., Lawton, S. L., and Meier, W. M., *Nature.* **275**, 119 (1978).

33. Fyfe, C. A., Gies, H., Kokotailo, G. T., Paztor, C., Strobl, H., and Cox, D. E., *J. Am. Chem. Soc.* **111**, 2470 (1989).

34. Bibby, D. M., Milestone, N. B., and Aldrige, L. P., *Nature.* **280**, 664 (1979).

35. Kennedy, G. F., Lawton, S. L., and Rubin, M. K., *J. Am. Chem. Soc.* **264**, 11000 (1994).

36. Kolodziejski, W., Wilson, C. Z., Corell, C., Pérez-Pariente, J., and Corma, A., *J. Phys. Chem.* **99**, 7002 (1995).

37. Fyfe, C. A., Feng, Y., Gies, H., Grondey, H., and Kokotailo, G. T., *J. Am. Chem. Soc.* **112**, 3264 (1990).

38. Hunger, M., Ernst, S., and Weitkamp, J., *Zeolites.* **15**, 188 (1995).

39. Engelhardt, G., and Michel, D., "High Resolution Solid-State NMR of Silicates and Zeolites", New York, (1984).

40. Ravishankar, R., Tapas. Sen, Sivasanker, S., and Ganapathy, S., *J. Chem. Soc. Faraday Trans.* **91(19)**, 3549 (1995).

41. Nagy, J. B., Gabelica, Z., Derouane, E. G., and Jacobs, P. A., *Chem. Lett.* 2003 (1982).

42. Ramdas, S., and Klinowski, J., *Nature.* (London), **398**, 521 (1984).

CHAPTER IV

SORPTION PROPERTIES OF MCM-22

4.1 INTRODUCTION

Acid-base property is an interesting characteristic of zeolites. As discussed in Chapter I, the acidity results from the protons associated with the trivalent metal ions,[1] whereas, basicity is due to the presence of hydroxyl groups and alkali or alkaline earth cations present in the exchangeable positions. Acidity of zeolites can be characterized by infrared spectroscopic study of adsorbed bases such as, NH_3, pyridine, pyrrole and n-butylamine.[2-7] Since, acid-sites are mostly located inside the pores of the zeolite, smaller basic molecules such as ammonia which can rapidly travel through the smaller pores and windows are more useful in evaluating the acid sites.

The exchange of the extra-framework cations, usually sodium, by other cations such as protons, and rare earth metals modifies the acid-strength and influences catalytic activities. The sorption of nitrogen or argon at liquid nitrogen temperature and fitting the results obtained into the BET equation yields the surface area of the zeolites. Sorption capacities of probe molecules such as, water, n-hexane, cyclohexane, m-xylene and 1,3,5-TMB yield information about the hydrophilicity/hydrophobicity, nature of pore structure and pore volume of the zeolites. Recently, Corma *et al.* have confirmed the presence of both 10-MR and 12-MR in MCM-22[8] through adsorption and catalytic studies. Infrared studies of CO_2 adsorbed on zeolites could yield information on cation site distribution.[9-11] CO_2 sorption has revealed the preferential occupation of Ca^{2+} and Mg^{2+} in specific sites in zeolite Y.[11] The sorption uptake of CO_2 was reported to be inversely proportional to the cation density at high degree of saturation, while at low coverages, it was found to be directly proportional.[11]

The sorption equilibrium and the application of various isotherm equations such as, Langmuir, BET, Dubinin-Radushkevich, Fruendlich and Sip's equations could be combined with other statistical models to gather information about the sorption characteristics of zeolites.[12-14] The adsorption of ammonia over zeolites can be used to obtain information about cation migration and cation site selectivity.[15-17] The number of acid sites and the strength of the acid sites could be determined, respectively, by chemisorption of ammonia and the temperature needed to desorb it.[18-22] Isosteric heats of adsorption provide information on the acid strength distribution in zeolites.[20,21]

The characterization of MCM-22 using various physico-chemical techniques[23,24] was discussed in Chapter III. In this chapter, the sorption properties of MCM-22 are reported. Sorption of probe molecules such as, water, n-hexane, cyclohexane, m-xylene and 1,3,5-trimethyl benzene (mesitylene) were carried out over MCM-22 samples with varying aluminum contents. Surface areas of samples were determined by argon sorption. Sorption of ammonia was studied upto 600 Torr in the temperature range of 303 K to 423 K. The results were fitted into different models and thermodynamic entities such as chemical potential and isosteric heats of adsorption were determined.

4.2 EXPERIMENTAL

4.2.1 SURFACE AREA MEASUREMENTS

Argon adsorption measurements were carried out using a commercial volumetric adsorption apparatus (Omnisorb 100CX, Coulter Corporation, USA). Approximately 200 mg of the calcined sample was degassed at 675 K at ~10^{-5} Torr prior to surface area

measurements. The samples were then cooled to 77 K and sorption of argon was carried out. The results were fitted into the BET equation to obtain the surface areas.

4.2.2 ADSORPTION MEASUREMENTS

Sorption of water and hydrocarbons was carried out in a vacuum microbalance (Cahn instruments, USA) at $p/p_o = 0.5$, for 2 h at 298 K. Initially, ~ 40 mg of the calcined sample was pressed into a small pellet and placed in the aluminum bucket (see Figure 4.1). The sample was degassed in vacuum ($\sim 10^{-5}$ Torr) at 673 K for 12 h prior to sorption measurements. The cell was then cooled and the temperature was maintained at 298 K during the measurements. The hydrocarbons used for sorption measurements were obtained from Aldrich Chem. Co., USA, (purity: > 99 %).

4.2.3 AMMONIA SORPTION

A conventional all glass unit was used for the sorption measurements of ammonia. The ammonia sorption isotherms were obtained volumetrically using the apparatus depicted in Figure 4.2. It consists of burettes (B_1 and B_2), a manometer (M) and a sample bulb (S). The sample bulb was immersed in a silicone-oil bath. The temperature was maintained to an accuracy of ± 1 K during the sorption measurements. The burette bulbs were precalibrated with mercury prior to the start of the experiments.

Approximately, 0.25 g of the sample was taken in the sample bulb and the bulb was immersed in the thermostat. The sorption measurements were carried out in the temperature range, 303 K - 453 K at intervals of 30 K. The sample was degassed at 753 K at a pressure of 10^{-6} Torr for 6 h. The sample was cooled to the desired temperature and the dead space calibrations were carried out using helium. The sample was again degassed
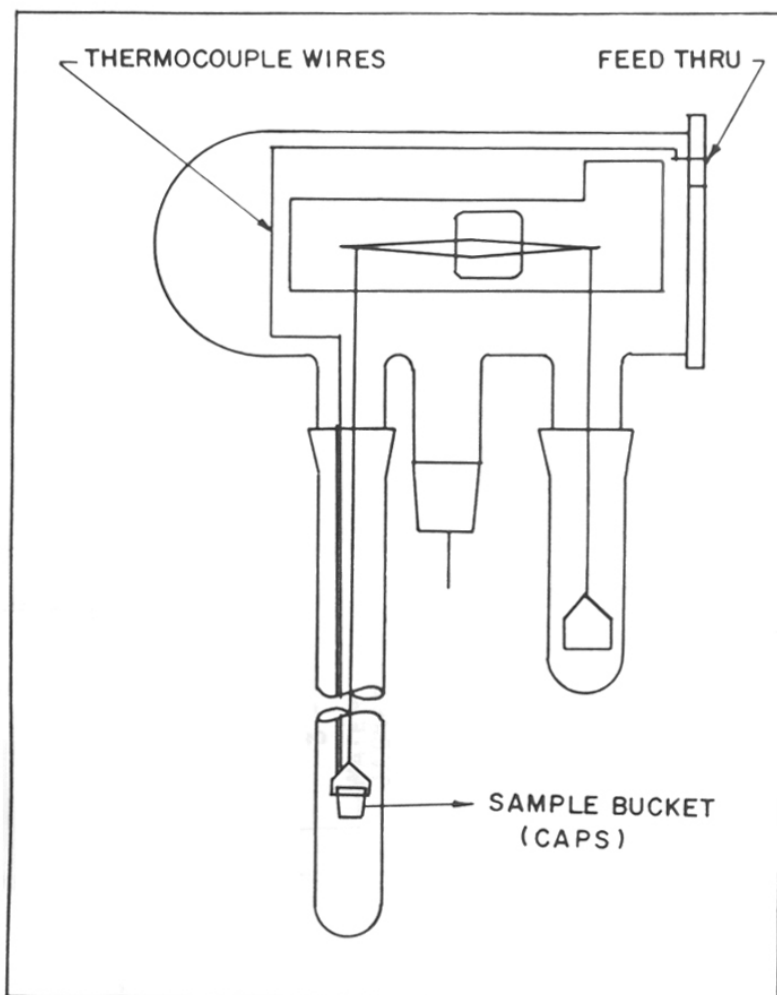
Figure 4.1   Cahn electromicro-balance used for adsorption of   probe
molecules.
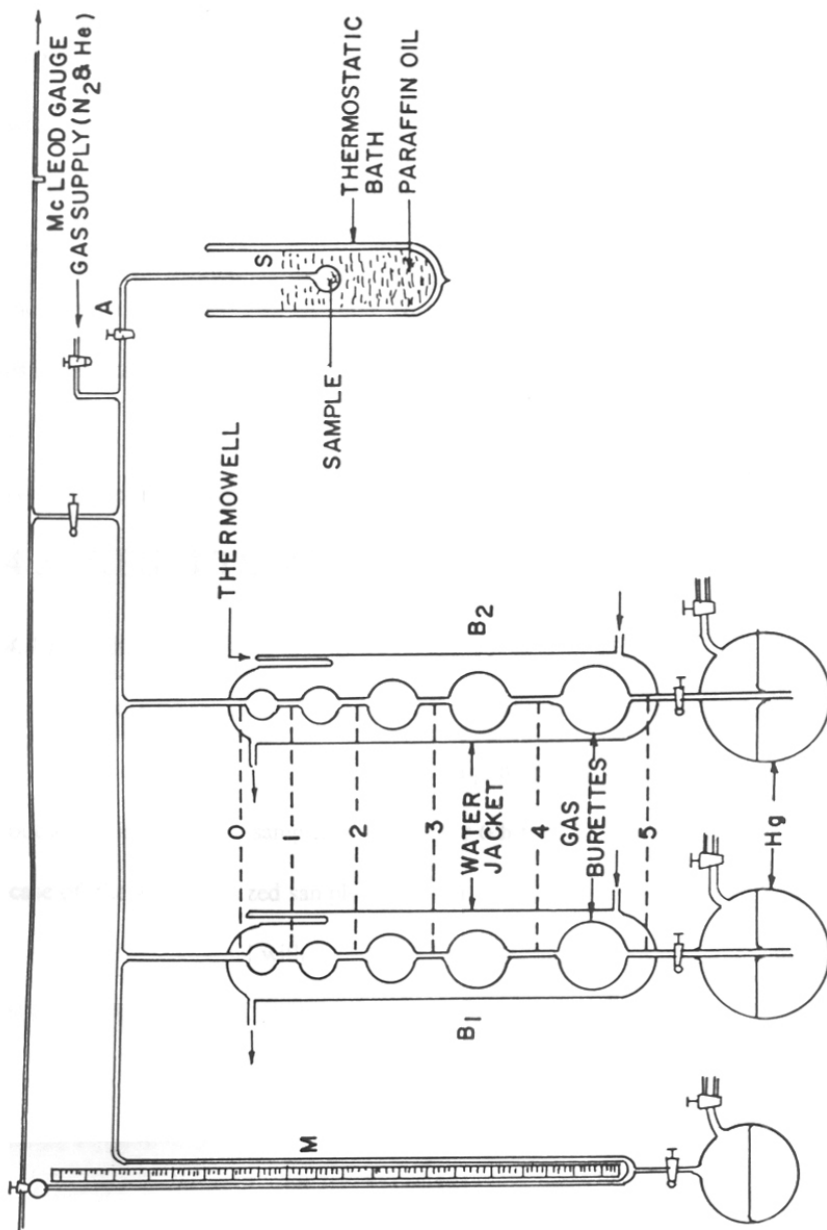
Figure 4.2   Adsorption unit for the measurement of ammonia uptake.

at 713 K for 6 h. The experiments were carried out at 453 K first and the temperature was lowered for other studies. Prior to the start of the experiments, the sample was immersed in the desired temperature bath for atleast 2 h for stabilization. A known amount of ammonia was admitted into the sample vessel and the sorption isotherms were measured upto a pressure of 600 Torr. The volume of the gas sorbed at STP was estimated as follows : $V_{Ads} = V_1 - V_2 - V_3$,

where, V_1, V_2 and V_3 are, respectively, the volumes of gas initially admitted into the system, gas remaining in the system and in the sample vessel.

4.3 RESULTS AND DISCUSSION

4.3.1 SURFACE AREA MEASUREMENTS

The surface areas of MCM-22 samples with different SiO_2/Al_2O_3 ratios are presented in Table 4.1. Argon sorption at liquid nitrogen temperature (77 K) was carried out after degassing the samples at 675 K for 6 h to a pressure of 10^{-5} Torr except in the case of the as-synthesized sample which was degassed at 323 K for 12 h. In general, the surface areas decreased with increase in SiO_2/Al_2O_3 ratios. The sample with SiO_2/Al_2O_3 ratio = 28 was found to have the highest area and the sample with SiO_2/Al_2O_3 ratio = 140, the lowest. As the amount of various hydrocarbons sorbed were similar for the different samples (Table 4.1), the decrease in surface area is not likely to be due to pore blockages. It is probably (atleast partly) related to the shrinkage in unit cell due to the decrease in Al^{3+} content. The surface area of the template filled as-synthesized sample was also determined. The surface area of the as-synthesized material is mostly due to the external

Table 4.1   Sorption of probe molecules and BET surface area of MCM-22 samples
              with varying SiO_2/Al_2O_3 ratios.

| SiO_2/Al_2O_3 | Sorption Capacity (Wt. %) | | | | | $S^{\bullet}_{BET}$ |
	Water	n-Hexane	Cyclohexane[+]	m-Xylene	Mesitylene	(m^2/g)
28[@]	15.1	11.5	9.5	9.8	8.7	425
40	14.1	10.8	9.4	9.3	7.9	371
58	12.2	-	9.7	9.0	7.8	360
80	11.6	9.4	10.0	8.2	-	344
96	10.7	8.1	10.2	8.9	8.0	340
140	12.1	11.1	8.0	9.0	8.3	336
30[#]	Not measured					74

[*]Sorption capacity measurements were carried out at 298 K at p/p_o = 0.5
[@]Sorption of 1,3,5-triisopropyl benzene was carried out. ~ 7.5 wt % after 24 hrs.
[+]Cyclohexane sorption attained equilibrium only after 24 hrs.
[*]S_{BET} : Sorption of argon at 77 K.
[#]SiO_2/Al_2O_3 = 30 : As-synthesized sample.

surface area as the pores are filled with the template and are hence not accessible to the sorbate argon, though some pores might have become accessible due to the removal of the template during decomposition. The surface areas of other zeolites including the medium pore ZSM-5 and the large pore zeolites ZSM-12 [MTW], beta [ß], USY, mordenite [MOR] were also estimated for comparison purposes. The results are presented in Table 4.2. It could be seen that the pore volume of MCM-22 (0.2 ml gm^{-1}) is between that of MTW (large pore, 1-D, pore system) and ß (large pore 3-D pore system).

4.3.2 ADSORPTION OF PROBE MOLECULES

The quantity of water and other hydrocarbons sorbed by MCM-22 (sample A) are presented in Figure 4.3 and Table 4.1. The sorption of water decreased as the aluminium content decreased indicating the decreasing hydrophilic nature exhibited by the zeolite (Table 4.1).

The sorption capacity of a zeolite for any specific molecule is dependent upon the relative dimensions of the pore openings and the size of the molecule. When the pore diameters are larger than the molecular diameters, the quantity sorbed depends on the total void volume inside the zeolite. Examination of Table 4.2 reveals that all the zeolites adsorb the small molecules such as H_2O and n-hexane whose kinetic diameters are smaller than the diameters of the pores of all the zeolites examined. In the case of 1,3,5-TMB in general, there is a sharp decrease in sorption when the pore diameter (longer diameter) is significantly smaller than the kinetic diameter of the molecule (0.75 nm).

The small amounts of 1,3,5-TMB sorbed by the zeolites with smaller pores is probably due to sorption at the external surface of the crystallites. Thus, the zeolites

131

Table 4.2   Studies on sorption characteristics of zeolites.

Zeolite	SiO_2/Al_2O_3 Ratio	N_2 Adsorption[a]		Sorption Uptake [(P/P$_o$), Wt. %]			Pore dimensions	Source
		V_m (ml/g)	S_{BET} (m²/g)	H_2O (0.265 nm)[b]	n-hexane (0.43 nm)[b]	1,3,5-TMB (0.75 nm)[b]	(nm)	
ZSM-5	39	0.14	413	7.7	10.5	0.5	2-D; 0.54 x 0.56 0.51 x 0.55	UCIL, India.
ZSM-12	81	0.17	465	9.2	8.3	2.6	1-D; 0.57 x 0.60	Synthesized.[25]
ß	35	0.28	600	20.1	15.9	17.0	3-D; 0.75 x 0.55	PQ, Holland.
Mordenite[+]	44	0.25	568	17.5	11.4	7.0	1-D; 0.67 x 0.70	Norton, USA..
H-Y	5.2	0.37	820	30.0	20.9	24.0	3-D; 0.74 with 1,3 nm cages	Linde, USA..
MCM-22[+]	28	0.20	425	15.0	11.5	8.5	2-D; 0.71 x 0.71 1.81 nm cages and 10-MR pores.	Synthesized.[23,24]

[+] Argon sorption in the case of MCM-22 and mordenite and N_2 in all the other cases.

[b] Values in paranthesis are kinetic diameters of molecules.[26]
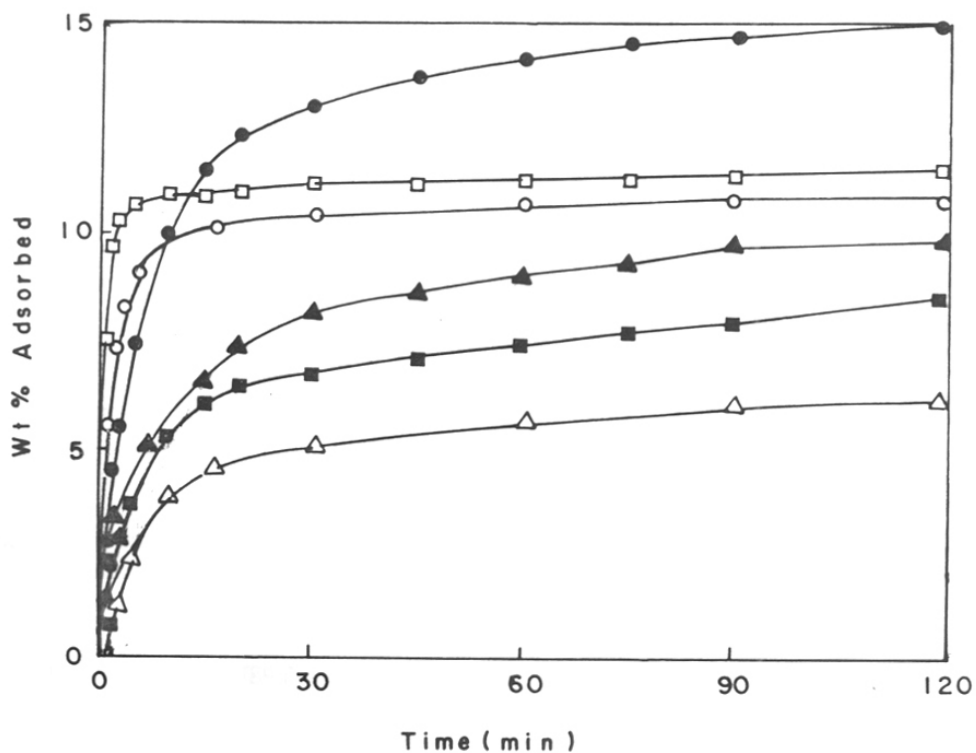
Figure 4.3 Sorption kinetics of probe molecules over MCM-22 sample with SiO$_2$/Al$_2$O$_3$ ratio = 28, at 298 K and p/p$_o$ = 0.5.

(●) Water, (□) n-hexane, (O) benzene, (▲) m-xylene, (■) Mesitylene and (Δ) cumene.

(ZSM-5 and ZSM-12) with maximum pore diameters less than 0.64 nm adsorb very little 1,3,5-TMB. MCM-22 which is believed to possess 10-MR pore openings[27] adsorbs moderate amounts of 1,3,5-TMB. It, thus, appears likely that some of the long 12.MR cages are accessible from the external surface. The access could be through defect centers or due to the presence of some of the 12-MR cages at the surface.

In Figure 4.4, the volumes of n-hexane and 1,3,5-TMB sorbed by the different zeolites is plotted against the pore volumes obtained experimentally from N_2 (Ar) adsorption data. The volumes of the hydrocarbons were obtained by dividing the weight sorbed by the liquid state density of the hydrocarbons (a gross approximation !) A reasonable straight line is obtained for n-hexane. Experimental pore volumes have been used instead of the theoretical volumes to minimize errors arising from differences in the quality of the zeolites which were obtained from different sources.

If we look at the 1,3,5-TMB data, we find that the points are close to the n-hexane line only for the large pore zeolites, ß and H-Y with pore diameters larger than the kinetic diameter of 1,3,5-TMB. While the points for ZSM-5, ZSM-12 and mordenite are farther away, that for MCM-22 is somewhat closer to the n-hexane line. This could probably due to adsorption on the large external platelet surface or due to the accessibility of a small number of the 12-MR cages from the external surface.

The diffusion coefficients of the probe molecules were calculated based on the sorption isotherm data obtained during the first 2 minutes using the relation given below:[28]

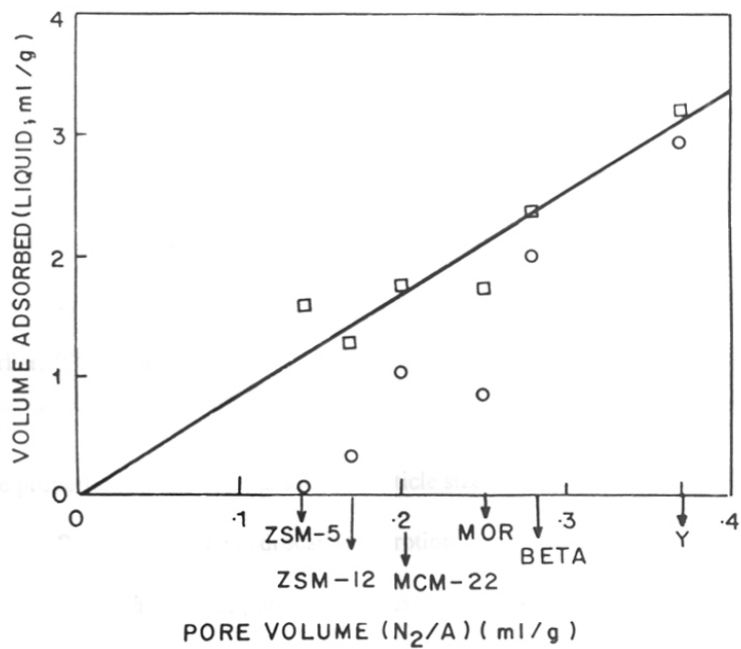$$\frac{Q_t - Q_0}{Q_\alpha - Q_0} = \frac{6}{r_0} \times \sqrt{(D/\pi) \times t}$$

Figure 4.4   Relationship between amount of n-hexane (□) and
1,3,5-TMB (O) sorbed vs the experimental pore volumes.

where, Q_o, Q_t and Q_∞ are the amounts of the sorbate at time '0' secs, 't' secs and at equilibrium,. 'D' and 'r_o' are diffusion coefficient and radius of the crystal, respectively. In view of the platelet nature of the crystals, r_o has been assumed to 0.05 µm (the platelet thickness being < 0.1 µm). By plotting, Q_t/Q_∞ vs $t^{1/2}$ and taking the slope of the linear portion in the graphs, the diffusion coefficients of the different probe molecules were calculated and are listed in Table 4.3. The diffusion coefficients decrease as expected with increasing size of the molecules. The diffusion coefficient values for n-hexane (Table 4.3) appear to be smaller than the diffusion coefficient values reported by earlier workers[29] for the diffusion of n-hexane in ZSM-5, a typical zeolite with 10 MR pore openings. However, the values for benzene and m-xylene are similar in magnitude to those reported earlier.[30,31] In any case, diffusion coefficient values estimated by different methods vary often by an order of magnitude (or even more, sometimes),[28,29] and are also influenced by the properties of the zeolites such as particle size, shape and composition.

Summing up, the hydrocarbon sorption data suggest that sorption occurs in MCM-22 mainly via the 10-MR pores (as suggessted by the earlier workers)[27] though some 12-MR cages (with dead-ends) may be accessible from the surface. These 12-MR cages will account for the significant amount of sorption of the bulky molecules like 1,3,5-TMB. Besides, the platelet nature of the crystals (with large external area) may also be responsible for the sorption of the bulky molecules.

4.3.3 AMMONIA ADSORPTION AND ISOTHERM EQUATIONS

Adsorption of ammonia over 3 samples of MCM-22 with SiO_2/Al_2O_3 ratios of 40, 80 and 140 was carried out and the families of isothems obtained are shown in Figure

Table 4.3   Diffusion coefficients of probe molecules adsorbed over MCM-22 sample.

| Probe molecule | Diffusion coefficients (x 10^{-14}) cm²/sec. | |
	Measured values	Literature data for ZSM-5[29-31]
n-Hexane	22	~ 100 [@]
Benzene	8.9	9[+]
m-Xylene	2.0	2[#]
Cumene	0.9	-

[@]n-Hexane : Diffusivity over H-ZSM-5 (Si/Al = 20; at 379 K) using Frequency Response technique.[29]

[+]Benzene   : Diffusivity over H-ZSM-5 (Si/Al = 30; at 386 K with crystal radius, r_c = 8 μm) using gravimetric and piezometric method.[32]

[#] m-Xylene : Diffusivity of m-xylene over H-ZSM-5 with r_c = 14 μm using gravimetric integral step.[31]

4.5. The sorption studies were carried out in the pressure range between 0 - 600 Torr. It could be seen that sorption uptake is higher at lower temperatures and decreases as the temperature is increased (as expected thermodynamically). The shape of the isotherms approximates "type I" based on Kieselev's classification.[32] The shape of the isotherm clearly shows that ~ 75 % of the sorption takes place within a narrow pressure region. At a particular temperature, for example, (303 K), the amount of NH_3 sorbed followed the order of SiO_2/Al_2O_3 ratios : 40 > 80 > 140 (Figure 4.5). This order is expected as the adsorption centers (acid sites) increase with increasing Al-content.

4.3.4 APPLICATION OF ISOTHERM EQUATIONS

The analysis of the NH_3-adsorption isotherms in terms of the different isotherm models such as Dubinin and Langmuir could provide information about the physical state of sorbed molecules and the nature of the sorbent.

(I) Langmuir adsorption isotherm model

The Langmuir isotherm is based on the assumption of the localized sorption centres without interactions with the energetically homogeneous sites located adjacent to each other. There is no sorbate-sorbate interaction. The plot of pressure (P) vs P/V did not yield linear plots (Figure 4.6) over the pressure range studied over the three samples. Thus, Langmuir isotherm assuming the absence of interactions between sorbate molecules and homogeneity of adsorption sites was not found to be suitable.

(II) Dubinin-Radushkevich equation

Polanyi potential theory is one of the earliest emperical approach that relates the adsorption free energy and the volume adsorbed. Later, the theory was modified by

138
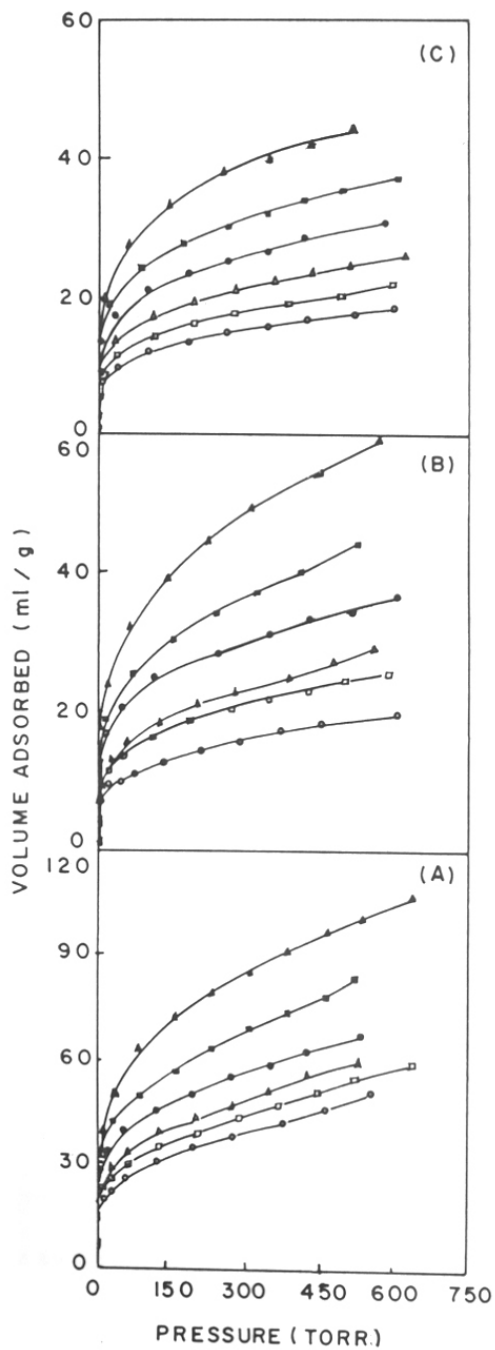
Figure 4.5 Adsorption isotherms of ammonia over samples with different SiO₂/Al₂O₃ ratios. SiO₂/Al₂O₃ ratios : (A) 40, (B) 80 and (C) 140, at different temperatures.

(O) 453 K, (□) 433 K, (Δ) 393 K, (●) 363 K, (■) 333 K and (▲) 303 K.
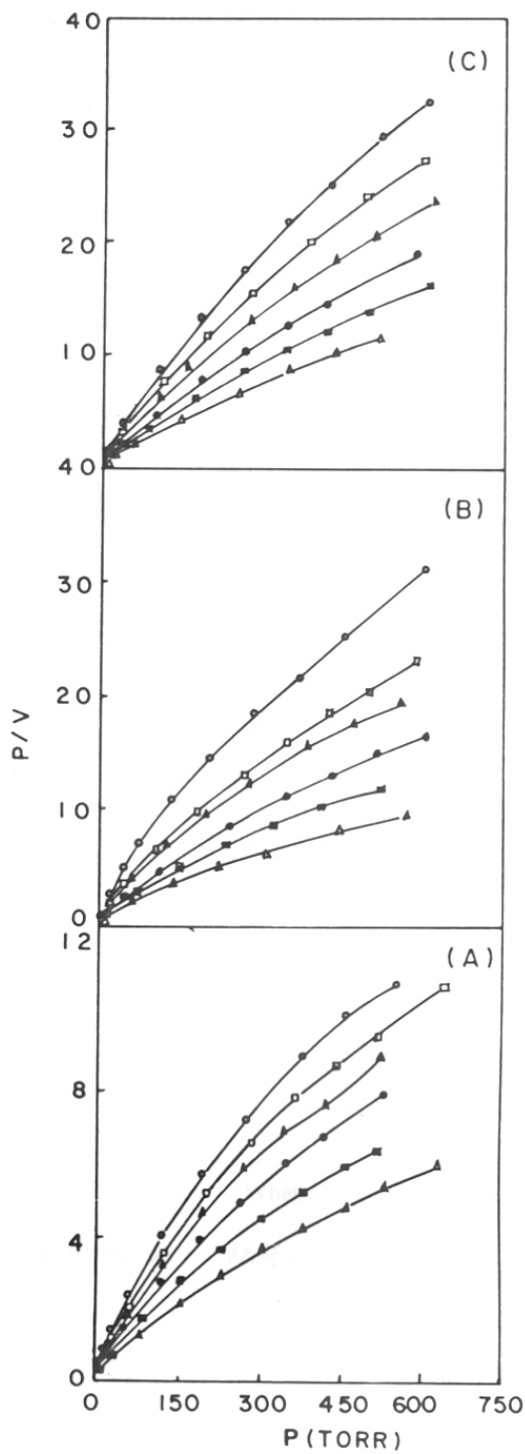
Figure 4.6   Langmuir plot of ammonia isotherms over samples with different
SiO₂/Al₂O₃ ratios. SiO₂/Al₂O₃ ratios : (A) 40, (B) 80 and (C) 140,
at different temperatures.
(O) 453 K, (□) 433 K, (▲) 393 K, (●) 363 K, (■) 333 K
and (Δ) 303 K.

Dubinin and his co-workers.[33-38]   The theory is applied to adsorption in micropores assuming the filling of void or pore-filling model. The equation was able to explain the statistical distribution of adsorption energies.   The final form of the equation is represented as:

$$Log(W) \ = \ Log(W_o) \ - \ \frac{B}{2.303 \ \beta^2} \ \times \ [TLog(\frac{P}{P_o})]^2$$

where, 'W'   is the amount sorbed at equilibrium pressure 'P' and P_o is the saturated

vapor pressure.

W_o is the total sorption capacity.

T   is the temperature (K) and

(B/β^2) is the affinity co-efficient.

Thus, by plotting $Log(W)$ against $[T\{log(P_o/P)\}]^2 \times 2.303$, straight lines were obtained, (Figure 4.7). In the Figure 4.7, the Dubinin plots obtained over MCM-22 sample with SiO_2/Al_2O_3 ratio = 40 are presented. Straight lines were obtained in the region studied. Similar results were obtained over the other two samples. From the slope and intercept, the total sorption capacity and affinity co-efficients were calculated.   The results are presented in Table 4.4. From the table, it could be seen that the affinity coefficient and amount adsorbed decrease as temperature increases.   Besides the affinity co-efficient increases with increase in SiO_2/Al_2O_3 ratio. Whether, this implies an increase in the acid strength of the zeolite (with increasing SiO_2/Al_2O_3 ratio) is not clear. On the other hand, the adsorption capacity decreases with increase in the SiO_2/Al_2O_3 ratio, apparantely due to the reduction in the number of adsorption sites. Linear Dubinin plots have earlier been
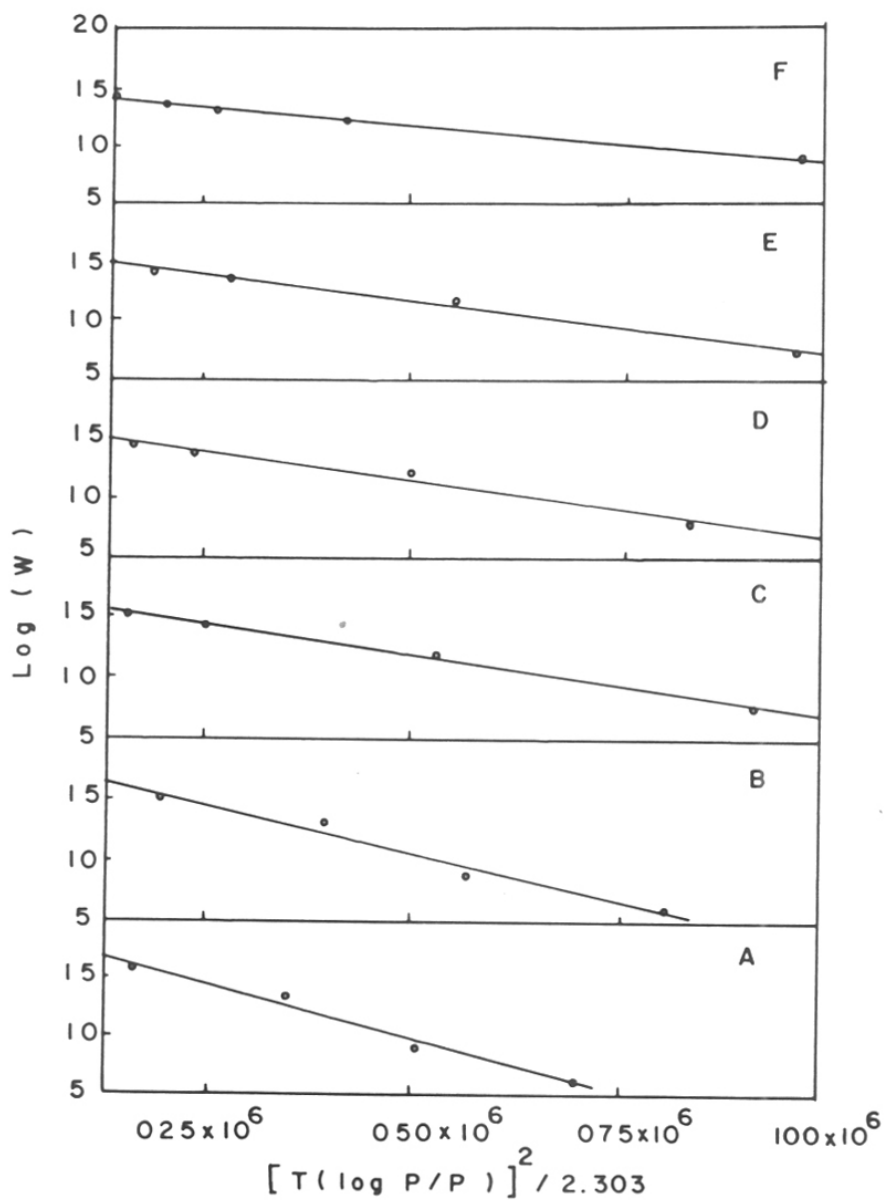
Figure 4.7   Dubinin plots for the adsorption of ammonia over sample with
$SiO_2/Al_2O_3 = 40$ at different temperatures.
(A) 303 K, (B) 333 K, (C) 363 K, (D) 393 K, (E) 423 K
and (F) 453 K.

Table 4.4   Total sorption capacity and affinity values obtained from Dubinin equation.

| Temperature (K) | SiO$_2$/Al$_2$O$_3$ | | | | | |
| | 40 | | 80 | | 140 | |
	B/ß^2 x 10$^{6@}$	W$_o$ [#]	B/ß^2 x 10^6	W$_o$	B/ß^2 x 10^6	W$_o$
303	18.7	75.86	31.50	51.29	35.5	48.98
333	9.44	46.77	23.70	38.02	25.9	35.48
363	9.73	42.64	19.90	32.36	21.1	28.84
393	9.22	39.81	16.50	26.30	17.4	22.91
423	8.16	36.31	12.40	20.42	13.4	20.89
453	6.12	28.18	9.03	14.13	11.2	15.49

[@]B/ß^2 : Affinity coefficient.

[#]W$_o$: Total sorption capacity.

reported for ammonia sorption over modified ß zeolites and CO_2 sorption over LTL and n-butylamine sorption over titanosilicates and Fe-Y zeolites.[2-4,20,21]

(III) Isosteric heats of adsorption

Vogt *et al.* have evaluated the thermodynamic parameters for the sorption of benzene, n-butylamine and ammonia on Ce-Na-Y and Cr-Na-Y.[37] Isosteric heats of adsorption of ammonia, pyridine and n-butylamine have been evaluated from microcalorimeteric studies on cation-exchanged zeolites such as X, Y and mordenite.[12, 19] Isosteric heats (q_{st}) are calculated from sorption isosteres by applying the Clausius Clapeyron equation at constant sorbate loadings.[38]

$$q_{st} = R[\{T_2 \times T_1\}/\{T_2 - T_1\}] \times Ln(P_2/P_1).$$

Plots of ln(p) vs (1/T) yielded straight lines at constant coverages in the present studies. From the slope, isosteric heats were calculated by the following relation :

$$q_{st} = (Slope \times 1.98 \times 4.186)/1000 \ kJ.$$

The results are presented in Table 4.5. At a constant coverage, q_{st} was found to decrease in the following order of SiO_2/Al_2O_3 ratio :

SiO_2/Al_2O_3 ratio : 40 > 80 > 140.

Besides, the heat of adsorption increases with increasing coverage (number of molecules/unit cell) and decreases beyond certain coverages for all those samples studied (Table 4.5).   Exactly similar results were obtained by Aurox *et al.*[39] during microcalorimetric studies of NH_3 adsorption over H-ZSM-5. The above authors have suggested that a combination of the three factors viz., (i) immobile adsorption of ammonia, (ii) mass-transfer limitations in the narrow zeolitic channels and (iii) non-

Table 4.5   Isosteric heats of adsorption (of ammonia) over
            MCM-22 samples at different sorption values.

Coverage (number of molecules/unit cell)	SiO_2/Al_2O_3		
	40	80	140
0.37	17.51	11.40	9.88
0.56	31.16	26.98	19.43
0.75	33.20	30.58	20.99
0.93	35.13	33.21	23.89
1.11	25.50	23.56	21.88
1.30	25.53	-	-
1.49	24.53	-	-

uniform energetic site distribution, is probably responsible for the initial increase in q_{st} with coverage. The q_{st} values obtained over MCM-22 are much smaller than those reported by Aurox *et al.* for ZSM-5 (> 100 kJ mole^{-1}).[39] This is probably due to the weaker acidity in MCM-22 than ZSM-5.

(IV) Chemical Affinity

A decrease in the chemical potential takes place when a gas is transferred reversibly and isothermally from a gas phase at a standard pressure p_o into an infinite amount of sorbent-sorbate mixture at an equilibrium pressure P. Neglecting the non-ideality of the sorbate, the chemical affinity may be expressed as :

$$-\Delta\mu = RT \ln(P/P_o).$$

The value of $-\Delta\mu$ may often be taken as the quantitative measure of the chemical affinity of the sorbate for the sorbent. Plots of $-\Delta\mu$ against the amount sorbed also serve as useful criteria for the comparison of the sorption affinities of a probe molecule in the lattices of different zeolites. Typical plots of $-\Delta\mu$ against the amount sorbed are shown in Figure 4.8 for H-MCM-22 samples.

From the plots, it could be seen that higher temperatures, the drop in affinity is steeper than at lower temperatures. Also, it could be seen that at higher temperatures, the decrease in chemical potential in the case of samples with low aluminum content (SiO_2/Al_2O_3 = 80 and 140) are nearly same but the chemical potential of the sample with SiO_2/Al_2O_3 = 40 decreases rather slowly.
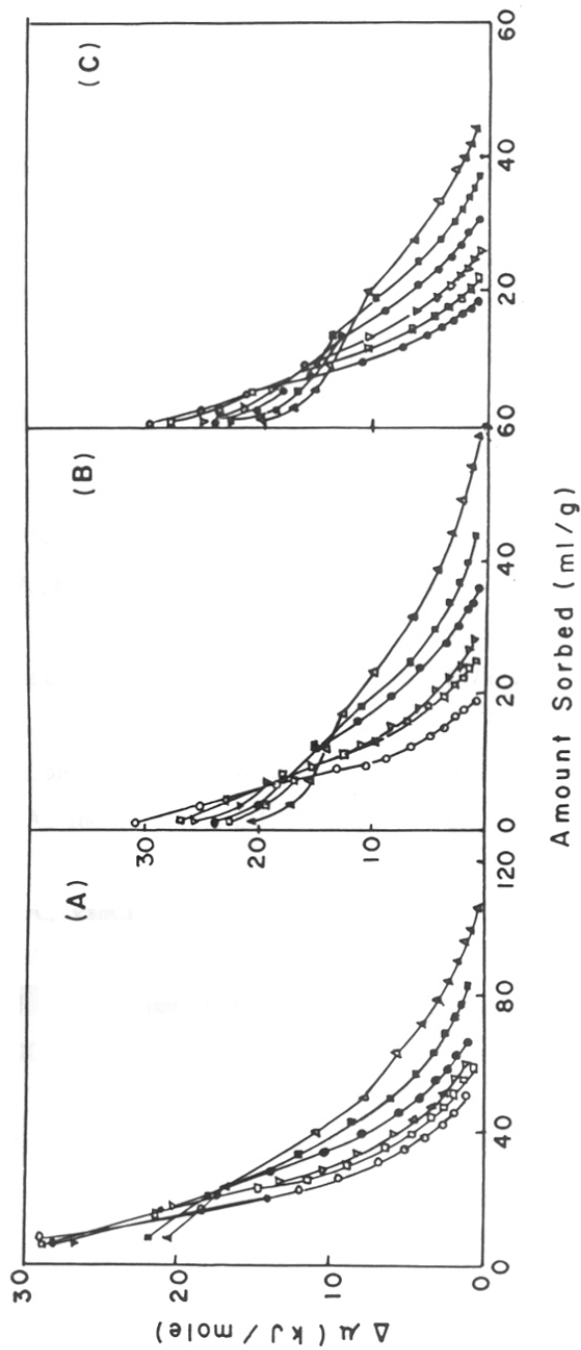
Figure 4.8   Chemical affinity plots for sorption of ammonia over MCM-22 samples with varying SiO₂/Al₂O₃ ratios. SiO₂/Al₂O₃ ratios : (A) 40, (B) 80 and (C) 140.

(△) 303 K, (■) 333 K, (●) 363 K, (▼) 393 K, (□) 423 K and (O) 453 K.

147

4.4 REFERENCES

1. Ward, J. W., `Zeolites Chemistry and Catalysis', (Rabo, J. A., Ed.,), *ACS Monograph.* **171**, 118 (1976).

2. Reddy, K. S. N., Eapen, M. J., Soni, H. S., and Shiralkar, V. P., *J. Phys. Chem.* **96**, 7923 (1992).

3. Rao, G. N., Joshi, P. N., Kotasthane, A. N., and Shiralkar, V. P., *J. Phys. Chem.* **94**, 8589 (1990).

4. Mirajkar, S. P., Thangaraj, A., and Shiralkar, V. P., *J. Phys. Chem.* **94**, 3073 (1992).

5. Yates, D. J. C., `Molecular Sieves', Soc. Chem. Ind., London, (1968) 334.

6. Ward, J. W., "Molecular Sieve Zeolites-1", *Adv. Chem. Ser.* (Gould, R. F., Ed.,) Am. Chem. Soc. **101**, 380 (1971).

7. Jacobs, P. A., and Heylen, C. F., *J. Catal.* **39**, 267 (1974).

8. Corma, A., Corell, C., Pérez-Pariente, J., Guil, J. M., López, R. G., Nicolopoulos, S., Gonzalez Calbet, J., and Regi, M. V., *Zeolites.* **16**, 7 (1996).

9. Angell, C. L., *J. Phys. Chem.* **70**, 2420 (1976).

10. Ward, J. W., and Hobgood, H. W., *J. Phys. Chem.* **70**, 1178 (1976).

11. Jacobs, P. A., and Utterhoeven, J. B., *J. Chem. Soc. Faraday Trans., I.* **69**, 339 (1973).

12. Jacobs, P. A., VanCauwelaert, F. H., Vansant, E. F., and Utterhoeven, J. B., *J. Chem. Soc. Faraday Trans. I.* **69**, 1056 (1973).

13. Egertone, T. A., and Stone, F. S., *J. Colloid Interface Sci.* **38**, 195 (1972).

14. Steinberg, K. H., Bremer, H., and Falke, P., *Z. Phys. Chem.* (Leipzig) **257**,.151 (1976).

15. Barrer, R. M., and Bratt, G. C., *J. Phys. Chem. Solids.* **12**, 130 (1956).

16. Barrer, R. M., and Gibbons, R. M., *Trans. Faraday Soc.* **59**, 2569 (1963).

17. Coughlan, B., and Kilmartin, S. J., *J. Chem. Soc. Faraday Trans. I* **71**, 1809 (1975).

18. Coughlan, B., and Larkin, P. A., *Chem. Ind.* 275 (1976).

19. Coughlan, B., and McCann, W. A., *J. Chem. Soc. Faraday Trans. I* 75, 1769 (1979).

20. Shiralkar, V. P., and Kulkarni, S. B., *J. Colloid and Interf. Sci.* 108(1), 1 (1985).

21. Shiralkar, V. P., and Kulkarni, S. B., *J. Colloid and Interf. Sci.* 109(1), 115 (1986).

22. Romanovskii, B., Topchieva, K .V., Stolyanova, L. V., and Alakseev, A. M., *Kinet. Catal.* 13, 1003 (1971).

23. Ravishankar, R., Sen, T., Ramaswamy, V., Soni, H. S., Ganapathy, S., and Sivasanker, S., *Stud. Surf. Sci. Catal.* 84(A), 329 (1994).

24. Ravishankar, R., Bhattacharya, D., Jacob, N. E., and Sivasanker, *Microporous Materials.* 4, 83 (1995).

25. Ernst, S., Jacobs, P. A., Martens, J. A., and Weitkamp, J., *Zeolites.* 7, 25 (1986).

26. Breck, D. W., `Zeolite Molecular Sieves', Wiley-Interscience, NY, 1974.

27. Leonowicz, M. E., Lawton, J. A., Lawton, S. L., and Rubin, M. K., *Science.* 264, 1910 (1994).

28. Karger, J., and Ruthven, D. M., "Diffusion in Zeolites and Other Microporous Solids", Wiley-Interscience, New York, (1992).

29. Bulow, M., Schlodder, H., Rees, L. V. C., and Richards, R. E., Proc. of 7th Intern. Conf. Zeolites, Tokyo, (1986).

30. Zikanova, A., Bulow, M., and Schlodder, H., *Zeolites.* 7, 115 (1987).

31. Deolle, H-J., Heering, J., and Riekert, L., *J. Catal.* 71, 22 (1981).

32. Kieselev, A. V., *Discuss. Faraday Soc.* 40, 205 (1965).

33. Dubinin, M. M., and Radushkevich, L. V., *Proc. Acad. Sci.* USSR, 55, 227 (1974).

34. Dubinin, M. M., *Chem. Rev.* 60, 309 (1960).

35. Dubinin, M. M., *Pure Appl. Chem.* 10, 309 (1965).

36. Dubinin, M. M., and Astakhov, V. A., *Bull. Acad. Sci.* USSR, 20, 3 (1971).

37. Vogt, V. F., Wolf, H., Bremer, H., Rubinshtein, A. M., Klyacho, A. L., Brueva, J. B., and Mishin, I. V., *Z. Anorg. Allg. Chem.* 439, 153 (1978).

38. Barrer, R. M., and Coughlan, B., `Molecular sieves', Soc. Chem. Ind., London (1968) p.141,233 and 241.

39. Auroux, A., Bolis, V., Wierzchowski, P., Gravelle, P. C., and Vedrine, J. C., *J. Chem. Soc. Faraday Trans. II.* 75, 2544 (1979).

CHAPTER V

CATALYTIC PROPERTIES OF MCM-22

5.1 INTRODUCTION

Catalytic reactions have been used in combination with other techniques, to estimate the pore dimensions of zeolites with unknown structures.[1,2] The catalytic tests yield data obtained under realistic conditions, which include mass-transfer and intrinsic chemical effects.[3] Eventhough characterization by spectroscopic techniques and adsorption of probe molecules provide general information about pore topology, the picture of the pore openings provided by these techniques is not complete. Catalytic test reactions often provide additional information on the nature of the pore openings, side pockets and windows. The test reactions generally used to gauge the pore dimensions of zeolites with unknown structures[4,5] have been discussed in Chapter I.

Apart from the catalytic test reactions such as, m-xylene isomerization, ethyl benzene disproportionation and n-decane cracking, there are a number of other reactions which are either acid or base catalyzed that are industrially important. Nowadays, zeolites are replacing conventional acid catalysts which are hazardous and pollute the environment. In contrast, zeolites are eco-friendly, non-hazardous and easy to handle. Zeolites are used in petroleum refining, petrochemical processing and also in the synthesis of fine chemicals and drug intermediates. One of the many advantages of zeolites arises from their inherent shape-selective nature and their ability to discriminate molecules by their shapes and sizes, which can lead to high selectivities for the desired product.

MCM-22 is a high-silica zeolite[6,7] which has been reported in the patent literature to have wide applications in acid-catalyzed reactions such as, disproportionation, FCC, octane boosting, production of low density jet fuel, isomerization and alkylation reactions.[8-13] It is also reported to be useful in the transformation of methanol to hydrocarbons [MTG process].[14]

150

The present chapter [Chapter V] discusses the use of the test reaction, isomerization of m-xylene, to gauge the pore dimensions of the MCM-22. This chapter also addresses the performance of MCM-22 as a catalyst in other acid-catalyzed reactions such as, the hydroisomerization and cracking of n-hexane and transformation of methanol to hydrocarbons.[15,16]

5.2 EXPERIMENTAL

5.2.1 PREPARATION OF CATALYSTS

The method of preparation of the MCM-22 samples and their modifications are described in Chapter II. The catalysts (MCM-22) used for all the acid-catalyzed reactions were in their protonic [H⁺] form except in the case of hydroisomerization reactions, where platinum impregnated H-forms were used. The catalyst powder (MCM-22) was pressed into pellets and sieved into -12 +18 mesh size particles. The catalytic activities of other zeolites were also examined for comparison purposes. Zeolite beta, mordenite and USY were obtained from PQ (Netherlands), Norton (USA) and Linde (USA), respectively. ZSM-12 was prepared following the synthetic procedure described by Ernst et al.[17] Mordenite was dealuminated using the procedures described in Chapter II.

5.2.2 CATALYTIC REACTIONS : METHODOLOGY

The catalytic reactions were carried out in a fixed bed, down flow, tubular silica reactor at atmospheric pressure. The tubular reactor consisted of a fused silica tube (40 cm long with 1.5 cm I.D.) equipped with a thermowell. The sieved catalyst material (2 g) was loaded in such a way that the tip of the thermocouple (kept inside a thermowell) was at the center of the catalyst bed. The catalyst was flanked by inert porcelain beads (both above and below) which provided a more uniform flow distribution. The top portion of the porcelain beads additionally served as a pre-heater zone and vaporizer. A condenser was attached to the outlet of the

151

reactor which was cooled by cold water circulation from a cryostat maintained at approximately 0 °c. A sample collector, (separating funnel), was connected to the condenser. An outlet to measure the gas evolved was connected to a gas collection system.

The products were analyzed by gas chromatography. The gas and liquid products [hydrocarbons] were analyzed by a gas chromatograph (HP 5890A), equipped with a capillary column coated with cross-linked methyl silicone gum [HP1; 50 m x 0.5 mm] and a FID. For m-xylene isomerization studies, a gas chromatograph (Shimadzu GC R1A) equipped with a 5 % bentone + 5 % diisodecyl phthalate column (2 m x 3 mm) was used.

Prior to the reaction, the catalyst, was activated under a flow of air at 773 K for 6 h. Later, the catalyst was cooled with flowing nitrogen to the desired reaction temperature. Whenever Pt containing catalysts were used, reduction of the catalyst was carried out with H_2 (100 ml min^{-1}) for 4 h at 573 K prior to injection of the feed at the desired temperature.

5.3 ISOMERIZATION OF m-XYLENE

Normally, the feed to a commercial xylene-isomerization unit contains the undesired xylene isomers (mostly m-xylene) and ethyl benzene. The role of the catalyst is to convert the m-xylene into an equilibrium mixture of xylene isomers and to eliminate the ethyl benzene from the feed stock with minimal xylene loss (which may occur through disproportionation/transalkylation reactions).

5.3.1 MECHANISM

In the presence of an acid catalyst, m-xylene undergoes two types of reactions, namely, (I) isomerization to ortho- and para-xylenes and (II) disproportionation or transalkylation to trimethyl benzenes and toluenes. This reaction network is depicted in Figure 5.1.

The isomerization of m-xylene mainly gauges the largest cavity and not the window size. Csicsery[18] has proposed two types of mechanisms and arrived at the conclusion that intramolecular 1,2-alkyl shift was favored at higher temperatures and intermolecular shifts are favored below 473 K. Later, Corma *et al.* proposed a bimolecular mechanism for the isomerization of m-xylenes.[19] Gnep *et al.* were the first to use m-xylene isomerization as a test-reaction to gauge the pore dimensions of zeolites.[20] Martens *et al.* explored the use of isomerization of m-xylene to estimate the void structure of zeolites.[21] The zeolites could be ranked as 10 MR or 12 MR pore-types depending on the distribution of trimethyl benzene [TMBs] isomers formed during m-xylene isomerization.[21] Three possible pathways are believed to account for the formation of TMBs. The reaction pathways are presented in Figure 5.1 [Scheme II].

Martens *et al.* proposed the formation of diphenyl methane type intermediates during the isomerization of m-xylene[21] (see Figure 5.1 (VI A-C)). Each intermediate leads to a particular of TMB isomer (Figure 5.1 (V A-C)). 1,3,5-Trimethyl benzene (V A) is bulkier than

153
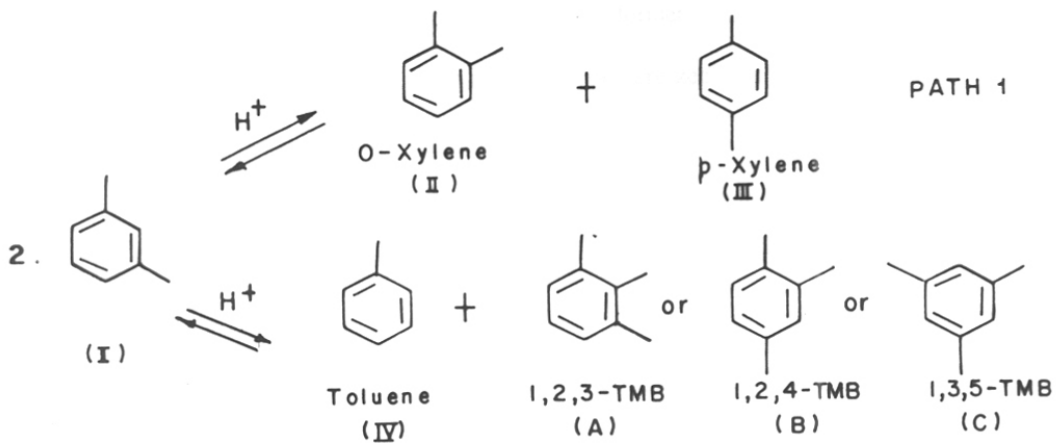
SCHEME − I

Reactions during the isomerization of m−xylene
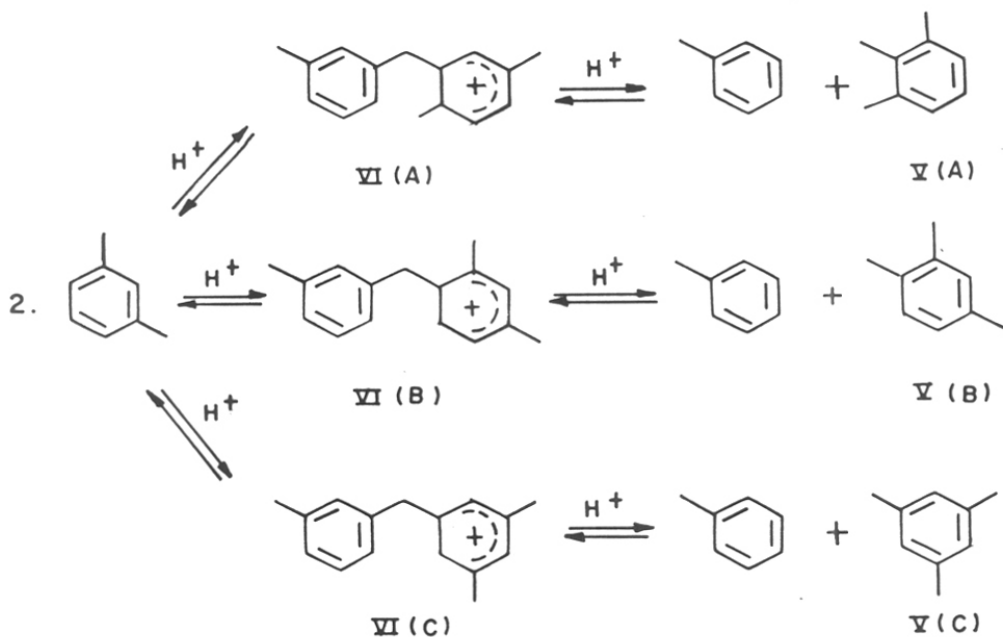
SCHEME − II

Probable transition states during the disproportionation of m−xylene

Figure 5.1   Reactions and transition states during the transformation of m-xylene.

154

the other isomers (VI B and C). The formation of the former will be sterically hindered in the case of medium pore zeolites, but in the case of large pore zeolites, they will be formed with relative ease due to the availability of space inside the pores/cages.

The presence of any specific TMB in the product is determined mainly by the extent of steric hindrance inside the zeolite cavity.[19,21] Thus, the difference in the diffusion of the TMB isomers (PSS) through the channels are believed to be less important than steric effects on the transition states (RTSS). Medium pore zeolites offer more steric hindrance leading to more isomerized products than the transalkylated products. Thus, (I/D) ratio is larger over medium pore zeolites.

Isomerization reactions were carried out over different MCM-22 samples and the influences of the various reaction parameters are discussed in the following sections.

5.3.2 PORE CHARACTERISTICS IN MCM-22

To understand the pore characteristics of MCM-22, the isomerization of m-xylene was carried out at different conversions levels at the same temperature (623 K) by varying the space velocity.

5.3.2.1 Isomerization

The p-xylene/o-xylene (p-/o-) ratio at various conversion levels of m-xylene are presented in Figure 5.2 (A). The same set of experiments were carried out over other zeolites and the results were used as standards for comparison of MCM-22. Earlier workers have shown that, when diffusion was absent, the probabilities of producing para- and ortho-isomers from m-xylene were nearly equal and p-/o- xylene ratio did not depend on the acid strength of the zeolite.[21] The important parameter that affected the p-/o- xylene ratio was diffusion selectivity. Dewing[22] reported that the diffusivity ratios of p-xylene to ortho-xylene (D_{para}/D_{ortho}) were 12.82 and 1.73, respectively, in the case of ZSM-5 (medium pore ; 0.55 nm) and mordenite (large pore; 0.67 nm) at 673 K. The p-/o- xylene ratios of the different zeolites
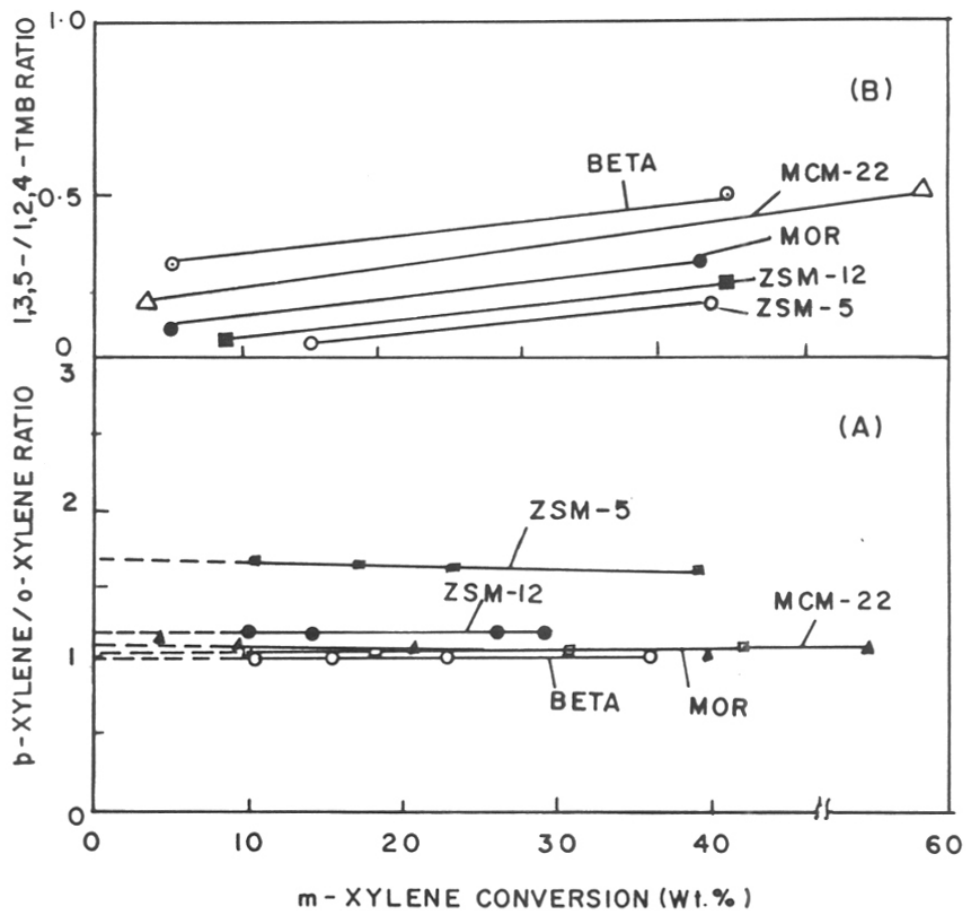
155

Figure 5.2 (A) p-Xylene/ortho-xylene ratios at different conversion levels of m-xylene over medium and large pore zeolites.

(B) The ratio of 1,3,5-TMB/1,2,4-TMB at different m-xylene conversion levels over different zeolites.

(at extrapolated zero conversions) were ZSM-5, 1.7; NCL-1, 1.1; beta and mordenite, < 1.1 and ZSM-12, ~ 1.2 (Figure 5.2 A). It is found that the p-/o- xylene ratio of ZSM-5 is well above the thermodynamic equilibrium value of 1.1. In medium pore zeolites, the **"diffusion controlled product shape selectivity"** (PSS)[21,23] is believed to be responsible for enhanced para selectivity, ie., more para xylene in the product stream. In the large pore zeolites, an equilibrium distribution of both ortho- and para-isomers were found (mordenite and beta (~ 1)), suggesting that there is no diffusion controlled product shape selectivity, as the pores are large enough to permit rapid diffusion of the xylene isomers. MCM-22 was found to have a p-/o- ratio of 1.01 (± 0.1), which is very near the equilibrium value. Thus, MCM-22 was found to behave as a large pore zeolite, eventhough structural studies have shown the existence of 10 MR channels normally associated with medium pore zeolites.[24]

5.3.2.2 Disproportionation

The isomerization of m-xylene is invariably accompanied by disproportionation over acid zeolites. m-Xylene disproportionates into toluene and trimethyl benzenes[21] [see Figure 5.1, Scheme II]. The ratio of isomerization (I) to disproportionation (D), (I/D) plotted as a function of m-xylene conversion and the values extrapolated to zero gives useful information about void space in the zeolite.[21]

During the isomerization of m-xylene, the product pattern is believed to be controlled by PSS, while **"Restricted transition state shape selectivity"** (RTSS) is believed to determine the product selectivities in disproportionation reactions. The facility or the ability of the transition state to be formed inside the void of the particular zeolite governs the formation of a particular type of TMB isomer. Thus, in medium pore zeolites, 1,3,5-TMB formation is sterically hindered and is present in negligible amounts in the products, while the least bulky isomer, 1,2,4-TMB is formed in relatively large quantities.

157

The void space in different zeolites can be estimated by comparing the ratios of 1,3,5-TMB and 1,2,4-TMB isomers at similar conversions. The ratio of 1,3,5- and 1,2,4- TMBs were plotted against the conversions of m-xylene. Data obtained over different zeolites were used for comparison. Figure 5.2(B), presents the results obtained over large and medium pore zeolites.[16,25] It is observed that MCM-22 occupies an intermediate position between beta and mordenite. As the formation of 1,3,5-TMB is easier in the case of large pore zeolites, the 1,3,5-/1,2,4- TMBs ratio is found to be larger over large pore zeolites. The 1,3,5-/1,2,4- TMB ratios for ß, MOR, MTW are 0.36, 0.16 and 0.08, respectively, at a conversion level of 10 % at 623 K.[25] The values reported by Martens et al. were 0.30 for MOR, 0.30 for BEA and 0.0 for MTW at a conversion range of 6.9 - 10.6 % at 623 K.[21] The ratio observed over MCM-22 at 9.5 % conversion level at 573 K is 0.25.

In addition to the 1,3,5-TMB/1,2,4-TMB values, the ratio of products formed by Isomerization reactions (I) to the Disproportionation reactions (D) can be used to guage the void space.[21] Disproportionation reactions are bimolecular and occur more easily in wide pore zeolites (relative to medium pore analogs). The Figure 5.2 (C) shows the plot of Log(I/D) at different conversions of m-xylene, the dotted lines indicate their extrapolation to `0 conversion'. At "0 conversion" levels, the ratios observed over different zeolites were : NCL-1, 0.11;[25] mordenite, 0.05; beta, 0.22 and MCM-22, 0.25. The ratios suggest that MCM-22 behaves similar to wide pore zeolites.

MCM-22 exhibits p-/o- xylene ratio of ~ 1.1 ± 0.1 (near equilibrium value), log(I/D) ratio of 0.66 and 1,3,5-/1,2,4-TMB ratio of ~ 0.25 (at extrapolated '0' conversion level). Thus, it behaves like a wide pore zeolite in m-xylene isomerization. However, Corma et al.[26] have observed an I/D ratio of 15 (Log(I/D) ~ 1.2) during their studies on m-xylene isomerization over MCM-22 and believe that its selectivity is in between that of 10 MR and 12 MR zeolites. The formation of 1,3,5-TMB over MCM-22 and mordenite at similar conversion levels and the
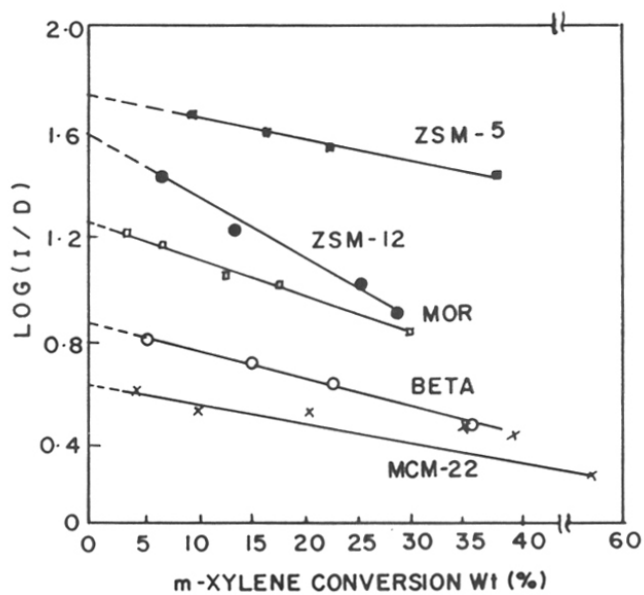
Figure 5.2   (C)   Plot of Log(I/D) at different m-xylene conversion levels.

absence of 1,3,5-TMB even at 17 % conversion of m-xylene over ZSM-5 supported their suggestion.

5.3.3 INFLUENCE OF SPACE VELOCITY

The results obtained during the studies on space velocity variations are presented in Table 5.1. The variation in the p-/o- xylene ratio was very small (1.02 to 1.16) in the conversion range of 9.5 % to 58 %. Thus, the p/o ratio was near to the equilibrium value of 1.1 even when the conversion was far from equilibrium. The formations of TMBs were more at high conversions (low space velocities) resulting in a decrease in I/D ratios (I/D = 4.0 and 1.6 at 4.1 % and 58.1 % conversions, respectively).

5.3.4 INFLUENCE OF REACTION TEMPERATURE

The results of the temperature variations on the distribution of products is presented in Table 5.2. It can be seen that, as temperature is increased, conversion and disproportionation increase. The rate of formation of transalkylated products is higher at higher temperatures and a slight decrease in p/o ratio is also noticed (from 1.15 to 1.02). The 1,3,5-/1,2,4- TMB ratios remains nearly constant (~ 0.42) in the temperature range of 523 K to 598 K. The ratio of 1,3,5-/1,2,4- TMBs is 0.42 at 598 K which is reasonably similar to the thermodynamic value of 0.32 expected during the disproportionation of m-xylene.

5.3.5 THE INFLUENCE OF ALUMINUM CONTENT OF THE ZEOLITE

The results of the isomerization studies carried out over samples with varying SiO_2/Al_2O_3 ratios are presented in Table 5.3. The results show that, conversion and disproportionation decrease with decrease in the aluminum content. Disproportionation proceeds by a bimolecular pathway requiring 2 adsorption sites located near each other.[21] This would facilitate the adsorption of two m-xylene molecules leading to a diphenyl methane type intermediate. When the aluminum content is decreased, the total number of acid sites decreases. The number of paired adsorption sites also decrease significantly with decrease in aluminum content. This

160

Table 5.1   m-Xylene isomerization over MCM-22 samples: effect of space velocity on product distribution.

Conditions : Temp. = 573 K; H_2/m-xylene = 4; TOS = 2 h and Catalyst = H-MCM-22 (SiO_2/Al_2O_3 = 30).

	WHSV (h^{-1})				
	1.76	3.47	6.50	8.68	13.02
% Conversion	58.1	39.7	20.2	9.5	4.1
Product Distribution					
Toluene	5.0	6.1	8.4	14.2	20.7
Para xylene	27.7	31.3	26.8	22.7	31.0
Ortho xylene	26.8	30.8	25.2	21.3	26.8
1,3,5-TMB	10.8	7.5	7.6	6.0	2.0
1,2,4-TMB	24.9	19.1	25.4	23.9	10.2
1,2,3-TMB	2.9	2.3	3.1	2.8	0.5
Others[a]	2.0	3.0	3.4	9.1	8.8
I/D	1.6	2.4	3.2	3.5	4.0
p-/o- Xylene ratio	1.0	1.0	1.1	1.1	1.2
1,3,5-/1,2,4- TMBs	0.4	0.4	0.3	0.3	0.2

[a]Others : Benzene and aliphatics.

Table 5.2   m-Xylene isomerization over MCM-22 samples: effect of reaction temperature.
Conditions : WHSV (h^{-1}) = 3.47; H_2/m-xylene = 4; TOS = 2 h and Catalyst = H-MCM-22
(SiO$_2$/Al$_2$O$_3$ = 30).

	Temperature (K)			
	523	1548	573	598
% Conversion	26.2	35.1	39.7	57.1
Product Distribution				
Toluene	12.8	15.5	6.1	18.2
Para xylene	36.4	30.6	31.3	26.5
Ortho xylene	31.4	27.6	30.8	25.2
1,3,5-TMB	4.8	6.7	7.5	7.5
1,2,4-TMB	11.4	16.0	19.1	17.9
1,2,3-TMB	1.1	1.8	2.3	2.3
Others[@]	2.0	1.80	3.0	2.5
Log(I/D)	0.7	0.4	0.4	0.3
p/o ratio	1.2	1.1	1.0	1.1
1,3,5-/1,2,4- TMBs	0.4	0.4	0.4	0.4

[@]Others : Benzene and aliphatics.

Table 5.3   Effect of aluminum content of MCM-22 samples on the isomerization of m-xylene.

Conditions :   Temp. = 573 K; WHSV (h^{-1}) = 3.47; H_2/m-xylene (mole) = 4;

                TOS = 2 h and Catalyst = H-MCM-22

	SiO_2/Al_2O_3					
	28	40	56	80	96	140
% Conversion	39.7	28.4	20.1	17.6	14.1	13.8
Product Distribution						
Toluene	6.1	5.3	4.0	3.6	2.7	1.6
Para xylene	31.3	34.4	34.9	39.3	39.8	45.5
Ortho xylene	30.77	33.4	33.9	37.2	37.8	43.0
1,3,5-TMB	7.49	5.6	4.1	3.2	3.0	1.0
1,2,4-TMB	19.09	14.5	10.4	8.6	8.5	7.7
1,2,3-TMB	2.27	1.8	1.4	1.3	1.0	1.0
Others[a]	2.96	5.0	6.0	6.8	7.1	8.0
(I/D)	2.44	3.5	4.9	6.6	7.0	7.9
Log(I/D)	0.39	0.6	0.7	0.8	0.9	0.9
p/o ratio	1.02	1.0	1.0	1.1	1.1	1.1
1,3,5-/1,2,3 - TMBs	0.30	0.3	0.3	0.4	0.3	0.4

[a]Others : Benzene and aliphatics.

163

aspect is apparent when we compare the I/D ratios observed at different conversion levels during WHSV-studies (using MCM-22 with SiO_2/Al_2O_3 = 28) and during Al-content studies. The I/D ratio increases marginally from 3.4 to 4.0 when the conversion decreases 10-fold from 39.7 to 4.1 % during the WHSV studies (Table 5.1) while it increases nearly three fold from 2.4 to 7.9 when the conversion decreases from 39.7 % to 13.8 % during the Al-content studies (Table 5.3). In other words, at the same conversion level, the I/D ratio is larger for the catalysts with higher SiO_2/Al_2O_3 ratio.

5.4 HYDROISOMERIZATION OF n-HEXANE

5.4.1. INTRODUCTION

The hydroisomerization of light naphtha (C_5 - C_6 fractions) is an industrially important process and is used in the production of high octane gasoline blend stocks.[27,28] The process involves the transformation (with minimal cracking) of the low octane normal (and less branched) paraffin components into high octane isomers with greater branching of the carbon - chain. For example, n-hexane has a blending research octane number (RON) of 19,[29] which on isomerization yields an equilibrium mixture of n- and i-hexanes, the overall RON of the mixture (at 503 K) being 74.9. The dimethyl butanes (2,2-dimethyl butane (2,2-DMC$_4$); RON = 92.3 and 2,3-dimethyl butane (2,3-DMC$_4$); RON = 103.5) have larger RON values than the monomethyl pentanes (2-methyl pentane (2-MP); RON = 73.4 and 3-methyl pentane (3-MP); RON = 74.5) and constitute a larger proportion of the equilibrium mixtures at lower temperatures.

Hydroisomerization reactions are generally carried out over bifunctional catalysts, containing, often, platinum. The metal component aids in increasing the rate of isomerization, besides lowering catalyst deactivation. The reactivity of n-alkanes increases as the carbon number increases but the selectivity towards isomerization decreases.[30] The mono-branched isomers are formed predominantly as they are the primary products. These undergo consecutive reactions to yield multiply branched isomers. The chain length has a marked influence on the reaction rate and over the formation of the multiply branched isomers, which increases on increasing the chain length.[30]

The hydroisomerization of n-hexane has already been studied over Pt-loaded zeolites such as Pt-Y,[31] Pt-beta (β)[32] and Pt-mordenite (MOR).[33] There is a general consensus on the mechanism of alkane hydroisomerization. n-Alkane molecules are adsorbed at

dehydrogenation/hydrogenation sites where n-alkenes are formed. These migrate and interact with acid sites and 2° carbenium ions are generated, which further rearrange to more stable 3° carbenium ions. Finally, the 3° carbenium ions are hydrogenated at the metallic sites yielding isoalkanes.[34,35] The isomerization of n-hexane over Pt supported on acidic zeolites is believed to proceed by a bifunctional mechanism.[31,32] The metal atoms act as dehydrogenation sites and generate reactive olefinic intermediates. The olefinic intermediates isomerize via carbocations over Brönsted acid sites. The iso-olefins transform into iso-paraffins over the metal atoms by hydrogenation. Studies on the influence of the metal content and the acidity (SiO_2/Al_2O_3 ratio) of the zeolite are important aspects of the overall investigations of bifunctional catalysis.

The hydroisomerization of n-hexane was carried out at atmospheric pressure in the temperature range 473 - 573 K over Pt-MCM-22. The influence of Pt-content, the SiO_2/Al_2O_3 ratio of the zeolite and reaction parameters on the isomerization efficiency of the catalyst was investigated. The optimum Pt-content for the reaction was found to be approximately 0.5 wt %. At a constant Pt content of 0.5 wt. %, increasing the Al-content of the zeolite increased catalytic activities and I/C ratios. The studies suggest that the reaction proceeds by a bifunctional mechanism.

5.4.2 INFLUENCE OF Pt-CONTENT ON n-HEXANE ISOMERIZATION

The transformation of n-hexane was carried out at atmospheric pressure in the temperature range of 473 K to 573 K over Pt-MCM-22 samples containing varying amounts of Pt (0.1 to 0.75 wt %). All the catalysts deactivated with increasing duration of the run (time on stream = TOS), the deactivation being more rapid during the first few minutes (Figure 5.3), the activity becoming reasonably stable after 30 - 45 minutes. The deactivation rate was also more rapid at higher temperatures, the effect being more pronounced when the Pt content was low (Figure 5.3 (A & B)). Also, at a given temperature, the deactivation rate increased with a decrease in Pt content (Figure 5.3 (C)). Therefore, the data reported in the following sections
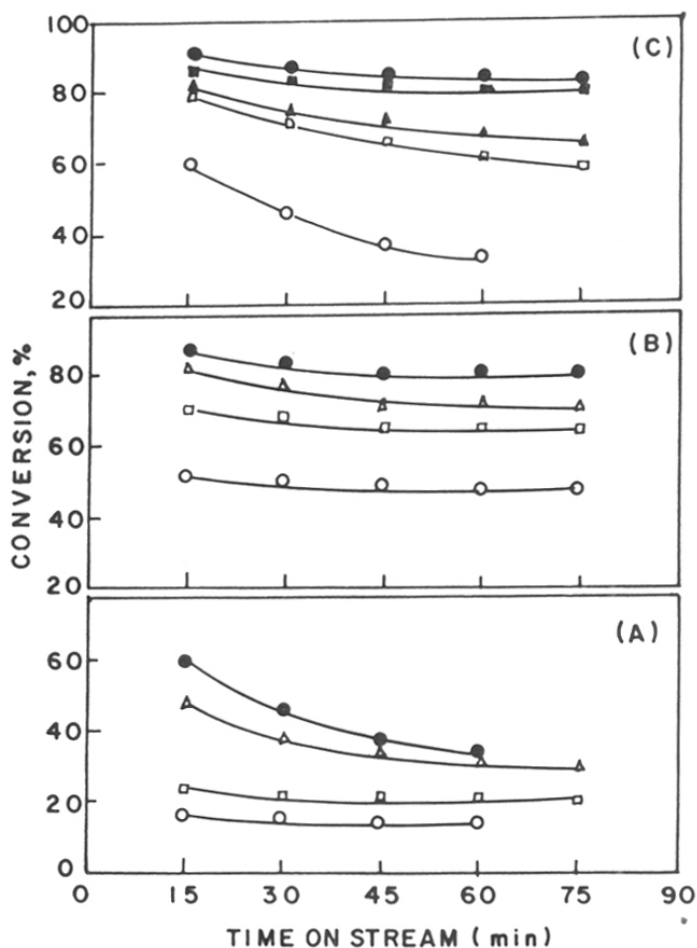
Figure 5.3   Effect of temperature and Pt-content on catalyst deactivation with duration of
run (time on stream = TOS).

(A):   Catalyst, Pt-(0.1 %)-H-MCM-22 (SiO$_2$/Al$_2$O$_3$ = 28); WHSV (h^{-1}) = 1.0;
H$_2$/n-hexane (mole) = 4.5; (O) 473 K; (□) 503 K; (Δ) 548 K and
(●) 573 K.

(B):   Catalyst, Pt-(0.5 %)-H-MCM-22 (SiO$_2$/Al$_2$O$_3$ = 28); WHSV (h^{-1}) = 1.0;
H$_2$/n-hexane (mole) = 4.5; (O) 473 K; (□) 503 K; (Δ) 548 K
and (●) 573 K.

(C):   Temp. = 573 K; WHSV (h^{-1}) = 1.0; H$_2$/n-hexane (mole) = 4.5; Pt-H-
MCM-22 (SiO$_2$/Al$_2$O$_3$ = 28) with Pt (Wt. %) : (O) 0.1; (□) 0.2; (▲) 0.3;
(■) 0.5 %; (●) 0.75.

167

were mostly collected over catalysts containing 0.5 wt % Pt and at 503 K at a TOS of 45 - 60 min. The influence of Pt-content (SiO_2/Al_2O_3 ratio of the zeolite = 28) on conversion at different temperatures is presented in Figure 5.4 (A). Conversion increases with increasing Pt-contents and reaches a maximum at about 0.5 wt % Pt. At temperatures above 523 K, the conversion remains constant with further increase in Pt content but decreases at lower temperatures. The observance of a maximum with Pt-loading is typical of bifunctional catalysis.[32,34,36] A similar decrease in the conversion at Pt-contents beyond 0.3 wt % was also observed by Leu et al.[32] during their studies on the isomerization of n-hexane over Pt-β.

The influence of Pt-content on the isomerization/cracking (I/C) ratios is presented in Figure 5.4 (B). Increasing the Pt-content increases the I/C ratio till a plateau is reached at around 0.5 wt % Pt. Increasing the temperature of the reaction, as expected, decreases the I/C ratios. The Pt-content does not appear to influence significantly the C_6-isomer distribution (Figure 5.4 (C)), and this is consistent with the role of platinum as a hydrogenation/dehydrogenation site rather than as a site for molecular rearrangements. The 2-methyl pentane/3-methyl pentane (2-MP/3-MP) ratio is ~ 1.63 ± 0.04 at all Pt-levels and is close to the equilibrium value of 1.74 expected at the reaction temperature (503 K). However, the dimethyl butanes are not formed in equilibrium amounts. The ratios of the methyl pentanes/dimethyl butanes (MP/DMB ~ 5.22 - 7.19) is larger than the expected equilibrium values of 2.43. Similarly, the 2,3-dimethyl butane/2,2-dimethyl butane ratio (2,3-DMB/2,2-DMB ~ 2.89 - 4.25) is also much larger than the expected equilibrium ratio of 0.59.

5.4.3 *INFLUENCE OF SiO_2/Al_2O_3 RATIO*

These studies were carried out at 503 K over Pt-MCM-22 samples containing the same amount of Pt (0.5 wt %) but different SiO_2/Al_2O_3 ratios. The results are presented in Table 5.4. The decrease in activity (conversion) with decreasing Al content (increasing SiO_2/Al_2O_3) is due
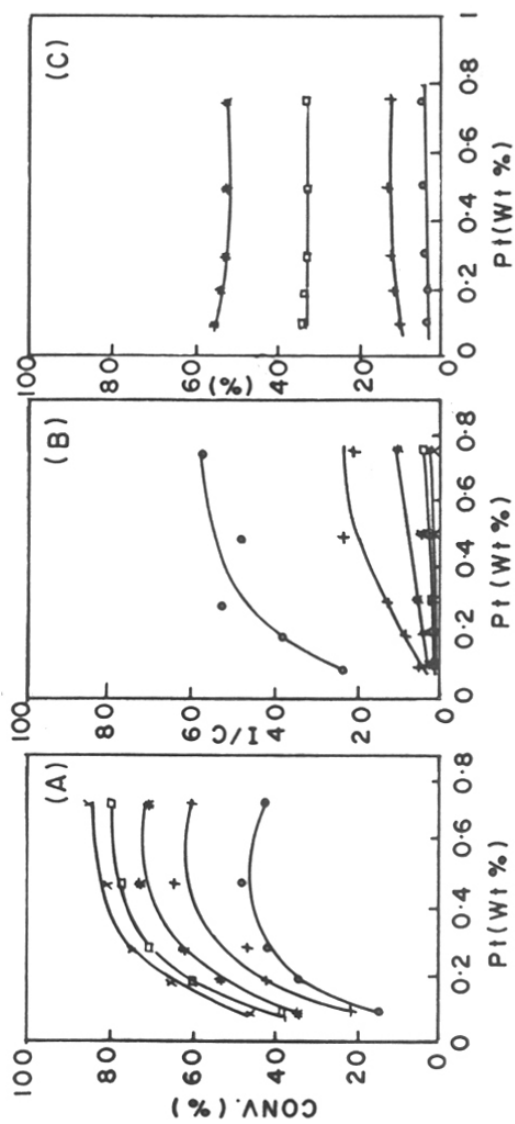
Figure 5.4   Influence of Pt-content on n-hexane isomerization.
Catalyst, Pt-(0.5 %)-H-MCM-22 (SiO$_2$/Al$_2$O$_3$ = 28); WHSV (h^{-1}) = 1.0;
H$_2$/n-hexane (mole) = 4.5; TOS = 45 min.

(A),(B):   (O) 473 K; (+) 503 K; (*) 523 K; (□) 548 K; (X) 573 K.

(C):   Temp. = 503 K; (O) 2,2-DMB; (+) 2,3-DMB, (□) 3-MP;
             (*) 2-MP.

Table 5.4   n-Hexane isomerization: Influence of aluminum content of MCM-22 on product distribution.

Conditions :   Temp. = 503 K; WHSV (h^{-1}) = 1.0; H_2/n-hexane (mole) = 4.5;
TOS (min) = 60 and Catalyst = Pt-(0.5 wt.%)-H-MCM-22 (SiO_2/Al_2O_3 = 28).

Product breakup (Wt. %)	SiO_2/Al_2O_3		
	28	58	80
C_1	0.02	0.01	0.01
C_2	0.07	0.07	0.05
C_3	1.65	1.35	1.19
i-C_4	1.19	1.12	1.39
n-C_4	0.44	0.51	0.44
i-C_5	0.76	0.82	1.06
n-C_5	0.24	0.41	0.45
2,2-DMC_4	2.28	1.72	0.45
2,3-DMC_4	6.54	5.68	2.16
2-MP	30.07	24.71	18.64
3-MP	18.26	15.45	11.34
n-Hexane	38.42	48.12	62.65
C_6+ Aliphatics	0.48	0.05	0.17
2-MP/3-MP[b]	1.65	1.60	1.64
MP/DMB[c]	5.48	5.43	11.49
2,3-DMB/2,2-DMB[d]	2.87	3.30	4.80
I/C Ratio	12.90	10.99	6.85

a)   Ratio of 2-methyl pentane/3-methyl pentane, equilibrium value = 1.74.

b)   Ratio of methyl pentanes/dimethyl butanes; equilibrium value = 2.34.

c)   Ratio of 2,3-dimethyl butane/2,2-dimethyl butane; equilibrium value = 0.59.

170

to the decrease in available acid sites for the isomerization/cracking reactions. The I/C ratio decreases with increasing SiO_2/Al_2O_3.

The interaction between the zeolite and the metal in zeolite supported catalysts has been investigated by many workers.[37,38] The general consensus now is that there is significant electron transfer between the support (zeolite) and the transition metal atoms such as Pd and Pt. Electron enrichment of the metal occurs in alkaline zeolites such as KL,[37] while a depletion of electrons occurs in the case of acidic zeolites such as HY.[38] In a given zeolite supported metal catalyst, any variation in the acid site content of the zeolite is expected to influence the net electronic properties of the metal and hence changes in activity or selectivity for specific products are likely when the SiO_2/Al_2O_3 ratio of the zeolite is changed. Besides, in the case of bifunctional catalysis, where migration of intermediates occurs between the metal and acid sites, the change in the relative densities of the two species should affect selectivities. For example, when the n_{Pt}/n_A (where n_{Pt} is number of platinum atoms and n_A is the number of acid sites) is large, hydrogenolysis due to the metal will be predominant and when n_{Pt}/n_A is small, acid cracking will be the main reaction. For example, Guisnet et al.[39] have reported that in Pt-H-Y, hydrogenolysis activity became important at $n_{Pt}/n_A > 0.4$ and the acid activity was important at $n_{Pt}/n_A < 0.03$. For the given value of $n_{Pt}/n_A = 0.03$, the cracking selectivity was found to be higher for Pt-H-ZSM-5 than for Pt-H-Y. This was attributed to the greater acid strength of the acid sites and the smaller pore dimensions of H-ZSM-5 slowing the diffusion of the intermediates inside them. The optimum n_{Pt}/n_A ratio for achieving the maximum I/C ratio, therefore, depends not only on the relative concentration of the exposed metal and the acid sites but also on the strength of the acid sites and pore characteristics.

As discussed above, the decrease in the I/C ratio observed at high SiO_2/Al_2O_3 ratios could be due to an increased hydrogenolysis activity from the 2.9 - fold increase in n_{Pt}/n_A ratio on increasing the SiO_2/Al_2O_3 ratio from 28 to 80. The influence of changes in the electronic

state of Pt (on changing the SiO_2/Al_2O_3 of the support) on the I/C ratio is not clear. An increase in hydrogenolysis activity is also suggested by the greater yield of C_4 and C_5 fractions. However, the light product distribution ($< C_6$) itself is not typical of n-hexane cracking or hydrogenolysis as more moles of C_4 and C_5 hydrocarbons are present in the product than can be accounted for by the yields of the C_2 and C_1 components. Earlier workers have also reported similar imbalance in product distribution and have attributed it to the occurrence of alkylation-cracking reactions during alkane transformations over metal loaded zeolites.[33]

The 2-MP/3-MP ratios are nearly constant, approximately equal to 1.6 over all the samples and are close to the thermodynamic value of 1.74. The MP/DMB ratios and the 2,3-DMB/2,2-DMB ratios increase with decreasing Al content and are larger than the expected equilibrium values. Apparently, though 2-MP/3-MP equilibrium is reached even over the catalyst with the least Al-content ($SiO_2/Al_2O_3 = 80$), the other equilibria are not attained even over the catalyst with maximum Al-content ($SiO_2/Al_2O_3 = 28$).

5.4.4 INFLUENCE OF TEMPERATURE

The influence of temperature on the reaction are presented in Figure 5.5. n-Hexane conversion increases with increasing temperature. The increase in conversion is accompanied by an increase in cracking resulting in a decrease in the I/C ratios (Figure 5.5 (A)). It is likely that the increase in n-hexane fragmentation (cracking) is a result of both increased hydrogenolysis activity of the metal and enhanced cracking over the acidic zeolite. The apparent activation energies (E_a) calculated using extrapolated initial (TOS = 0 min) conversion data in the temperature range 470 K to 510 K is 30 kcal mole^{-1} and it is 17 kcal mole^{-1} at "steady-state" conversion at TOS = 45 minutes. The lower E_a value observed at TOS = 45 minutes is due to the greater activity drop at higher temperatures with duration of the run. The E_a values are similar in magnitude to the values (22 - 36 kcal mole^{-1}) reported by earlier workers during n-hexane transformation over different samples of Pt-mordenite.[35]

172
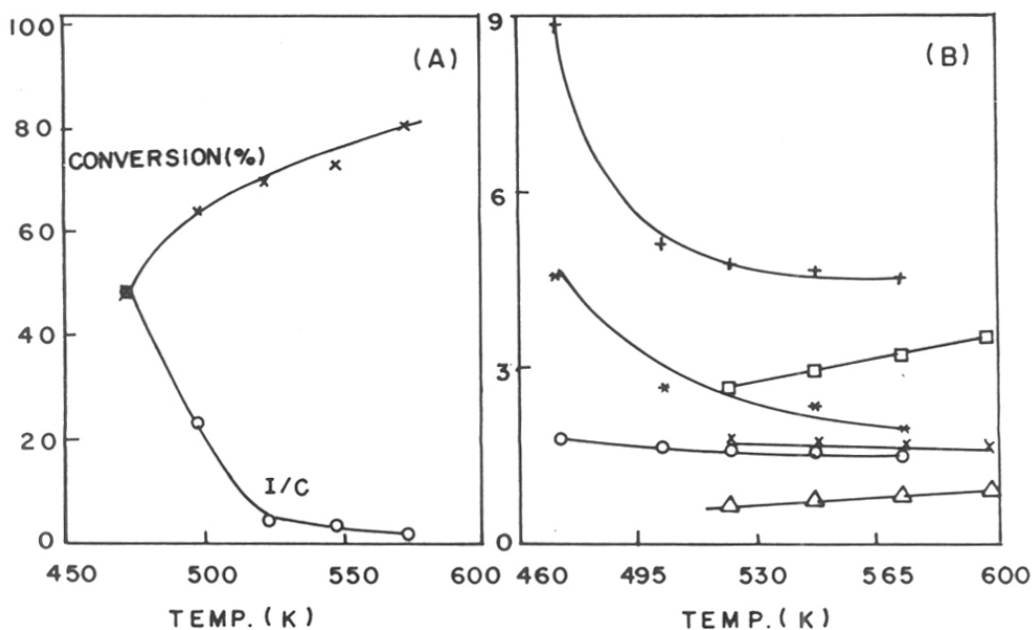
Figure 5.5   Influence of temperature on isomerization of n-hexane.
Catalyst, Pt-(0.5 %)-H-MCM-22 (SiO$_2$/Al$_2$O$_3$ = 28); WHSV (h^{-1}) = 1.0; H$_2$/n-hexane (mole) = 4.5; TOS = 45 min.

B :   Isomer ratio (Experimental :- (O) 2-MP/3-MP; (+) MP/DMB; (∗) 2,3-DMB/2,2-DMB. Thermodynamic data :- (Δ) 2-MP/3-MP; (□) MP/DMB; (X) 2,3-DMB/2,2-DMB).

The ratio of hexane isomers at different temperatures are presented in Figure 5.4 (B). The 2-MP/3-MP ratios are close to the equilibrium values, but the MP/DMB and 2,3-DMB/2,2-DMB ratios are larger than the equilibrium values. There is, however, a tendency for these ratios to approach the equilibrium values at higher temperatures (Figure 5.4 (B)).

5.4.5 INFLUENCE OF CONTACT TIME

Increasing the contact time (1/WHSV) increases conversion and decreases the I/C ratios (Figure 5.6 (A)). The decrease in I/C ratios is a result of an increase in cracking reactions, which, being slower than the isomerization reactions are enhanced at higher residence times. The 2-MP/3-MP ratio is ~ 1.63 (at WHSV (h^{-1}) = 0.5), though a slight increase is noted at the lowest contact time (WHSV (h^{-1}) = 5; 2-MP/3-MP = 1.71, Figure 5.6 (B)). A near equilibrium value of 2-MP/3-MP was observed at WHSV (h^{-1}) = 5 even at the low conversion of 23 %. The MP/DMB and 2,3-DMB/2,2-DMB values are larger than expected at equilibrium and increase with decreasing contact time (Figure 5.5 (B)). Plots of the yield of the hexane isomers at different conversions (Figure 5.5 (C)) suggest that the methyl pentanes are the primary products of the reaction while 2,3- and 2,2- dimethyl butanes are formed subsequently from the methyl pentanes.

The ratio of MP/2,3-DMB is 6.14 at WSHV (h^{-1}) = 1 (equilibrium value = 6.54) and increases to 9.97 at WHSV (h^{-1}) = 5. The 2,3-DMB/2,2-DMB ratio is 2.23 at WHSV (h^{-1}) = 0.5 and is far away from the equilibrium value of 0.59. The near attainment of the MP/2,3-DMB equilibrium, the non-attainment of equilibrium between the two dimethyl butanes, and the rapid increase in the 2,3-DMB/2,2-DMB ratio from 2.23 at WHSV (h^{-1}) = 0.5 to 3.44 at WHSV (h^{-1}) = 5, suggest that the transformation of the methyl pentanes to 2,3-DMB is faster than the isomerization of 2,3-DMB to 2,2-DMB. The difficulty in transforming a more stable tertiary carbocation (2,3-DMB-carbocation) into a less stable secondary carbocation (2,2-DMB-
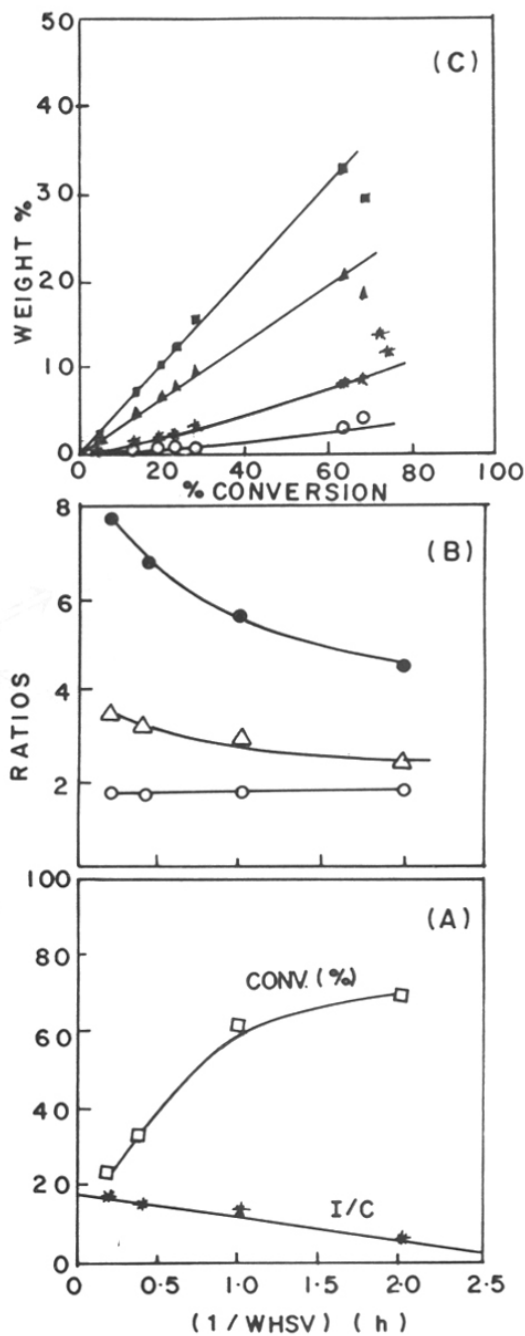
Figure 5.6   Influence of contact time on n-hexane isomerization.
Catalyst, Pt-(0.5 %)-H-MCM-22 (SiO$_2$/Al$_2$O$_3$ = 28); Temp. = 503 K; H$_2$/n-hexane (mole) = 4.5; TOS = 45 min.
(B): (O) 2-MP/3-MP; (●) MP/DMB;(Δ) 2,3-DMB/2,2-DMB.
(C): Distribution of n-hexane isomers in product at different conversions.
    Catalyst, Pt-(0.5 %)-H-MCM-22 (SiO$_2$/Al$_2$O$_3$ = 28); Temp. = 503 K; H$_2$/n-hexane (mole) = 4.5; TOS = 45 min; WHSV varied; (●) 2-MP; (▲) 3-MP; (✳) 2,3-DMB; (O) 2,2-DMB.

carbocation) has been attributed to the slowness in the formation of 2,2-DMB.[34] McCaulay[40] has reported that the relative rates of isomerization of the different hexane isomers over HF/BF_3 are as follows: 2-MP to 3-MP, 58 x 10^3; MP to DMB, 58; 2,3-DMB to 2,2-DMB = 8.6. Though, the relative rates could be different inside the zeolite pores, our studies also point to similar trends in isomerization rates; isomerization of 2-MP to 3-MP >> MP to 2,3-DMB > 2,3-DMB to 2,2-DMB.

The following reaction sequence suggested by earlier workers[34,41] appears to be likely in our case also.
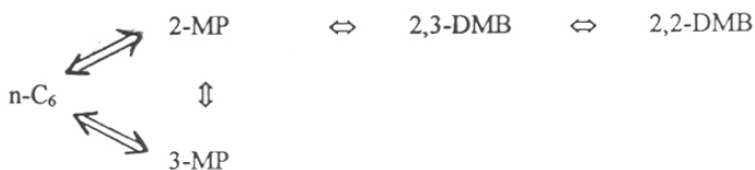
5.4.6 INFLUENCE OF H_2/n-C_6 (MOLE) RATIO

The results of the experiments carried out at different H_2/n-C_6 (mole) ratios at constant n-hexane feed rate are presented in Table 5.5. Increasing the partial pressure of hydrogen from 0.82 to 0.93 (H_2/n-hexane (mole) from 4.5 to 15) resulted in a decrease in conversion and an increase in I/C ratio. A similar increase in I/C ratios with decreasing conversion was also observed during contact time studies (Figure 5.5). Generally, I/C ratios increase with decreasing conversions as isomerization reactions are faster than cracking reactions. Besides, as cracking of isohexanes is faster than the cracking of n-hexane, cracking reactions are more prevalent at high conversions when the isoproducts were present in large amounts. As the studies were conducted at a constant feed rate of n-hexane (WHSV (h^{-1}) = 1), the decrease in conversion could possibly be due to the increase in overall (n-C_6 + H_2) space velocity. Earlier workers have reported reaction orders of 0 to 0.3 with respect to n-C_6 and 0.3 to −0.6 with respect to H_2 for the hydroisomerization of n-C_6 over Pt-mordenite at atmospheric pressure.[35] Therefore, the

Table 5.5   n-Hexane isomerization: Influence of H_2/n-hexane (mole) ratio over product distribution

Conditions : Temp. = 503 K; WHSV (h^{-1}) = 1.0; Press = 0.1 MPa; TOS = 60 min and Catalyst = Pt-(0.5 Wt. %)-H-MCM-22 (SiO_2/Al_2O_3 = 28);

	H_2/n-hexane (mole) Ratio		
	4.5	10.0	15.0
Conversion (%)	61.58	51.05	46.13
I/C Ratio	12.89	17.83	24.84
Products (Wt. %)			
C_1 - C_5	7.08	5.17	3.70
2-MP	48.83	48.87	50.10
3-MP	29.65	31.06	32.00
2,3-DMC$_4$	10.62	11.20	10.71
2,2-DMC$_4$	3.70	3.66	3.32
Others	0.11	0.14	0.18
2-MP/3-MP	1.65	1.57	1.57
MP/DMB	5.48	5.37	5.85
2,3-DMB/2,2-DMB	2.87	3.06	3.23

decrease in conversion at high H_2/n-C_6 ratio could also be due to a negative order with respect to H_2.

The 2-MP/3-MP ratios were close to equilibrium values at all H_2/n-C_6 ratios studied, while the MP/DMB and 2,3-DMB/2,2- DMB ratios were far from the equilibrium values. The ratios deviate more from equilibrium values at higher H_2 partial pressures.

5.4.7 COMPARISON OF MCM-22 WITH BETA AND MORDENITE

A comparison of the activites of Pt-loaded ß (SiO_2/Al_2O_3 = 35) and mordenite (SiO_2/Al_2O_3 = 21) with MCM-22 (SiO_2/Al_2O_3 = 28) are presented in Table 5.6. All the zeolites were loaded with the same amount of Pt (0.5 wt. %). The zeolites can be arranged in decreasing order of activities and I/C ratios at constant experimental conditions as : ß > MCM-22 > MOR. The 2-MP/3-MP ratios are nearly the same (1.64 ± 0.1) being similar to the equilibrium value (1.74) over all the catalysts. The MP/DMB and 2,3-DMB/2,2-DMB values are different over the three zeolites (Table 5.6), the values being close to equilibrium values only in the case of MOR. The isohexanes distribution observed over MOR, viz., 2-MP : 3-MP : 2,2-DMB : 2,3-DMB = 43.5 : 28.3 : 15.1 : 13.0, is similar to the equilibrium distribution, 44.9 : 25.9 : 18.3 : 10.9. The above distribution is noticed over MOR even when the n-hexane content of the C_6 fraction is 54.3 % (i.e., even at low conversions), while the equilibrium value is 16.9 %. The rapid attainment of equilibrium between the isohexanes over mordenite even at a low n-hexane conversion (much less than the equilibrium value) is attributed to the strong acidity of the Brönsted sites and the slow diffusion of the products through the uni-dimensional pore system. The production of large amounts of the cracked (secondary) products support the above explanation.

The isomerization of n-hexane rich light naphtha fractions with low octane numbers (RON = 60 - 70) into octane rich products (RON = 90 +) is already commercially practiced.[27,28] Maximum octane advantage is realized when the feed is converted into an equilibrium mixture of

Table 5.6   n-Hexane isomerization : Product distribution over different Pt-zeolites

Conditions :   Temp. = 503 K; WHSV (h^{-1}) = 1.0; $H_2/n-C_6$ (mole) = 4.5; TOS = 60 min and Press. = 0.1 MPa.

	MCM-22	ß	Mordenite	Equilibrium values[34]
C_6 - break up (%)				
n-C_6	40.20	25.23	54.30	16.9
2-MP	31.46	38.07	19.95	37.4
3-MP	19.11	23.27	12.93	21.5
2,2-DMB	2.39	4.10	6.91	15.2
2,3-DMB	6.84	9.34	5.92	9.0
I/C	12.90	16.89	1.18	-
2-MP/3-MP	1.65	1.64	1.54	1.74
MP/DMB	5.48	4.57	2.56	2.43
2,3-DMB/2,2-DMB	2.87	2.28	0.86	0.59
C_6 - RON[a]	58.88	69.02	49.83	74.91
ATE (%)[b]	71.3	89.9	55.1	-
RON yield[c]	56.3	66.5	35.4	-

a)   RON of the C_6 fraction calculated from RON values of individual components.[29]

b)   ATE = Approach to equilibrium.

$$ATE = \frac{\sum C_{ip} (RON)_i - (RON)_{n-C_6}}{\sum C_{ie} (RON)_i - (RON)_{n-C_6}} \times 100$$

C_{ip} =   Weight fraction of the component i in the C_6 fraction of the product;

C_{ie} =   Weight fraction of the component at thermodynamic equilibrium of the C_6 alkanes.

$(RON)_i$ =   Blending octane number of the component i.

$(RON)_{n-C_6}$ =   Blending octane number of n-hexane.

c)   RON yield = {(C_6 - RON) x % C_6 in product}/100

isomers at as low a temperature as possible. Hence, the extent to which the equilibrium composition is realized over a catalyst determines its usefulness. The calculated RON values of the C_6 fraction from MCM-22, ß and MOR are presented in Table 5.6 using blending RON values for the individual components.[29] The extent to which equilibrium has been achieved over the different zeolites can be quantified as approach to equilibrium (ATE) based on the RON of the C_6 fraction in the product and the expected RON at thermodynamic equilibrium of the C_6 alkanes. The method of calculating ATE and the ATE values for the three zeolites are presented in Table 5.6. ß and MCM-22 lead to attractive RON benefits, the ATE being higher (89.9 %) over ß. It should be noted that the ATE could exceed 100 % even when equilibrium of the products is not attained, if the mixture is rich in 2,3-DMB which has the highest blending RON of 96. However, the concept is useful in comparing the abilities of catalysts for RON improvement. Due to its large cracking activity, the RON yield (= RON of the C_6 fraction x weight fraction of the C_6 components in the reaction product) is lowest over MOR. However, it is emphasized that the above zeolites have been compared at common operating parameters which may not be the most suitable conditions for the different zeolites. Besides, the specific ß and MOR samples used in this study might not be optimal for the reaction.

The studies reveal that the isomerization of n-hexane proceeds through a dual functional mechanism over Pt-MCM-22. Both conversion and isomerization/cracking ratio increase with increasing Pt content of the sample and reach a plateau at about 0.5 wt. % Pt. High H_2-partial pressures increases the I/C ratio, while a high Al content increases the conversion and rapid equilibration of the isomers. The octane number (RON) enhancement over Pt-MCM-22 (at 503 K and WHSV (h^{-1}) = 1) is significant.

5.5 CRACKING OF n-HEXANE OVER MCM-22

5.5.1 INTRODUCTION

n-Hexane readily cracks over acidic zeolites to produce lighter hydrocarbons, (C_2 - C_4 gases). Above 723 K, the cracked products often oligomerize to yield aromatics. The formation of aromatics is especially significant over the medium pore zeolites of the high silica type such as ZSM-5 or ZSM-11, the aromatization reaction presumably being assisted by the medium sized pores (~5.5 Å) in these zeolites.[42]

In the present study, n-hexane cracking experiments were conducted over H-MCM-22 samples without platinum loading. As a comparitive study, experiments under identical conditions were conducted over the large pore zeolites beta, mordenite and ZSM-12 and the medium pore zeolite, ZSM-5. The results are discussed in the following sections. The studies were carried out over MCM-22 samples with SiO_2/Al_2O_3 = 28 except where specified.

5.5.2 EFFECT OF REACTION TEMPERATURE ON CRACKING

The reaction was carried out at different temperaures ranging from 473 K - 773 K. At lower temperatures, isomerization predominated and at higher temperatures, the cracking reactions became dominant. The results are presented in Figure 5.7.

The cracking activity increased from approximately 25 % at 473 K to approximately 96 % at 773 K. As expected, C/I (cracking/isomerization) ratio increased as the temperature was increased. The distribution of products are presented in Table 5.7. The formation of aromatics was negligible even at temperatures beyond 773 K. The major products were C_3 and C_4 fractions followed by C_2 and C_1 fractions. The formation of the latter light hydrocarbons is attributed to secondary cracking reactions. The isobutane/n-butane [(i-C_4)/(n-C_4)] ratio is found to be 1.64 at 473 K and 0.50 at 773 K. The decrease in ratio is in accordance with that expected from thermodynamics, the thermodynamic equilibrium values being 1.17 and 0.56 at
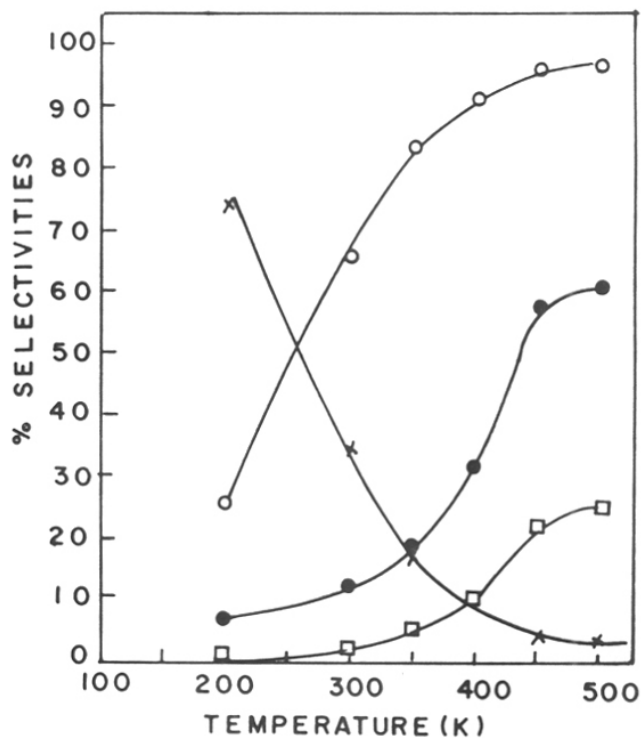
Figure 5.7   Effect of temperature on cracking over MCM-22
sample with $SiO_2/Al_2O_3 = 28$.
WHSV (h^{-1}) = 2.0; TOS = 1h, H_2/n-hexane = 1.5.

(O) % Cracking, (*) % Isomerization,
(●) % Conversion and (□) C/I ratio.

Table 5.7   n-Heane cracking : The effect of reaction temperature.

Conditions :   WHSV (h^{-1}) = 2.0; H_2/n-hexane (mole) = 1.5; TOS : 1 h and

Catalyst = MCM-22 (SiO_2/Al_2O_3 = 28; 2 g).

Product (% w/w)	Temperature (K)					
	473	573	625	673	725	773
$C_1 + C_2$	0.3	7.6	7.4	16.4	24.8	29.8
C_3	5.4	20.5	42.1	45.5	48.1	48.6
C_4	9.8	23.7	24.6	22.8	17.8	15.5
C_5	7.4	12.2	5.6	2.6	1.5	0.9
C_6	74.2	34.3	16.8	8.8	4.4	3.9
C_6+ Aromatics	3.0	1.6	3.5	4.0	3.4	1.3
i-C_4/n-C_4	1.6	1.1	1.1	0.9	0.7	0.5
C_4 (ole)/C_4 (para)	-	-	0.1	0.2	0.4	0.5
2-MP/3-MP	1.4	0.7	0.5	0.6	0.3	0.3

500 K and 800 K, respectively. The 2-MP/3-MP ratio decreases from 1.43 at 473 K to 0.29 at 773 K. The values expected at thermodynamic equilibrium are 2.13 at 500 K and 1.79 at 800 K. The deviation of the observed ratios from the thermodynamic equilibrium values is a result of the rapid cracking of the 2-MP and the consequent non-attainment of equilibrium (see below).

$$n\text{-}C_6 \quad \leftrightarrow \quad 2\text{-MP} \quad \leftrightarrow \quad 3\text{-MP}$$
$$\downarrow \qquad\qquad \downarrow$$
$$\text{Cracked Products}$$
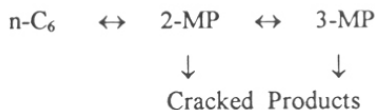
5.5.3 EFFECT OF SiO_2/Al_2O_3 RATIOS

The influence of aluminum content was studied by carrying out experiments over samples with varying aluminum contents (SiO_2/Al_2O_3 = 28, 56, 80, respectively). The conversions are found to decrease as the aluminum content decreased. The yield of the C_3 and C_4 fractions increases as the SiO_2/Al_2O_3 ratio is increased. Among the C_4 components, the yield of the olefins increases with decrease in aluminum content. This stems from the fact that, the hydrogen transfer ability[43] decreases as the framework SiO_2/Al_2O_3 ratio increases. The hydrogen transfer ability depends primarily on the density of the Brönsted acid sites.[43] The results are presented in Figure 5.8 and Table 5.8. Corma *et al.* have attributed the decrease in olefin/paraffin ratio to a decrease in the density of Brönsted acid sites in HY and Hß.[44] The C/I ratio decreases with an increase in the framework Si/Al ratio.

5.5.4 COMPARISON WITH OTHER ZEOLITES

The cracking activity of MCM-22 was compared with those of zeolite ZSM-12 (MTW), beta (ß), mordenite (MOR) and the medium pore zeolite, ZSM-5 (MFI). The reactions were carried out over the H-form of the samples without Pt loading, under identical reaction conditions.

5.5.4.1 Comparison with ZSM-5

The reactions were carried out at 798 K, WHSV (h^{-1}) = 2.5, H_2/n-hexane (mole) ratio = 1.5 and time on stream (TOS) of 4 h. The results are presented in Table 5.9. A comparison of
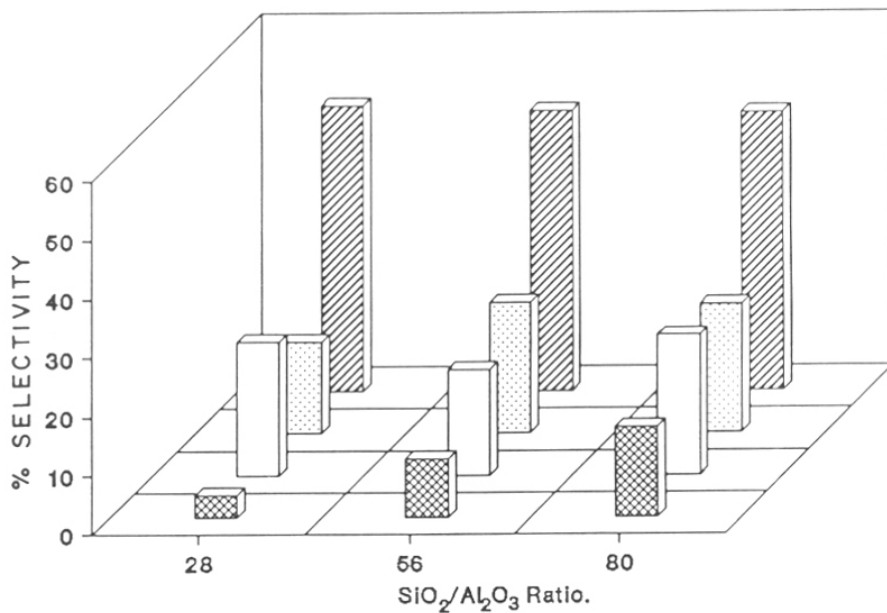
Figure 5.8   Influence of aluminum content over n-hexane cracking.
Temp. = 773 K; WHSV (h^{-1}) = 2.0; TOS = 1h and H$_2$/n-hexane = 1.5.

$C_1 + C_2$, $C_5 + C_6$, C_4 and C_3.

Table 5.8   The effect of aluminum content upon the efficiency of cracking.

Reaction Conditions   Temp. = 773 K; WHSV (h^{-1}) = 2.0; H$_2$/n-hexane (mole) =
:   1.5; TOS = 1 h and Catalyst = H-MCM-22.

	SiO$_2$/Al$_2$O$_3$		
	28	56	80
% Conversion	60.9	34.5	20.9
% Cracking	96.1	91.1	85.3
C/I	24.6	10.2	5.1
C$_4$ (olefin)/C$_4$ (paraffin)	0.5	1.5	1.7
C$_4$/C$_2$	0.8	1.2	1.3

Table 5.9 n-Hexane cracking : a comparative study over MCM-22 and ZSM-5:

Reaction Conditions :   Temp. = 798 K; WHSV (h^{-1}) = 2.5; H_2/n-hexane (mole) = 1.5;

TOS = 4h and Catalyst = H^+-form, [SiO_2/Al_2O_3 = 80] (2 g).

	MCM-22	ZSM-5
Conversion Wt. %	63.4	100
$C_1 + C_2$	14.4	27.1
C_3	28.8	36.3
C_4	10.0	3.9
C_5 + Aliphatics	40.4	0.3
C_6 - C_7 Aromatics	1.5	21.2
C_7 + Aromatics.	1.4	10.9
Σ Aromatics	2.9	32.1
p-/o- Xylene	1.1	0.7

ZSM-5 and MCM-22 is made in Table 5.9. At identical conditions, conversion is more over H-ZSM-5 (100 %) than over MCM-22 (63.4 %). The lower cracking activity of MCM-22 compared to ZSM-5 could be due to lower strength of the acid sites in MCM-22 and the absence of a "Nest Effect" in MCM-22.[45] The major difference is the larger amount of aromatics produced over ZSM-5 (32.1 %) than over MCM-22 (2.9 %). Apparently, the pore-topology of MCM-22 is much less conducive to the formation of cyclic (C_6) intermediates, the precursors to aromatics. Besides, the poorer aromatization activity could also be due to lower H-transfer activity and weaker acidity of MCM-22.

5.5.4.2 Comparison with large pore zeolites

Among the large pore zeolites used for the comparison purposes, ZSM-12 [MTW] with uni-dimensional channels of 0.57 nm x 0.6 nm was found to exhibit good reactivity (Table 5.10). Based on conversion, the activities of the zeolites can be arranged in decreasing order as follows : MTW > ß > MCM-22 > DMOR.

The C_3 fraction is the major product in all the cases. In the case of MCM-22, the C_1 + C_2 mixture was higher than the C_4 fraction. However, the same trend was not observed over the other zeolites. The i-C_4/n-C_4 ratio was closer to the equilibrium value of 0.56 (at 800 K) in the case of MCM-22. C_4 (olefin)/C_4 (paraffin) ratio was highest over DMOR with higher SiO.$_2$/Al$_2$O$_3$ ratio (~ 70) than over the other zeolites. This is attributed to the lower H-transfer activity of dealuminated mordenite due to the lower acid site density.

Table 5.10   n-Hexane cracking : a comparative study over MCM-22 and
              large pore molecular sieves.

Conditions : Temp. = 773 K; WHSV (h^{-1}) = 2.0; H_2/n-hexane (mole) = 1.5;
              TOS = 1 h; Press. = Atmospheric and Catalyst = 2 g.

Products	Large pore molecular sieves			
	MCM-22	ß	Mordenite	MTW
$C_1 + C_2$	3.8	11.3	14.4	11.4
C_3	48.6	54.3	54.8	53.1
C_4	15.5	21.1	15.3	21.2
$C_5 + C_6$	22.8	5.4	13.5	4.6
% Conversion	68.7	60.9	71.2	24.9
% Cracking	97.1	96.1	97.0	90.9
C/I	33.9	24.6	32.8	10.0
$i-C_4/n-C_4$	1.5	0.5	0.9	0.8
C_4 (ole)/C_4 (para)	0.3	0.5	0.7	0.9
C_4/C_2	2.3	0.8	1.9	1.2

5.6 TRANSFORMATION OF METHANOL TO HYDROCARBONS

Light olefins, the key components of petrochemical intermediates, are often obtained by the thermal cracking of petroleum gases and naphtha. The transformation of methanol to compounds with higher carbon number could be of industrial importance in the production of light olefins and fuels. The process could become important especially when the present efforts to convert methane to methanol are successful.

The first report of the transformation of methanol was made by Label and Greene in 1880.[46] The conversion was carried out over molten $ZnCl_2$. Hexamethyl benzene was observed as the major product in addition to traces of methane. The mechanism proposed by Label and Greene[46] involved the dehydration of methanol to form "CH_2" (active methylene/carbene) which cyclized to benzene and exhaustive ring alkylation by methyl chloride generated *in situ* (Friedel Crafts alkylation) which produced hexamethyl benzenes (HMBs). Later, other researchers examined a variety of catalysts such as P_2O_5,[47] $ZnCl_2$,[46,48] Al_2O_3,[49] silicagel, Al_2O_3 and silica-alumina,[50a] activated alumina,[50b] and metal-molybdate catalysts for the tranformation of methanol into hydrocarbons.[51]

Mobil Oil Corporation achieved a major technological breakthrough by successfully converting methanol into gasoline in a catalytic process called the Mobil MTG process.[52,53] The catalyst used was the shape-selective, medium pore zeolite, ZSM-5, with a high silica to alumina ratio.[54] Till today, ZSM-5 has proven to be the best catalyst for the conversion of methanol with good selectives for aromatics.

The major hydrocarbons produced from methanol transformation over ZSM-5 zeolite are C_1 - C_4 alkanes, C_2 - C_4 alkenes, C_6 - C_{10} aromatics. No higher aromatics were found in the product stream of the shape selective pentasil zeolite.[55]

Apart from ZSM-5,[56] ZSM-8,[57] small pore zeolite such as NU-1[58,59] and large pore zeolite such as offretite,[60] have also been used in the conversion of methanol. Cormerais *et al.*[61] have investigated the influence of acidity of zeolite Y on this reaction. Later, Sulikowski and Popierlaz have reported the selective formation of HMBs over ultra stable zeolite Y.[62]

5.6.1 *MECHANISM*

The mechanism of the conversion of methanol to hydrocarbons over an acid catalyst comprises of three key steps :

(I)   Formation of the ether.

(II)   The first C-C bond formation leading to reactive olefins

(III)   Cyclization and aromatization with H-transfer.

Ether formation occurs via adjacent surface methoxyls. Since, methanol does not possess any parent olefin, the formation of ether and subsequent formation of the C-C bond appears to be the important route. Many researchers have reported ethene as the primary intermediate during methanol transformation.[56,57] Nováková *et al.*[63] have suggested that the reaction of gaseous methanol resulted in a very reactive surface C_1 species which further led to the formation of the first C-C bond.

Hydrocarbon formation was considered to occur by condensation of methoxy groups accompanied by dehydration and hydride transfer as proposed by Topchieva *et al.*[50a] Salvador *et al.*[64] have proposed the α-elimination mechanism. Chang *et al.* have proposed an intermediate of carbenoid type during the α-elimination mechanism.[56] Van der Berg *et al.* have proposed oxonium ylide types of intermediates to explain the formation of C-C bond, which also involved Stevens type rearrangement.[65]

Many reaction mechanisms have been proposed for the cyclization and aromatization. Dejaifve *et al.* have proposed a carbenium ion mechanism and have accounted for the formation of higher aliphatics and aromatics.[66]

5.6.2 RESULTS AND DISCUSSION

The transformation of methanol was carried out over MCM-22 samples. In addition to gaseous and liquid products, solid products were also observed. During the course of the reaction, these solid products were found to condense over the walls of the reactor near the outlet.

After each run, the reactor was cooled and washed with acetone. The washings were then evaporated to get the solid products. The solid product thus obtained was characterized by GC, GC-MS, FTIR, ^{1}H and ^{13}C NMR and elemental microanalysis. The solid and liquid products were mixed and analyzed. The gaseous products were estimated separately and combined mass-balances were carried out.

The major solid component was found to be hexamethyl benzene (HMB). GC-MS data were recorded for the solid sample. Two peaks were observed with molecular weights corresponding to 162 and 148, respectively, with the base peaks (in both cases) corresponding to the $[M-15]^+$ fragment. This is a characteristic of poly alkyl benzenes (PABs.). ^{1}H NMR spectrum of the sample dissolved in CDCl$_3$ indicated only a peak at $\delta = 2.3$ ppm, corresponding to only CH$_3$ group. ^{13}C NMR spectrum of the same sample revealed 2 signals corresponding to 2 sets of carbon atoms (first being methyl carbon and the second being aromatic ring carbon atoms). The elemental analysis results of the neat sample matched the theoretical wt. % of C and H present in HMB.

The solid product obtained during the course of reaction was found to contain > 95 % of HMB and < 5 % of penta methylbenzene (PMB) and tetra methylbenzene isomers such as, durene.

5.6.2.3. Effect of temperature

The reaction was carried out over MCM-22 samples with SiO$_2$/Al$_2$O$_3$ ratio = 80 in the temperature range from 373 K to 673 K. The results are presented in Table 5.11. At lower

192

Table 5.11   The effect of temperature over product distribution during the transformation of methanol.

Reaction Conditions :   WHSV (h^{-1}) = 6.0; N$_2$/methanol (mole) = 1.5; TOS = 1 h and Catalyst = H-MCM-22 [SiO$_2$/Al$_2$O$_3$ = 80, 1.5 g].

	Temperature (K)				
	373	473	573	643	673
Conversion (%)	10.1	72.3	85.0	87.7	92.7
Products (Wt. %)					
C$_1$ + C$_2$	-	-	1.5	2.5	4.6
C$_3$	0.1	0.2	4.0	8.3	13.3
C$_4$	99.9	99.8	63.4	68.2	51.7
C$_5$ + Aliphatics	-	-	10.7	12.1	20.4
C$_6$ - C$_8$ Aromatics	-	-	0.4	0.6	0.3
> C$_8$ Aromatics[b]	-	-	20.0	8.3	9.7

[b] >C$_8$ Aromatics : ≥ 95 % Hexamethyl benzene [HMB] and ≤ 5 % PMB and durene.

temperatures, the conversions were low and the major products were C_4 hydrocarbons. At higher temperatures, a decrease in the yields of C_4 and an increase in C_1 - C_2 yields was noticed.

At 673 K, the formation of HMB and PMB was found to be maximum. The formation of PABs suggests the presence of reasonably strong acid sites and large pore dimensions, which facilitate their formation and easy diffusion, respectively. The critical diameters[67] of 1,2,4,5-, 1,2,3,4-, 1,2,3,5- tetramethyl benzenes are 6.1 Å, 6.4 Å and 6.7 Å, respectively. 6.9 Å and 7.1 Å are the critical diameters of the penta- and hexa- methylbenzenes.

Durene was the largest molecule found in the product obtained over ZSM-5[53,54] which has a pore diameter ~ 5.5 Å. In the case of MCM-22, eventhough large 12-MR cages are present, only the 10-MR pores have been suggested to be directly accessible from the outside; the cages can however be reached by the 10-MR pores. The formation of the large molecules such as HMBs over MCM-22 suggests that either a small fraction of the 12-MR cages are accessible directly from the surface or a large amount of the reaction occurs on the external surface of the crystals (platelets).

5.6.2.4   Effect of SiO_2/Al_2O_3 ratio

The reaction was carried out over samples with varying aluminum contents. The results are presented in Table 5.12. The conversion was larger for samples with higher aluminum content and decreased as the aluminum content decreased. The selectivty to PMB was found to be greater in the case of samples with lower aluminum content. It is possible that an increase in acid strength generally associated with decreasing Al-content is responsible for greater yields of HMB. The formation of the C_5+ aliphatics fraction was more in the case of samples with higher aluminum content.

5.6.2.5   Comparison with ZSM-5 and large pore zeolites

The reaction was also carried out over ZSM-5 and the large pore zeolite beta. The activities and product selectivities observed over these zeolites and those of mordenite and US-

194

Table 5.12   Transformation of methanol : influence of the aluminum content of MCM-22.

Conditions   Temp. = 643 K; WHSV (h^{-1}) = 1.0 and other conditions are same as listed in Table 5.14.

	SiO_2/Al_2O_3 ratios			
	28	40	56	80
Conversion %	100	100	98	95.76
Product Distribution (Wt. %)				
$C_1 + C_2$	6.8	6.6	7.2	6.8
C_3	27.8	23.0	19.1	16.1
C_4	23.1	26.7	29.4	36.2
$\geq C_5$ + Aliphatics	37.9	37.8	28.0	18.4
Σ BTX[b]	1.5	0.6	0.5	0.3
A_{10} + Aromatics[c]	3.0	5.5	15.9	22.3

[b]Σ BTX corresponds to Benzene, Toluene and Xylene.

[c]Aromatics : Same composition as listed in Table 5.14.

Y obtained from the literature have been compared with MCM-22 (Table 5.13). It is obvious from the table that the formation of heavier aromatics ($> C_{10}$) is favored to a greater extent over the large pore zeolites. In the case of the medium pore ZSM-5, the formation of benzene, toluene and xylenes [BTX] was more pronounced when compared to higher ($> C_8$) aromatics.

Sulikowski and Popierlaz have carried out methanol conversion over USY[62] (see Table 5.13). The major product was hexamethyl benzene, along with traces of unreacted methanol, water and dimethyl ether. Chang *et al.* have carried out the same reaction over mordenite and have observed the formation of PABs.[56]

The formation of PABs is favored in the case of the large pore zeolites and MCM-22. The formation of HMB was more over MCM-22 than over beta or mordenite. ZSM-5 produced more light hydrocarbons and BTX, whereas, the large pore zeolites and MCM-22 produced more PABs relative to BTX. In the case of MCM-22, the product stream was found to contain a considerable amount of PABs, being similar to that produced over mordenite but much less than that obtained over US-Y.

Table 5.13   Transformation of methanol: a comparative studies over MCM-22 and other

zeolites.

Zeolites	H-ZSM-5	H-MCM-22	H-ß	H-MOR[56]	H-USY[62]
% Conversion	100	95.8	95.8	-	-
Product Distribution					
$C_1 + C_2$	6.4	6.8	21.4	17.8	-
C_3	33.7	16.1	19.1	21.6	-
C_4	21.8	36.2	31.2	23.6	-
$C_5 +$ Aliphatics	18.2	18.3	20.8	18.6	-
$C_6 - C_8$					
Aromatics	14.8	0.3	0.3	2.3	-
$> C_8$ Aromatics	5.1[+]	22.3	7.2	18.1	100[*]

[+]$> C_8$ Aromatics : Only upto C_{10} aromatics in the case of ZSM-5.

[*]$> C_8$ Aromatics :   Pure HMB in the case of USY.[62]

197

5.7 REFERENCES

1. Jacobs, P. A., and Martens, J. A., *Stud. Surf. Sci. Catal.* **28**, 23 (1988).

2. Weitkamp, J., and Ernst, S., *Stud. Surf. Sci. Catal.* **38**, 367 (1988).

3. Csicsery, S. M., *Zeolites.* **4**, 202 (1984).

4. Weitkamp, J., and Ernst, S., *Catal. Today.* **19**, 107 (1994).

5. Martens, J. A., Tielen, M., Jacobs, P. A., and Weitkamp, J., *Zeolites.* **4**, 98 (1984).

6. Rubin, M. K., and Chu, P., US Patent No. 4,954,325 (1990).

7. Ravishankar, R., Tapas Sen, Veda Ramaswamy, Soni, H. S., Ganapathy, S., and Sivasanker, S., *Stud. Surf. Sci. Catal.* **84(A)**, 331 (1994).

8. Absil. R. P. L., Marler, D. O., and Shihabi, D. S., US Patent No. 4,962,257 (1990).

9. Kirker, G. W., Mirzahi, S., and Shih, S. S., US Patent No. 5,000,839 (1991).

10. Absil, R. P. L., Angevine, P. J., Brundens, R. G., and Horbat, J. A., US Patent No. 4,983,276 (1991).

11. Chu, P., Kirker, G. W., Kushnerick, J. D., and Marler, D. O., US Patent No. 5,043,512 (1991).

12. Huss, A., Kirker, G. W., Keville, K. M., and Thomson, R. T., US Patent No. 4,992,615 (1991).

13. Kushnerick, J. D., Marler, D. O., McWilliams, J. P., and Smith, C. M., US Patent No. 4,992,606 (1991).

14. Chu, C. T. W., Degnan, T. F., and Huh, B. K., US Patent No. 4,982,032 (1991).

15. Puppe, L., and Weisser, J., US Patent No. 4,439,409 (1984).

16. Ravishankar, R., Bhattacharya, D., Jacob, N. E., and Sivasanker, S., *Microporous Materials.* **4**, 83 (1995).

17. Ernst, S., Jacobs, P. A., Martens, J. A., and Weitkamp, J., *Zeolites.* **7**, 25 (1986).

18. Csicery, S. M., *J. Org. Chem.* **34**, 3338 (1969).

19. Corma, A., and Sastre, E., *J. Catal.* **129**, 177 (1991).

20. Gnep, N. S., Tejada, J., and Guisnet, M., *Bull. Soc. Chem. Fr.* **I**, 5 (1982).

21. Martens, J. A., Péréz-Parienté, J., Sastre, E., Corma, A., and Jacobs, P. A., *Appl. Catal.* **45**, 85 (1988).

22. Dewing, J., *J. Mol. Catal.* **27**, 25 (1984).

23. Kumar, R., Rao, G. N., and Ratnasamy, P., *Stud. Surf. Sci. Catal.* **49(B)**, 1141 (1989).

24. Leonowicz, M. E., Lawton, J. A., Lawton, S. L., and Rubin, M. K., *Science.* **264**, 1910 (1994).

25. Kumar, R., and Reddy, K. R., *Microporous Materials.* **3**, 195 (1994).

26. Corma, A., Corell, C., Llopis, F., Martinez, A., and Pérez-Parienté, J., *Appl. Catal.* **115**, 121 (1994).

27. Cusher, N. A., Greenouch, P., Rolfe, J. R. K., and Weiszmann, J. A., in Chap.5, Handbook of Petroleum Refining Processes, (Meyers, R. A., Ed.), McGraw-Hill Book Co., New York, p.5.1 (1986).

28. Refining Handbook,'92, Hydrocarbon Processing, **71**, 195 (1992).

29. Ciapetta, F. G., Dobres, R. M., and Baker, R. N., *Catalysis*, Vol. IV (Emmett, P. H., Ed.), Rheinhold Pub. Corpn., New Yord, p.495 (1958).

30. Farneth, W. E., and Gorte, R. J., *Chem. Rev.* **95**, 615 (1995).

31. Giannetto, G. E., Perot, G. R., and Guisnet, M., *Ind. Eng. Prod. Res. Dev.* **25**, 481 (1986).

32. Leu, L. J., Hou, L-Y., Kang, B-D., Li, C., Wu, S-T., and Wu, J-C., *Appl. Catal.* **69**, 49 (1991).

33. Guisnet, M., Fouche, V., Belloum, M., Bournonville, J. P., and Travers, C., *Appl. Catal.* **71**, 283 (1991).

34. Chen, J. K., Martin, A. M., Kim, Y. G., and John, V. T., *Ind. Eng. Chem. Res.* **27**, 401 (1988).

35. Guisnet, M., Fouche, V., Belloum, M., Bournonville, J. P., and Travers, C., *Appl. Catal.* **71**, 295 (1991).

36. Weisz, P. B., *Adv. Catal.* **13**, 137 (1962).

37. Besoukhanova, C., Guidot, J., and Barthomeuf, D., *J. Chem. Soc. Faraday Trans. I.* **77**, 1595 (1981).

38. Dalla Betta, R. A., and Boudardt, M., Proc. 5th Intern. Congr. Catal., p.1329 (1973).

39. Guisnet, M., Alvarez, F., Giannetto, G., and Perot, G., *Catal. Today.* **1**, 483 (1987).

40. McCaulay, D. A., *J. Am. Chem. Soc.* **84**, 6437 (1959).

41. Marin, G. B., and Froment, G. F., *Chem. Eng. Sci.* **37 (5)**, 759 (1982).

42. Gianetto, G., Perot, G., and Guisnet, M., *Acta. Phys. Chem.* **31**, 467 (1985).

43. Pines, L. A., Maher, P. J., and Watcher, W. A., *J. Catal.* **85**, 466 (1984).

44. Corma, A., Monton, J. B., and Orchilles, A. V., *Appl. Catal.* **16**, 89 (1985).

45. Derouane, E. G., Proceedings, Ketgen Catalysts Symposium 86, Kurhams, The Netherlands, May 25-28, 1986, p.G-3.

46. LaBel, J. A., and Greene, W. H., *Am. Chem. J.* **2**, 20 (1980).

47. Sernagiotto, E., *Gazz, Chim. Ital.* **44(1)**, 587 (1914).

48. Grosse, A. V., and Snyder, J. C., US Patent No. 2,492,984 (1950).

49. Adkins, H., and Perkins, P. D., *J. Phys. Chem.* **32**, 223 (1928).

50. (A) Topchieva, K. V., and Ballod, A. U., *Doki. Akad. Nauk. SSSR*, **75**, 247 (1950).

    (B) Cullinane, N. M., Chart, S. J., and Meatyard, R., *J. Soc. Chem. Ind.* **67**, 142 (1948).

51. Fawcett, F. S., and Howk, B. W., US Patent No. 2,744,151 (1956).

52. Meisel, S. L., McCullough, J. P., Lechtlhaler, C. H., and Weisz, P. B., *Chem. Tech.* **2**, 86 (1976).

53. Chang, C. D., Silvestri, A. J., and Smith, R. L., US Patent Nos. 3,894,103 and 3,928,483 (1975).

54. Chang, C. D., and Silvestri, A. J., *J. Catal.* **47**, 249 (1977).

55. Lee, W., Mazio, J., Weekmann, V. W., and Yurchak, S., in Froment, G. F., (Ed.), "Large Chemical Plants", Elseview, Amsterdam, (1974) p.171.

56. Chang, C. D., *Catal. Rev. Sci. Eng.*, **25(1)**, 1 (1983).

57. Khadziev, S. N., Levinbuk, M. I., Shumovskii, Yu, V., and Topchieva, K. V.,

Kinet. Katal. **20(6)**, 347 (1979).

58. Chang, C. D., Lang, W. H., and Silvestri, A. J., US Patent No. 4,062,905 (1977).

59. Spencer, M. S., and Whittam, T. V., *Acta. Phys. Chem.* **29**, 347 (1978).

60. Ceckiewicz, S., *J. Chem. Soc. Faraday Trans. I*, **80**, 2989 (1989).

61. Cormerais, F. X., Clen, Y. S., Kern, M., Gnep, N. S., Perot, G., and Guisnet, M., *J. Chem. Res.* **5**, 290 (1981).

62. Sulikowskii, B., and Popierlaz, A., *Appl. Catal.* **42**, 195 (1988).

63. Nováková, J., Kubelková. L., and Dolejsck, Z., *J. Catal.* **108**, 208 (1987).

64. Salvador, P., and Kladnig, W., *J. Chem. Soc. Faraday Trans.* **1**, 1153 (1977).

65. Vanden Berg, J. P., Wolthuizen, J. P., and Van Hoff, J. H. C., Proc. V Conf. Zeolites, Naples, Italy (1980), p. 649.

66. Dejaifve, P., Vedrine, J. C., Bolis, V., and Derouane, E. G., *J. Catal.*, **63**, 331 (1980).

67. Chang, C. D., Lang, W. H., and Bell, W. K., "Catalysis of Organic Reactions" (Moser, W. R., Ed.), Dekker, New York, (1981), p.73.

CHAPTER VI

SUMMARY AND CONCLUSIONS

6.1 SUMMARY AND CONCLUSIONS

6.1.1 SYNTHESIS AND KINETICS

MCM-22 could be synthesized in the SiO_2/Al_2O_3 range between 30 - 150 using hexamethyleneimine as the template. Even a small modification in the structure of the template led to an amorphous phase. The synthesis of the zeolite was feasible only in a narrow temperature window (~ 423 K).

Sodium silicate was found to be a better source of silica compared to silica sol or fumed silica for synthesizing MCM-22. The samples synthesized using sodium silicate were found to possess higher crystallinity. Besides, the yields were also larger when sodium silicate was used. The OH^-/SiO_2 ratio of the precursor gel could be varied between 0.075 to 0.3, beyond which ZSM-5 and ferrierite were found to co-crystallize, either as pure phases or as a mixture along with MCM-22.

Finally, MCM-22 samples with high phase purity and good crystallinity were produced by stirring at the rate of 200 rpm. Stirring also shortened the crystallization time. Static conditions did not lead to the formation of MCM-22.

6.1.2 CHARACTERIZATION

X-ray powder diffraction analysis of the samples demonstrated that no impurity phases were present in the synthesized samples. The XRD patterns of the samples matched the pattern reported by Rubin and Chu. The XRD patterns of the synthesized material was carefully examined for peaks from dense phases such as, crystobalite and quartz and zeolitic phases such as, ZSM-5, mordenite and ferreirite. The samples were found to be free from all the above phases. The XRD lines were indexed based on an orthorhombic crystal symmetry with a Cmmm space group. The unit cell parameters of the MCM-22 sample with SiO_2/Al_2O_3 ratio = 28 were 'a' = 24.606 ± 0.005 Å, 'b' = 14.395 ± 0.005 Å and 'c' = 24.753 ± 0.005 Å.

Scanning electron micrographs revealed that MCM-22 crystals have a platelet morphology with platelet diameters of approximately 1 - 2 μm diameter and thickness of about 0.1 μm. The platelets are bunched into 4 -5 μm particles. No difference in morphology was observed between the as-synthesized and calcined samples. FTIR studies indicated the presence of pentasil rings and 12 MR units. I.R. bands corresponding to -OH groups, associated with extra-framework aluminum, were detected in the samples with higher aluminum contents. Sorption of pyridine provided details about the acid sites present in the zeolite samples.

From the thermo-analytical studies, two stages of template decomposition were observed. The decomposition was exothermic even in an inert atmosphere (helium), which indicated that, the template probably underwent oxidation with surface -OH groups. The zeolite structure was stable up to 1000 K. The temperature-programmed decomposition (TPD) of the template revealed information regarding the nature of the decomposition. The main fragments of the decomposition, namely, CH_4 and NH_3, being richer in hydrogen led to the build up of "difficult to burn" carbon skeleton on the surface.

Detailed, multinuclear MAS NMR studies were carried out over the as-synthesized, calcined and dealuminated samples. The as-synthesized sample exhibited a sharp NMR spectrum, whereas, spectra of the calcined and dealuminated samples were broad. The existence of a **"buried T"** site was confirmed by ^{29}Si NMR studies. ^{27}Al MAS NMR studies confirmed that there was no dealumination upon calcination. ^{1}H - ^{29}Si CP-MAS NMR and ^{1}H NMR studies confirm the assignment of a signal at $\delta = -99.39$ ppm to silanol groups. A ^{29}Si NMR signal at $\delta = -104.3$ ppm attributed by earlier workers to the $Q^4(1Al)$ species is more likely to be due to both $Q^4(1Al)$ and $Q^4(0Al)$ species. The ^{13}C NMR spectrum of the template in the as-synthesized sample was similar to the one exhibited by the template adsorbed over silica gel except for the splitting of the downfield signal into two lines in the case of the former sample. This splitting of

the ^{13}C NMR signals suggests that the template has to orient itself to fit inside the channels/cages of MCM-22 in such a way that the environments of the carbon atoms are different.

6.1.3 SORPTION PROPERTIES

Sorption of argon was carried out at 77 K over all the samples studied, and the surface areas were measured. The samples had surface areas ranging from 425 m^2/g to 300 m^2/g. Sorption of probe molecules such as, water, n-hexane, cyclohexane, m-xylene and 1,3,5-trimethyl benzene (mesitylene) was carried out at 298 K over all the samples. The amount of water sorbed decreased as the Si/Al ratio of the samples increased indicating a decrease in hydrophilicity. Considerable sorption (> 7.5 wt. %) of bulky molecules like m-xylene and mesitylene was observed over MCM-22 samples suggesting the possible access of some 12 MR cages from the crystal surface. The adsorption data also indicated that the internal void volume of MCM-22 was larger than that of MTW and mordenite. Sorption of ammonia was carried out in the temperatures range of 303 K - 453 K. It was found that the Langmuir equation was not applicable to NH$_3$ adsorption over MCM-22. The monolayer capacities and affinity co-efficients were calculated from the Dubinin equation. Isosteric heats of adsorption and chemical affinities of ammonia were calculated for the various samples. The ammonia sorption studies indicated that the acid sites were not uniform and were hetergeneously distributed.

6.1.4 CATALYTIC PROPERTIES OF MCM-22

6.1.4.1 Isomerization of m-Xylene

Catalytic reactions were carried out over MCM-22 samples. During the isomerization of m-xylene, the para-xylene/ortho-xylene ratio was found to be 1.1 ± 0.1. The 1,3,5-TMB/1,2,4-TMB ratio was 0.25 ± 0.05. The isomerization/disproportionation ratio (I/D) of 3.98 (Log(I/D) = 0.6) suggested that MCM-22 behaved as a wide-pore zeolite, eventhough it possesses 10 MR channels. The results were compared with those obtained over other large pore molecular sieves such as, ß, MOR and ZSM-12.

6.1.4.2 Hydroisomerization of n-hexane

n-Hexane hydroisomerization was found to proceed via a dual-functional mechanism over Pt-H-MCM-22. Both conversion and isomerization/cracking (I/C) ratio increased with increasing Pt content of the samples and reached a plateau at about 0.5 wt. % Pt. High partial pressures of hydrogen led to an increase in I/C ratio, while the samples with high aluminum content exhibited higher conversion and the production of an equilibrium distribution of hexane isomers. The octane number (RON) enhancement over Pt-MCM-22 (at 503 K and WHSV $(h^{-1}) = 1$) was significant. The activity of MCM-22 was comparable to ß and was better than mordenite or MTW.

6.1.4.3 Cracking of n-hexane

The cracking of n-hexane was also studied over MCM-22 samples. At higher temperatures, the thermodynamically favored n-alkanes were preferentially formed and a decrease in iso-alkane to n-alkane ratio was observed for the C_4 fraction. As the aluminum content decreased, the hydrogen transfer capacity decreased and olefin yields increased. The activity of MCM-22 was compared with ZSM-5. The yield of C_1 and C_2 hydrocarbons was more over ZSM-5 than over MCM-22. Also, the formation of aromatics was pronounced in ZSM-5 (selectivity towards aromatics ~ 35 %) and negligible over MCM-22.

6.1.4.4 Transformation of methanol to hydrocarbons

Transformation of methanol to hydrocarbons over MCM-22 resulted in the formation of poly alkylbenzenes (PABs). The formation of PABs are favored only in large pore zeolites. Thus, MCM-22 was found to exhibit a large pore behaviour. But the other hydrocarbon distributions indicated that some medium pore characteristics also prevail. MCM-22 exhibited greater selectivity towards hexamethyl benzene and pentamethyl benzene rather than the lighter aromatics such as BTX (benzene, toluene and xylenes) which are formed in large quantities over ZSM-5.

LIST OF PUBLICATIONS

1. Synthesis, Characterization and Catalytic properties of Zeolite PSH-3/MCM-22.
    R. Ravishankar, Tapas Sen, Veda Ramaswamy, H.S. Soni, S. Ganapathy
    and S. Sivasanker.
    Studies in Surface Science and Catalysis, 84(A) (1994) 331.

2. Characterization and Catalytic properties of Zeolite MCM-22.
    R. Ravishankar, D. Bhattacharya, N.E. Jacob and S. Sivasanker,
    Microporous Materials, 4 (1995) 83.

3. Multinuclear MAS NMR Spectroscopic study of the Zeolite MCM-22.
    R. Ravishankar, Tapas Sen, S. Sivasanker and S. Ganapathy.
    J. Chem. Soc. Faraday Trans., 91(19) (1995) 3549.

4. Transformation of methanol to Olefins/hydrocarbons over zeolite MCM-22.
    R. Ravishankar and S. Sivasanker.
    Catalysis, Modern Trends, (Eds., N.M. Gupta and D.K. Chakraborthy),
    Narosa Publishing House, New Delhi, p. 81, (1995).

5. Hydroisomerization of n-hexane over zeolite MCM-22.
    R. Ravishankar and S. Sivasanker.
    Applied Catalysis, (in Press) 1996.

6. Sorption Properties of zeolite MCM-22.
    R. Ravishankar, S.S. Tamhankar, V.P. Shiralkar and S. Sivasanker.
    (Manuscript submitted for publication).

7. Catalytic Properties of zeolite MCM-22: Part I. Alkylation of benzene.
    R. Ravishankar and S. Sivasanker.
    (Manuscript submitted for publication : React. Kinet. Catal. Lett.)

8. Catalytic Properties of zeolite MCM-22: Part II. n-Hexane cracking over
    zeolite MCM-22.
    R. Ravishankar and S. Sivasanker.
    (Manuscript submitted for publication : Catal. Lett.)

9. Vapor Phase Beckmann Rearrangement of cyclohexanone oxime
    over MEL-type zeolites.
    J. Sudhakar Reddy, R. Ravishankar, S. Sivasanker and P. Ratnasamy.
    Catalysis Letters, 17 (1993) 139.

10. Location of titanium in the MEL lattice by Computer Modelling Studies.
    R. Ravishankar, R. Vetrivel and S. Kaliaguine.
    Catalysis, Present & Future,International Series on Chemical Engineering,
    (Eds.,) P. Kanta Rao and R.S. Beniwal (1995) p.139.

11. Synthesis and Characterization of molybdenum containing
    MFI type silicalite.
    P.S. Raghavan, R. Ravishankar and A.V. Ramaswamy.
    Catalysis, Modern Trends, (Eds., N.M. Gupta and D.K. Chakraborthy),
    Narosa Publishing House, New Delhi, p. 168 (1995).

12. Synthesis and Characterization of molybdenum containing
    MFI type silicalite.
    P.S. Raghavan, R. Ravishankar, S. Sivasanker and A.V. Ramaswamy.
    (Manuscript submitted for publication : Catal. lett.)

13. Computer Simulation of the magnetic phase transition.
C. Vijayan and R. Ravishankar.
Physics Education, 11(2) (1994) 125.

14. Computer Modelling Studies over Titanosilicate molecular sieves.
R. Ravishankar, R. Vetrivel and S. Sivasanker.
(Submitted for Publication : Mol. Simul.,)

15. The Stability of Silicalite-1 and Silicalite-2 and their
Titanium Substituted Analogues.
J.S. Reddy, R. Ravishankar, R. Vetrivel and S. Sivasanker.
(Communicated to Microporous Materials) 1995.

PATENTS

1. Synthesis and Characterization of Mo-containing MFI type molecular sieves.
P.S. Raghavan, R. Ravishankar and A.V. Ramaswamy.
Indian Patent No. 1719/DEL/94.

2. A process for the preparation of cyclopropyl amine, an intermediate for fluoro quinolone antibiotics.
T. Ravindranathan, S. Sivasanker, B. Chanda, K.R. Kamble and R. Ravishankar,
Indian Patent filed.